Aus dem Institute of Lung Health and Immunity des Helmholtz Zentrum München
Direktor: Dr. Ali Önder Yildirim

Und dem
Institut für Medizinische Informationsverarbeitung Biometrie und Epidemiologie (IBE) des
Institut der Universität München
Direktor: Prof. Dr. Ulrich Mansmann

Mechanism underlying environmental nanoparticle exposure triggered gammaherpesvirus reactivation

Dissertation
zum Erwerb des Doktorgrades der Humanbiologie
an der Medizinischen Fakultät der
Ludwig-Maximilians-Universität zu München

vorgelegt von
Lianyong Han

aus

Shandong, China

Jahr

2023

Mit Genehmigung der Medizinischen Fakultät
der Universität München

Berichterstatter:	Prof. Dr. Annette Peters
Mitberichterstatter:	Prof. Dr. Lars Lindner
Mitbetreuung durch den promovierten Mitarbeiter:	Dr. Tobias Stoeger Prof. Dr. Heiko Adler
Dekan:	Prof. Dr. med. Thomas Gudermann
Tag der mündlichen Prüfung:	08.08.2023

Table of content

Zusammenfassung:

Das Einatmen von Umweltpartikeln und die dauerhafte Herpesvirusinfektion sind zwei allgegenwärtige Umweltfaktoren die beide mit chronischen Lungenerkrankungen im Zusammenhang stehen. Nach der Erstinfektion, die oft durch eine Phase lytischer Infektion, Virusausbreitung und entsprechender Immunreaktion begleitet wird, begeben sich Herpesviren in einen Zustand sogenannter Latenz, indem sie vom Immunsystem kaum erkannt werden. Einmal infiziert, verbleiben Herpesviren lebenslang im Wirt, können jedoch durch bestimmte Stress-Stimuli reaktiviert, d.h. in den lytischen Zustand versetzt werden. Vor einigen Jahren konnte unsere Arbeitsgruppe im Mausmodell zeigen, dass eine Exposition mit rußartigen Kohlenstoff-Nanopartikeln (CNP) oder faserförmigen, doppelwandigen Kohlenstoff-Nanoröhren (DWCNT) in der Lunge von latent mit Murinen Gammaherpesvirus-68 (MHV-68) infizierten Mäusen, eine Zunahme der lytischen viralen Proteinexpression induziert. Dabei zeigen die Lungen ein ähnliches Muster an Zellulären Metaboliten, wie es bei einer akuten MHV-68 Infektion beobachtet wird, was erstmals auf eine Virusreaktivierung durch inhalierte Partikel hindeutete. Die genaue, zelluläre Lokalisierung der MHV-68-Reaktivierung sowie die zugrunde liegenden Mechanismen waren jedoch erstmal noch unklar.

Es ist bekannt, dass die MAP-Kinase-Weg (mitogen-activated protein kinase, MAPK), ein zentraler Signalweg der zellulären Stressreaktion, der auch durch bestimmte Partikel-Zell-Wechselwirkungen aktiviert wird, zur Herpesvirus-Infektion beiträgt. Wir untersuchten daher, ob CNP und DWCNT latentes MHV-68 über den MAPK-Signalweg reaktivieren.

Im latent MHV-68-infizierten Mausmodell konnten wir erneut zeigen, dass eine pulmonale CNP-Exposition latentes MHV-68 reaktiviert, indem wir die lytische Virusproteinexpression in der Lunge immunhistologisch quantifizierten. Weitere Untersuchungen ergaben, dass die durch CNP induzierte MHV-68-Reaktivierung in der Lunge hauptsächlich auf CD11b+, infiltrierende Makrophagenähnlichen Zellen lokalisiert war.

Um den zugrundeliegenden Mechanismus der Reaktivierung zu untersuchen, wurden persistent latent MHV-68-infizierte, aus dem Knochenmark stammende Makrophagen (Ana-1/MHV-68) etabliert, die ebenfalls stark CD11b exprimieren

und somit den Zelltyp der Virusreaktivierung nachahmen, wie er in der Mauslunge auftritt. Wir exponierten Ana-1/MHV-68-Zellen mit CNP und DWCNT und untersuchten die Aktivierung des MAPK-Signalweg sowie transkriptionelle Veränderungen. Hierbei zeigte sich, dass die MAP-Kinasen ERK1/2, JNK und p38 bereits innerhalb der ersten Stunde nach CNP- und DWCNT-Exposition aktiviert bzw. phosphoryliert wurden, gefolgt von der Induktion der lytischen viralen Genexpression (24 h) und dem Anstieg des Titers infektiöser Viruspartikel (72 h). Allerdings konnte innerhalb von 3 und 9 Stunden nach CNP- und DWCNT-Exposition keine klassische pro-inflammatorische Transkriptionssignatur beobachtet werden. So erwiesen sich Marker-Gene wie IL1b-, Ptgs2, Nos2 und Saa3 in ihrer Expression entsprechend unverändert, wurden jedoch durch LPS stark induziert.

Die Hemmung der p38-Aktivierung durch einen pharmakologischen Inhibitor konnte die MHV-68 Rekativierungs-Wirkung von CNP völlig aufheben, nicht jedoch die von DWCNT. Auch in vivo zeigte die immunhistochemische Färbung, dass die p38-Inhibitor-Vorbehandlung bei latent infizierten Mäusen die durch pulmonale CNP-Exposition induzierte MHV-68-Reaktivierung deutlich abschwächt.

Unsere Ergebnisse deuten darauf hin, dass Luftverschmutzung durch Partikel eine Herpesvirus-Reaktivierung auslösen kann, was wiederum einen immunmodulierenden Effekt in der Lunge bewirkt. Für die Reaktivierung latenter Herpesviren durch Kohlenstoffnanopartikel spielt der p38-MAPK-abhängige Signalweg eine wichtige Rolle und seine pharmakologische Hemmung könnte somit die Exazerbationen von Krankheiten im Zusammenhang mit der Partikelexposition in der Umgebung lindern.

Abstract:

Environmental particle inhalation and persistent herpesvirus infection are omnipresent and associated with chronic lung diseases. Herpesviruses have a lifespan consisting of two phases: lytic infection and latent infection. Once infected, the herpesvirus can stay lifelong in hosts and can be reactivated by certain stimuli. In a previous work, Sattler and colleagues in our group showed that pulmonary exposure to soot-like carbonaceous nanoparticles (CNP) and fiber-shaped engineered double walled carbon nanotubes (DWCNT) induced an increase in lytic viral protein expression in latently murine gammaherpesvirus-68 (MHV-68) infected mouse lungs, with similar lung gene expression and metabolome pattern as during acute infection suggesting virus reactivation. However, the exact localization of MHV-68 reactivation as well as the underlying mechanisms remain unclear.

The mitogen-activated protein kinase (MAPK) signaling, a stress response pathway also known to be activated by certain particle-cell interactions, has in addition to that been reported to also contribute to herpesvirus infection. We therefore studied whether CNP and DWCNT reactivate MHV-68 via MAPK signaling.

In a MHV-68 infected murine model, we confirmed that pulmonary CNP exposure reactivated latent MHV-68 by immunohistological quantifying lytic virus protein expression. Further investigation revealed that MHV-68 reactivation induced by CNP was mainly localized to CD11b+ infiltrating macrophage-like cells in the lung.

To study the underlying mechanism in a cell model, persistently latent MHV-68 infected bone marrow-derived macrophages (Ana-1/MHV-68) had been established, which highly expressed CD11b and mimic the virus reactivation occurring cell type in mouse lung. We exposed Ana-1/MHV-68 cells with CNP and DWCNT and MAPK signaling and transcriptomic changes were investigated. Here, we found that ERK1/2, JNK and p38 MAPK were rapidly activated within the first hour after CNP and DWCNT exposure, followed by the upregulation of lytic viral gene expression (24 h) and increased infectious virus titer (72 h). However, in contrast to LPS exposure, which was used as reactivation inducing positive control, no classical pro-inflammatory transcriptional signature, such as

IL1b, Ptgs2, Nos2 and Saa3 upregulation was detected within 3 & 9 h after CNP and DWCNT exposure.

Further pharmacological inhibition of p38 activation abrogated CNP but not DWCNT triggered virus reactivation *in vitro*. *In vivo*, immunohistochemistry staining showed that p38 inhibitor pretreatment of latently infected mice attenuated MHV-68 reactivation induced by pulmonary CNP exposure.

Our findings suggest that similar to CNP, environmental particle pollution triggers latent herpesvirus reactivation via a p38 MAPK dependent signaling, and the preventive pharmacological inhibition might alleviate ambient particle exposure related health effects and disease exacerbations.

List of figures

List of tables

List of abbreviations

No.	Abbreviations	Full name
1	AD	Antibody diluent
2	APS	Ammonium persulfate solution
3	BAL	Bronchoalveolar Lavage
4	BCA	Bicinchoninic acid
5	BMDM	Bone marrow-derived macrophage
6	BSA	Bovine serum albumin
7	CAST	Computer-assisted stereological toolbox
8	CMV	Cytomegalovirus
9	CNP	Carbonaceous nanoparticle
10	COPD	Chronic obstructive pulmonary disease
11	d	Day
12	DPBS	Dulbecco’s Phosphate Buffered Saline
13	DWCNT	Double-walled carbon nanotube
14	EBV	Epstein-Barr virus
15	EDTA	Ethylenediaminetetraacetic acid
16	ELISA	Enzyme-linked immunosorbent assay
17	FACS	Fluorescence-activated single cell sorting
18	g	Gravity
19	GSEA	Gene Set Enrichment Analysis
20	h	Hour
21	HHV-6	Human Herpesvirus 6
22	HHV-8	Human Herpesvirus 8
23	HIER	Heat-Induced Epitope Retrieval
24	IF	Immunofluorescence
25	IHC	Immunohistochemistry
26	IPF	Idiopathic pulmonary fibrosis
27	KSHV	Kaposi's sarcoma-associated herpesvirus
28	L	liter
29	LDH	Lactate Dehydrogenase

30	LPS	Lipopolysaccharide
31	LSFM	Light-sheet fluorescence microscopy
32	MAPK	Mitogen-activated protein kinase
33	MHV-68	Murine gammaherpesvirus 68
34	min	Minutes
35	ml	milliliter
36	MWCNT	Multi-walled carbon nanotube
37	NACA	N-acetylcysteine amide
38	NPs	Nanoparticles
39	PFA	Paraformaldehyde
40	PFU	Plaque-forming unit
41	qPCR	Quantitative polymerase chain reaction
42	ROS	Reactive Oxygen Species
43	rpm	Revolutions per minute
44	RT	Room temperature
45	s	second
46	SD	Standard division
47	SDS	Sodium dodecyl sulfate
48	TEMED	Tetramethylethylenediamine
49	V	Voltage
50	µl	microliter

1. Introduction

1.1 Environmental nanoparticle exposure, inflammation and chronic lung diseases

Nowadays, air pollution has been recognized as a global problem and is of great concern to human health. Worldwide air pollution causes respiratory as well as cardiovascular diseases and is thereby an important environmental cause of morbidity and mortality. As latest estimated by World Health Organization (WHO), 7 million death per year can be attributed to air pollution worldwide. Similarly, the Global Burden of Disease study also announced that air pollution causes a great global public health challenge and contributes to around 6.7 million death (Landrigan et al., 2018, Collaborators, 2018).

Six pollutants are identified as main air contaminants, which are carbon monoxide, lead, nitrogen oxides, ground-level ozone, sulfur oxides, and particle pollution. As one of the major components of air pollutants, particle pollution is often referred to particulate matter (PM). Dust, dirt, soot, and smoke are common sources of PM, and they are either emitted directly from sources such as construction places, factory smokestacks, and vehicles, or relative consumption products (EPA, 2022). Increasing studies reported that PM exposure and especially exposure to the most respirable fraction, namely ultrafine or nanoparticles, with a diameter less than 100 nm, is largely responsible for associated respiratory as well as cardiovascular diseases (Schraufnagel, 2020).

1.1.1 Pulmonary nanoparticle exposure causes inflammation

Nanoparticles (NPs) exhibits diameter less than 100 nm. Due to the ultrafine size of NPs, they can be suspended in the air for a long time. Compared to big size particles, NPs are easily to reach deep into the respiratory tract and cause further health problems.

In recent years, the rapid development of nanotechnology brings great benefits to humans, some nanomaterials (NMs) are used for energy storage, as chemical catalyst and as well for medical applications. However, these new developed

NMs may also pose uncertain or unknown risks to humans in daily life. Therefore the health hazard of NMs needs more careful observations and investigations.

Carbonaceous nanoparticles (CNP) or carbon black (CB), is a type of soot-like nanomaterial, typically consisting of primary particles of a diameter from 10 - 30 nm forming larger chain-like aggregates and agglomerates. CNP is therefore a fundamental component of inhaled combustion particles and has been frequently reported to trigger acute lung inflammation (Bourdon et al., 2012, Renwick et al., 2004, Ganguly et al., 2017).

Our research group has previously (André et al., 2006) reported that inhalation of moderate doses of CNP triggered a mild increase of airspace neutrophils in mice, detected by bronchoalveolar lavage (BAL), indicating low-grade neutrophilic inflammation in the lungs. Further microarray analysis identified several genes related to the pro-inflammatory response, such as Serum amyloid A-3 (Saa3), Osteopontin (Spp1) and Lipocalin 2 (Lcn2). BAL fluid interleukin-1β (IL-1β) and CXCL1 protein release after 24h CNP exposure also reflect the pro-inflammatory response in mice. To understand the cellular initiation of lung inflammation, isolated alveolar macrophages (AMs) from CNP exposed mice were analyzed for particle phagocytosis. 12h after CNP exposure more than 90% of BAL recovered AMs showed to be CNP laden (Chen et al., 2016). However, unless lung expression analysis demonstrated a significant induction of pro-inflammatory gene expression, no pro-inflammatory signature was detected in isolated AMs. In contrast, neutrophil chemoattractant Cxcl5 was significantly induced in alveolar epithelial type II (ATII) cells, suggesting the epithelial cell response or injury as a driver of the acute neutrophilic inflammation in response to CNP.

Inoue and colleagues found that CNP as well as diesel exhaust particles (DEPs) exposure exacerbated LPS-caused lung inflammation in mice, accompanied with IL-1β, CXCL1, CC-chemokine ligand 2 (CCL2), macrophage inflammatory protein-1alpha (MIP-1alpha) and MIP-2 activation (Inoue et al., 2006, Takano et al., 2002). Furthermore, oxidative stress and the transcription factor nuclear factor-kappaB (NF-κB) have also been described to be activated, suggesting a potential mechanism related to nanoparticle exposure induced lung inflammation.

Carbon nanotubes (CNTs) are tube-like engineered nanomaterial that are made up of elemental carbon and can reach micrometers in length with only a few

nanometers in diameter (Tasis et al., 2006). CNTs are made from graphite sheets and these sheets can roll up to rigid and highly resilient hexagonal like mesh structure, with different layers of carbon sheets. Depending upon the number of carbon layers, CNTs are classified into single-walled carbon nanotubes (SWCNTs), double-walled carbon nanotubes (DWCNTs), and multi-walled carbon nanotubes (MWCNTs) (Awasthi et al., 2005).

CNTs exhibit incessantly increasing applications with at the same time rising environmental concerns due to their fiber-like shape similar to asbestos. DWCNTs have been shown to induce acute lung inflammation at an equal surface dose compared to CNP (Tian et al., 2013). Differently, however, CNT induced persistent inflammation lasting over weeks and thus much longer than that of CNP (Ganguly et al., 2017).

Shvedova *et al*. found that SWCNT exposure caused progressive lymphocytes and macrophages influx in mouse lungs for up to 7 days, except for an acute neutrophils accumulation after 24 h. Importantly, transforming growth factor-beta1 (TGF-β1) release as well as granuloma formation in mouse lungs at day 7 demonstrated a pro-fibrotic effect of SWCNT (Shvedova et al., 2005). Similar to CNP, CNT also shows the ability to enhance lung inflammation caused by bacterial infection, via disturbing the phagocytosis and nitric oxide production of alveolar macrophages (Shvedova et al., 2008a). DWCNT and MWCNT showed a similar effect on lung inflammation, but MWCNT exhibits overall more toxic effects in a profibrotic manner. MWCNTs were reported to mediate alternative macrophage activation and trigger the production of TGF-β1, followed by the activation of fibroblasts (Wang et al., 2013). Furthermore, MWCNTs activated TGF-β/Smad signaling pathway and further directly promote epithelial-mesenchymal transition (EMT) and fibroblast-to-myofibroblast transition (Wang et al., 2015), all together pointing to the pro-fibrotic potential of these materials.

Thus, nanoparticle exposure can trigger acute and chronic lung inflammation.

1.1.2 Mechanism study uncovered the signaling pathway

Several important toxicological key events and signaling pathways participate in the pro-inflammatory responses and injury induced by nanoparticle exposure, reaching from the production of reactive oxygen species (ROS) and subsequent

oxidative stress, which in turn is known to stimulate mitogen activated protein kinases (MAPKs) signaling and NF-κB activation (Li et al., 2003, Stoeger et al., 2009).

Reactive oxygen species (ROS) and oxidative stress

ROS are chemically reactive molecules containing oxygen, including hydrogen peroxide (H_2O_2), superoxide (O_2^-), hydroxyl radical (·OH), and singlet oxygen (O_2). As small and reactive molecules, ROS can oxidize lipids, proteins and DNA. Besides, ROS play roles in signal transduction, gene expression, and activation of receptors in physiological condition. When the anti-oxidant homeostasis is disturbed, excessive ROS are produced in cells and tissues and cannot be controlled or neutralized by antioxidants, this is referred to oxidative stress (Li et al., 2017). The disturbance of the oxidative state thus causes the generation and prolonged persistence of free radicals and peroxides. In this context, disproportionate ROS has been implicated to initiate and enhance lung inflammation through activation of MAPK signaling and redox-sensitive transcription factors, such as NF-κB and activator protein-1 (AP-1).

Nanoparticles are widely reported to trigger oxidative stress (Li et al., 2003, Nel et al., 2006, Stoeger et al., 2009). Shvedova et al. found that SWCNT exposure caused oxidative stress and inflammation in mouse lungs (Shvedova et al., 2008b). Decreased Glutathione (GSH) level and increased protein thiols level indicate the oxidative damage in mouse lung, and Malondialdehyde (MDA), one type of final lipid peroxidation product, is increased upon SWCNT exposure also demonstrates the oxidative stress compared to control. Meanwhile, dichloro-dihydro-fluorescein diacetate (DCFH-DA) is widely used to measure intracellular ROS level and quantify oxidative stress *in vitro*. Silica nanoparticles are widely reported to cause epithelial damage and trigger lung inflammation. Wang et al. found that silica nanoparticles triggered a 2-fold increase of DCFH-DA intensity in human bronchial epithelial (BEAS-2B) cells, reflecting ROS production and can be significantly blocked by the application of ROS scavenger, N-acetyl-L-cysteine (NAC), which finally rescue cellular damage (Wang et al., 2020). Tian *et al.* found that DWCNT exposure resulted in a decrease of GSH levels and anti-oxidant catalase enzyme activity in mouse lungs (Tian et al., 2013).

Mechanistically, nanoparticle induced oxidative stress further mediates MAPK signaling activation, NF-and κB, AP-1, which are implicated in the process of lung inflammation and diseases.

Mitogen activated protein kinases (MAPKs) signaling

MAPK signaling contains three widely defined stress kinase cassettes, c-Jun N-terminal kinases (JNK), extracellular signal-regulated kinase (ERK, including ERK-1 and ERK-2 isoforms) and p38 MAPKs. MAPK signaling is one of the major intracellular signaling transduction pathway which regulates a wide variety of cellular processes.

In nanotoxicology, MAPK signaling is reported to be activated by certain particle-cell interactions. For instance, amorphous silica nanoparticles (nanosilica) have been proved to activate MAPK signaling in early exposure time in RAW264.7 macrophages due to oxidative stress, exhibiting fast phosphorylation of p38, ERK1/2 and JNK MAPK. Nanosilica further triggers a pro-inflammatory response characterized by increased Tnf, Ptgs2, Ccl2, and Cxcl2 mRNA levels and TNFa release (Fritsch-Decker et al., 2018). Inhibition of JNK and ERK1/2 but not p38 decreased these pro-inflammatory gene expression caused by nanosilica. A similar effect was found to suppress the release of TNFα.

The epidermal growth factor receptor (EGFR) is expressed in the epithelial cell membrane and is essential to activate MAPK signaling. Stoeckmann and colleagues reported that, CNP exposure caused the activation of EGFR and subsequent ERK1/2 phosphorylation in rat lung epithelial cells (RLE-6TN) (Weissenberg et al., 2010, Stöckmann et al., 2018). Also in primary rat epithelial lung cells, CNP induced IL-1α, IL-1β and IL-6 release via the activation of p38, ERK and JNK MAPK signaling (Totlandsdal et al., 2010).

Nuclear factor-κB (NF-κB) activation

NF-κB is a key transcription factor and play roles in inflammation and immune regulation. Beyond MAPK signaling activation, CNP triggered IL-6 release from rat primary lung epithelial cells is also depending on NF-κB. CNP especially at 100 μg/ml caused the degradation of IκBα, indicating the activation of NF-κB (Totlandsdal et al., 2010). Besides, 100 μg/ml CNP triggered the translocation of p50 and p65 subunit of NF-κB into nuclear in human monocytes and can be reduced by antioxidant application.

Thus, nanoparticle exposure causes oxidative stress and lung inflammation via the activation of MAPK signaling and NF-κB, and thus may contribute to the development of chronic lung diseases (CLDs).

1.1.3 The association between nanoparticle exposure and chronic lung diseases (CLDs)

Asthma

Asthma is a chronic inflammatory lung disease, affects long-term to airways and structural remodeling, resulting in narrowed airways and difficulties to breath for humans. Increasing epidemiological studies have focused on exposure to particulate air pollutants and asthma exacerbation. During the winter of 1991 to 1992, short-term exposure to different air pollutants was associated to respiratory symptoms, increase school absence rate and medication use in asthmatic children (Peters et al., 1997). Another study evaluated the effect of particulate air pollution and medication use among adult asthma populations. Elevated ambient particle concentrations resulted in high prevalence of asthma symptoms. Corticosteroid and beta2-agonist use for asthmatic adults was also associated with particulate air pollution (von Klot et al., 2002). Furthermore, not only exposure to fine or ultrafine particle, but higher average coarse particulate levels are also associated with increased asthma prevalence and morbidity among children (Keet et al., 2018).

In an experimental model, pulmonary exposure to CNP before allergen challenge enhanced allergic airway inflammation (Alessandrini et al., 2006). Compared to relevant control mice, particle inhalation before allergen challenge caused more infiltrating inflammatory cells and higher IL4, IL-5, and IL-13 level. Furthermore, CNP caused progressive mucus production and peribronchiolar and perivascular inflammation, and also increased airway hyperresponsiveness. There are counted as a strong adjuvant effect on allergic airway inflammation. A similar effect was also found by other researchers (Kroker et al., 2015, Inoue et al., 2005). Indeed, Kroker and colleague found that the application of the cell stress effects reducing solute ectoine, isolated from extremophilic bacteria, significantly suppressed the allergic airway inflammation(Kroker et al., 2015).

Taken together, these studies give a clear impression that populations with asthma pose more susceptibilities to particulate air pollution and thus need extra protection and healthcare.

Chronic obstructive pulmonary disease (COPD)

Facing a worldwide exposure to air pollution, the development and exacerbation of COPD is another great concern. COPD is a disease that is characterized by airway obstruction and loss of alveolar surface, both resulting in impaired breathing-related failures. Emphysema and chronic bronchitis are two phenotypes that depict the clinical picture of COPD. As estimated by WHO, COPD leads to 3.23 million deaths in 2019, which is accounted as the third leading death cause worldwide (WHO, 2022). A lot of factors have been recognized to be causes of COPD. Besides the leading factor of smoking, environmental factors, like harmful gases and ambient particles pollutants, genetic factors and respiratory infections have also been recognized as risk factors for COPD.

In 2018, the China Pulmonary Health (CPH) study, a cross-sectional study, assessed the prevalence and risk factors of COPD in China, and reported that the overall spirometry-defined COPD prevalence is 8.9%, with 11.9% in men and 5.4% in women (Wang et al., 2018). This study also proved that particulate matter is an important risk factor for COPD. A similar conclusion was addressed in another cross-sectional study in Japan. Kotaki and colleagues reported a high estimated prevalence of 16% for non-smokers and 29% and 37% for seniors and elders smokers, respectively (Kotaki et al., 2019). They also found correlation between levels of suspended particulate matter and COPD. As signs of COPD, chronic and progressive pulmonary inflammation and respiratory symptoms are persistence in those individuals.

Increasing studies have demonstrated that nanoparticle exposure can cause emphysema. For instance, as one major component of cigarette smoke, nano-sized carbon black (nCB) was found to deposit in dendritic cells (DCs) of lungs from emphysema patients and in mouse CD11c positive antigen presenting cells (APCs) (You et al., 2015). Experimentally, nCB exposure activated APCs, and promoted T helper 17 cell differentiation in the lung and finally caused emphysema in mice. Thus, nanoparticle exposure serves as a risk factor for the

development of emphysema and it potentially serves as a more susceptible factor to adverse health effects for COPD patients. Furthermore, Beyeler *et al.* reported that MWCNT exposure increased the frequencies of lung DCs and affected the mucosal immune system in mice with COPD (Beyeler et al., 2020). Thus, exposure to environmental nanoparticle poses health effect to individuals on the development of COPD.

Beyond ambient air pollution, indoor pollution especially cooking emission particles is also an emerging risk factor. A study undertaken in China revealed that, the prevalence of COPD among non-smoking women in rural area is higher compared to those who live in urban areas (7.2% vs 2.5%), mainly due to biomass fuel use in the kitchen (Liu et al., 2007). High PM10 and carbon monoxide (CO) concentration was measured in the kitchens from rural areas. Moreover, a systematic review and meta-analysis also demonstrated the association between cooking fuels use and COPD (Kurmi et al., 2010, Pathak et al., 2020).

Idiopathic pulmonary fibrosis (IPF)

IPF is a chronic, progressive interstitial lung disease, with key feature of fibrosis, IPF patients suffer worsening lung function. Exposure to air pollution is reported to be associated with lung functional decline, disease exacerbation, and increased risk of mortality in IPF patients. In a single center study in the US between 2007 and 2013 (Winterbottom et al., 2018), 135 IPF patients were included to assess the association between average particulate number concentration (PM2.5 and PM10) and the decline of forced vital capacity (FVC). There was a significant association between PM10 concentration and decline of FVC in those patients. Besides, low FVC of IPF patients was also associated with the level of NO_2, PM2.5 (Johannson et al., 2018). These studies suggest a potential promoting effect of ambient air pollution on the lung function decline of IPF patients.

Meanwhile, air pollution contributes to the exacerbation of IPF. In Beijing, clean air policy was implemented since 2013 and the air quality was largely improved. However, acute air pollution occurrence between 2013 and 2017 significantly caused more IPF hospitalizations (Liang et al., 2022). Currently, only carbon monoxide (CO), and nitrogen dioxide (NO_2) concentration were distinguished to

be associated with increased mortality in elder male IPF patients (Aguilar et al., 2021, Yoon et al., 2021). Thus, improving and controlling air quality remain a public health policy to protect IPF patients.

Carbon nanotubes (CNTs) are newly developed nanomaterials in recent years and have posed various applications. Animal studies have shown that CNTs, especially certain types of MWCNTs are potent inducers to trigger lung fibrosis, with excessive deposition of collagen and the remodeling of lung tissue (Wang et al., 2015, Wang et al., 2013). In recent years, CNTs are found in the airway of children (Kolosnjaj-Tabi et al., 2015), posing increasing concerns on the development of lung fibrosis in humans.

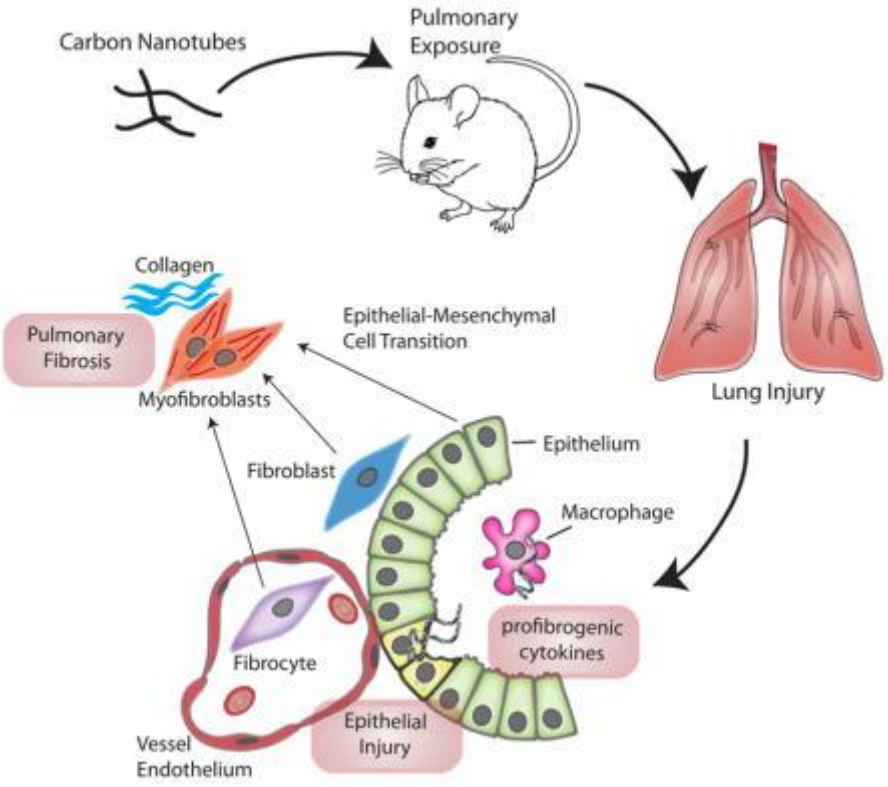

Figure 1.1 Pulmonary carbon nanotube exposure induced lung fibrosis in mice

Pulmonary carbon nanotubes exposure results in direct interaction with cells in the lung and result in epithelial cell injury, epithelial-Mesenchymal transition, fibroblast to myofibroblast transition and thereby contribute to fibrogenesis (adapted from (Duke and Bonner, 2018)).

Lung cancer

Environmental factors especially air pollution contribute to the development of lung cancer (Christiani, 2021). In 2013, International Agency for Research on

Cancer (IARC) evaluated outdoor air pollution as well as main component in outdoor air pollution, PM, as a Group I carcinogen to humans. A meta-analysis including 18 studies examined the association between PM2.5 and PM10 with lung cancer incidence and mortality (Hamra et al., 2014). The relative risk for PM2.5 associated lung cancer is 1.09 (95% CI: 1.04, 1.14), whereas PM10 associated lung cancer risk is 1.08 (95% CI: 1.00, 1.17). Smoking status also contributes to the lung cancer risk associated with PM2.5, which former smokers showed the greatest risk compared to never-smokers and current-smokers. Other air pollutants, such as NO_2, nitrogen oxides (NOx) also contribute to lung cancer incidence (Huang et al., 2021). Furthermore, air pollution shows additional interaction with genetic factors and arises the lung cancer risk in populations. A study based on UK Biobank revealed that lung cancer risk is associated with high genetic risk and air pollution in populations, compared to those who have low genetic risk and air pollution exposure.

MWCNT poses asbestos-like structure, especially MWCNT-7 (Mitsui-7) has been proved to have carcinogenicity in animal model. Inhalation of Mitsui-7 induced lung carcinoma in rats after 2 years, with male rats posing more susceptibilities than female rats. Another study demonstrated that, by 2 weeks exposure of MWCNT-N (Nikkiso) to rats, pleural malignant mesothelioma and lung tumors was developed after 109 weeks (Suzui et al., 2016). These studies proved the carcinogenicity of MWCNT in experimental model. In 2014, Mitsui-7 was classified as possibly carcinogenic to human by IARC (Barbarino and Giordano, 2021).

Thus, long-term exposed to air pollution poses risk to develop lung cancer especially for high genetic susceptibility individuals. Air quality improvement and personal protections reduce these risk factors and protect humans to develop lung cancer.

1.2 Pathogenesis of herpesvirus infection

1.2.1 Overview of herpesvirus and life cycle

Herpesviruses are a big family of DNA viruses, having accompanied their hosts including humans for millions of years, thus being very well adapted to their hosts. Herpesviruses are divided into alpha-, beta-, and gammaherpesviruses

(Sehrawat et al., 2018). Herpes simplex virus (HSV) -1, HSV-2 and varicella zoster virus (VZV) are alphaherpesviruses. Betaherpesviruses contain cytomegalovirus (CMV), human herpesvirus (HHV)-6 and HHV-7. Epstein Barr Virus (EBV) and Kaposi's sarcoma-associated herpesvirus (KSHV), also named human herpesvirus 8 (HHV-8), are gammaherpesviruses. Almost all populations worldwide are infected with at least one type of herpesvirus during the whole life (Boshoff and Weiss, 2001, Virgin et al., 2009, Sehrawat et al., 2018).

EBV infection can cause infectious mononucleosis, lymph node enlargement, chronic fatigue and hepatosplenomegaly in human (Marzouk et al., 2005). KSHV contributes to the development of Kaposi's sarcoma (KS), which is the most common cancer in acquired immunodeficiency syndrome (AIDS) patients. Besides, KSHV infection also contributes to primary effusion lymphoma and multicentric Castleman's disease (Ye et al., 2011).

Like all herpesviruses, gammaherpesviruses have a life cycle with both lytic and latent infection. During primary infection, gammaherpesviruses infect host cells in the respiratory tract causing the initial lytic infection. During lytic infection, infectious virus is produced and most of the viral genome is expressed. With the help of the immune response, in particular of cytotoxic T lymphocytes (CTL), the infectious virus is cleared but some virus remains lifelong in infected cells of the host in a latent stage. This is accompanied by downregulation of the lytic viral genes. Latency can be established in a variety of host cells including B cells, macrophages and dendritic cells. Latent virus can be reactivated towards lytic virus production by multiple challenges including classical and non-classical triggers. Known classical triggers include UV-light, fever, microbial co-infection, stress, tissue injury, hyperthermia, hormonal imbalance, allogeneic stimulation, cytokines, cell differentiation, immunosuppression and other toxic stimuli (Stoeger and Adler, 2018). In recent years, so-called nonclassical or novel challenges like helminth co-infection have been recognized as triggers of reactivation (Reese et al., 2014). In a previous work, Sattler and colleagues found that pulmonary exposure to carbon nanoparticles (CNP) and fiber-shape double-walled carbon nanotubes (DWCNT) also triggered herpesvirus reactivation in

lungs and restored a pattern similar to acute infection (Sattler et al., 2017).

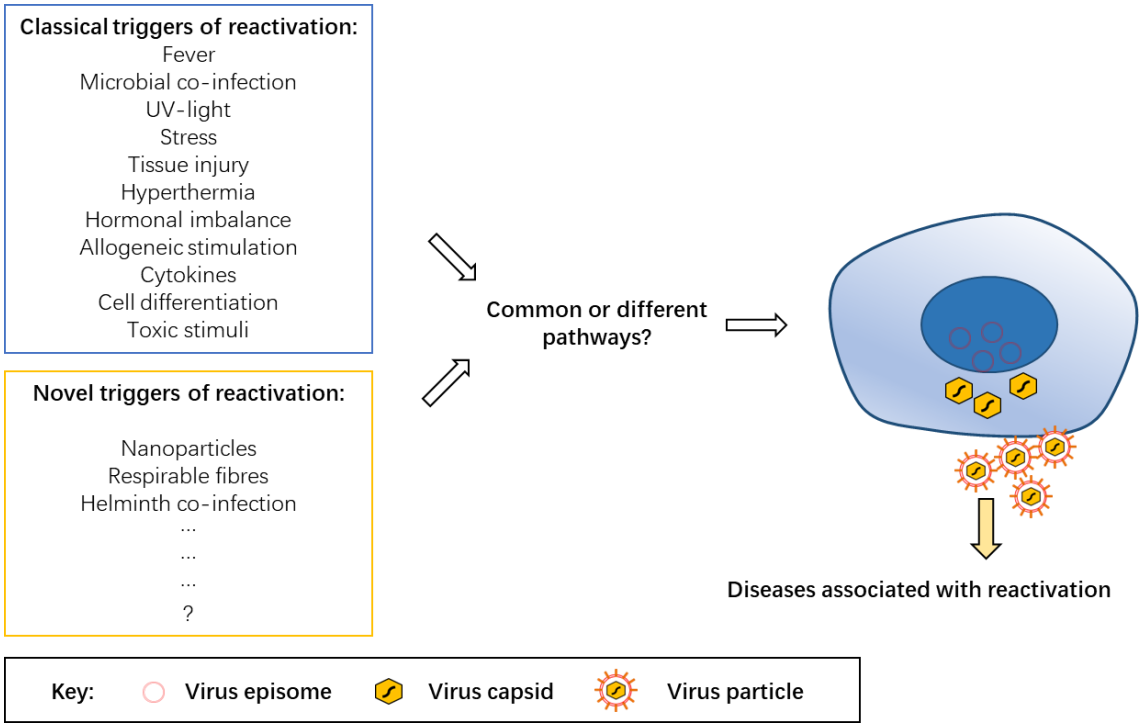

Figure 1.2 Classical and non-classical triggers of virus reactivation.

Both classical and non-classical triggers can reactivate latent herpesvirus. Known triggers were shown here. (adapted from (Stoeger and Adler, 2018))

1.2.2 Murine gammaherpesvirus 68 (MHV-68) provides a small animal model to study herpesvirus

Due to the species specificity of gammaherpesviruses, studies on the pathogenesis of human infection and reactivation are restricted. Murine gammaherpesvirus 68 (MHV-68), genetically related to EBV and KSHV, provides a good robust small animal model.

MHV-68 shares a lot of features with EBV and KSHV. MHV-68 and KSHV express the replication and transcriptional activator gene (RTA/ORF50), which is required for lytic replication as well as for reactivation. Thus, the expression of ORF50 is a marker for lytic viral gene expression. Meanwhile, gammaherpesviruses also express genes along latent infection which help the virus to stay latent in the host. Latency-associated nuclear antigen (LANA) for KSHV and murine LANA (or ORF73) for MHV-68 are required to establish and maintain the latent infection. Thus, the ratio of ORF50 and ORF73 can be used to characterize the different phases of infection.

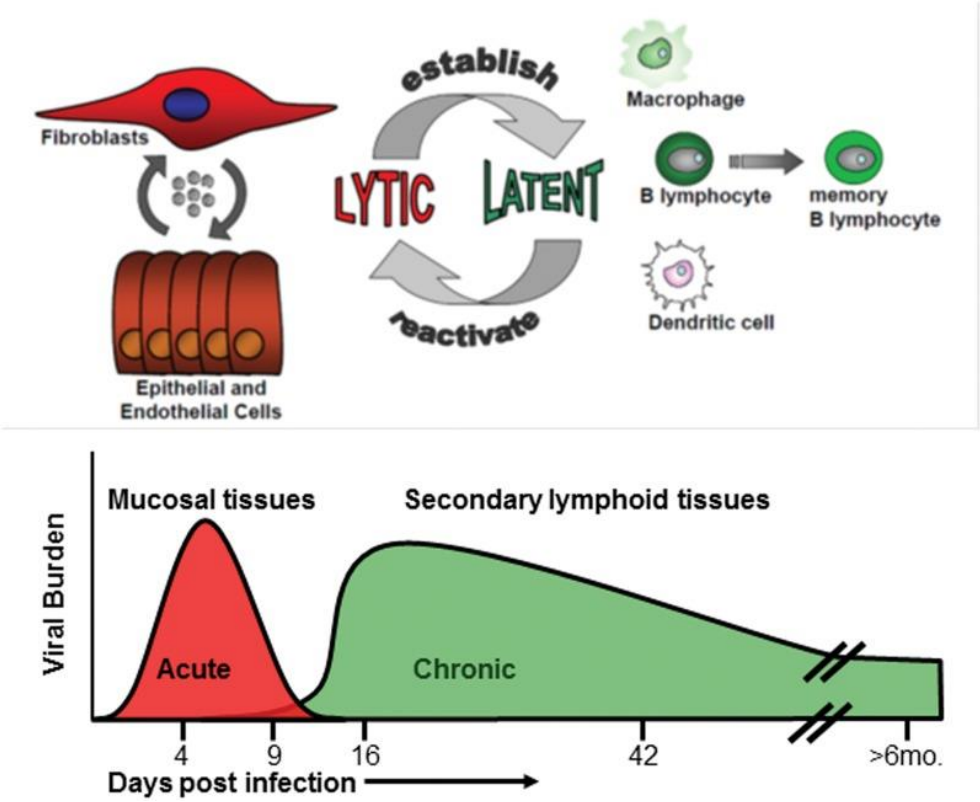

Figure 1.3 Course of MHV-68 infection in mice.

After infection, lytic MHV-68 replication mainly happens in epithelial cells of the lung. Afterwards, lytic virus is cleared by the immune response, and latent infection is established mainly in macrophages, dendritic cells and B lymphocytes. Acute MHV-68 infection occurs within 12 days after intranasal infection and peaks around 6 days. Latency is established afterwards. (adapted from (Cieniewicz et al., 2016))

1.2.3 Mechanism of herpesvirus infection and reactivation

Herpesviruses are able to hijack various signal transduction pathways that are essential for cellular functions to ensure acute infection, latency as well as reactivation. Common molecular mechanisms include oxidative stress, protein kinase C (PKC) signaling, Phosphatidylinositol 3-kinase (PI3K)-Akt signaling, NF-kB and MAPK signaling. In all cases, activation of RTA plays the central role.

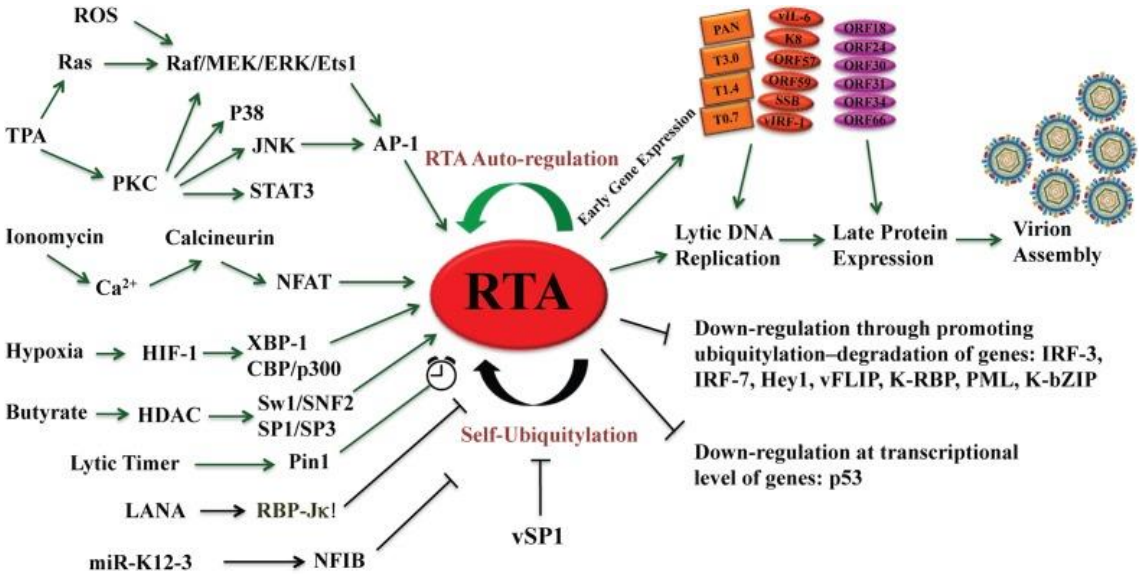

Figure 1.4 Signaling activation in KSHV reactivation from latency

Various signaling pathways are involved in KSHV reactivation, such as ROS, hypoxia and MAPK signaling. RTA plays a central role to link these pathways and reactivation. (Adapted from (Aneja and Yuan, 2017)).

Oxidative stress

Elevated ROS production, especially H_2O_2, induced the expression of RTA in KSHV latently infected human umbilical vein endothelial cells (HUVEC) and BCBL1 cells (Aneja and Yuan, 2017). Antioxidant enzymes, such as catalase and glutathione peroxidase, are expressed during oxidative stress and help cells to remove excessive H_2O_2 (Ye et al., 2011). The depletion of catalase and glutathione in turn induced stronger lytic viral gene expression (Li et al., 2011). Application of antioxidants N-acetyl-L-cysteine (NAC), catalase and glutathione significantly reduced KSHV reactivation induced by H_2O_2. Besides, NAC administration prolonged the lifespan of lymphoma mice induced by KSHV infection.

Protein kinase C signaling

Protein kinase C (PKC), which contains 12 structurally related serine-threonine kinases, is posing an important role in the transduction of cellular functions and proliferation signals (Ron and Kazanietz, 1999). PKC contains α, β, γ, δ, and ε isoforms. 12-O-tetradecanoylphorbol-13-acetate (TPA) is a common PKC activator and can reactivate latent herpesvirus in certain latently infected cells (Deutsch et al., 2004, Moore et al., 1996b, Renne et al., 1996, Sarid et al., 1998).

BCP-1 cells are KSHV positive lymphoma cells, derived from a HIV seronegative patient, have been used as an *in vitro* model to investigate KSHV reactivation. BCBL-1 cells are another KSHV-infected lymphoma cell line. TPA treatment caused early KSHV/ORF45 transcript (Zhu et al., 1999) and T1.1 early transcript induction (Zhong and Ganem, 1997), and early lytic protein viral IL-6 production (Moore et al., 1996a), suggesting KSHV reactivation. By application of GF 109203X (a pan-PKC inhibitor) as well as rottlerin (PKC ε isoforms inhibitor), KSHV reactivation was abolished in BCP-1 cells and BCBL-1 cells.

Phosphatidylinositol 3-kinase (PI3K)-Akt signaling

PI3K-Akt signaling is essential for several cellular processes, including protein synthesis, cell proliferation, cell growth and inflammation (Liu and Cohen, 2015). Herpesviruses express many proteins targeting and manipulating PI3K-Akt signaling to ensure virus replication, latency and reactivation. Viruses bind to B cell receptors (BCR), G protein coupled receptors (GPCRs) or integrins on cell membranes, then activate PI3K, resulting in the translocation of PI3K complex from the cytoplasm to plasma membrane, and finally inducing Akt phosphorylation. A lot of cellular responses are regulated downstream of Akt signaling, such as protein synthesis, cell cycle regulation and apoptosis.

Herpes simplex virus type 1 (HSV-1) infection activates the PI3K-Akt signaling pathways (Hsu et al., 2010). Blocking PI3K enhances apoptosis but attenuates viral gene expression in oral epithelial cells. Furthermore, HSV-1 infection also plays an important challenge to reactivate KSHV. In BCBL-1 cells, HSV-1 infection activates the PI3K-Akt signaling pathway and enhances KSHV lytic replication from latency, suggesting the effect of HSV-1 on KSHV reactivation (Qin et al., 2011).

NF-κB signaling

NF-κB signaling pathway is a well-known signaling pathway playing critical roles in cell survival, inflammation as well as B cell biology (Cieniewicz et al., 2016).

NF-κB signaling is involved in gammaherpesvirus lytic infection regulation and latency establishment. During EBV and KSHV latency, NF-κB activity remains high in lymphocytes, when cells are treated with NF-κB inhibitor, the lytic vial gene expression process starts and turns into reactivation. When KSHV is reactivated, NF-κB is downregulated (Chaudhary et al., 1999). In B cells and endothelial cells,

high NF-κB activity during latency suppresses downstream AP-1 and then blocks lytic viral gene expression. In fibroblasts and epithelial cells, the overexpression of NF-κB signaling repressed MHV-68 replication (Brown et al., 2003).

Thus, NF-κB signaling contributes to the maintenance of herpesvirus latency.

MAPK signaling pathway

MAPK signaling contains three widely defined stress kinase groups, which are JNK, ERK1/2 and p38 MAPKs. MAPK signaling plays important roles in cell growth, proliferation, differentiation and apoptosis (Yong et al., 2009).

During primary infection, KSHV activates ERK1/2, JNK and p38 pathways followed by AP-1 activation, which is mainly mediated by virus entry events at the early stage of KSHV infection. The activation of AP-1 then modulates the activation of RTA to enhance lytic infection. Specific inhibition of three MAPK pathways attenuates AP-1, RTA activation and virus infectivity in both HUVECs and HEK293 cells in a dose-dependent manner (Xie et al., 2005, Pan et al., 2006).

Beside primary infection, MAPKs also mediate KSHV reactivation from latency (Xie et al., 2008). In KSHV-infected BCBL-1 cells, three MAPKs are constitutively activated whereas TPA further enhances ERK1/2 and p38 MAPK activation but not JNK MAPK activation. However, inhibition of three MAPKs effectively reduced lytic viral gene expression as well as infectious virus production mediated by downstream target AP-1, confirming the role of MAPK signaling not only during primary infection but also reactivation from latency.

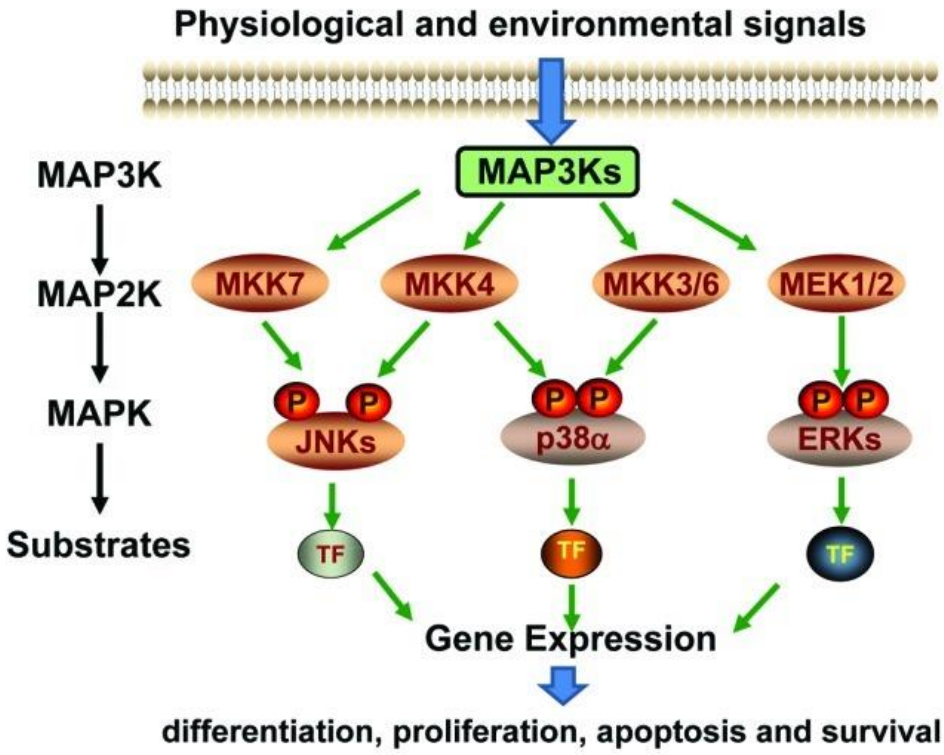

Figure 1.5 Schematic diagram of the MAPK signaling pathways

MAPK signaling contains three stress kinase groups, which are JNK, ERK1/2 and p38 MAPK, and they play important roles in cell differentiation, proliferation, apoptosis and cell survival (adapted from (Wang and Xia, 2012)).

1.3 Gammaherpesvirus prevalence and the association with chronic lung diseases (CLDs)

1.3.1 The prevalence of gammaherpesvirus infection in humans

Herpesviruses are highly prevalent in humans worldwide. According to epidemiological studies, more than 90% of human beings are seropositive for EBV (Tzellos and Farrell, 2012). The prevalence of KSHV differs in geographic regions (de Sanjose et al., 2009). Within adult populations, the seroprevalence is more than 50% in sub-Saharan Africa, 20% to 30% in the Mediterranean region and only 5% to 10% in Western and Northern Europe, Asia and the Americas (Labo et al., 2015).

1.3.2 The association of herpesvirus infection and CLDs

Studies have implied the important contribution of herpesvirus infection to the development of CLDs.

In the lungs of IPF patients, herpesvirus DNA has been detected, especially EBV, CMV and HHV-8 were significantly increased compared to controls, which suggested an potential link between herpesvirus infection and IPF (Tang et al., 2003). Similarly, Pulkkinen and colleagues also found more than 80% (11 out of 12) IPF patients lungs were EBV DNA positive whereas no controls were positive (Pulkkinen et al., 2012).

The attention has also been addressed on the association between EBV infection and the pathogenesis of COPD. A study assessed the presence of EBV DNA in sputum from 68 stable COPD patients and 136 exacerbation COPD patients compared to 16 non-obstructed smokers (McManus et al., 2008). Among them, only one control was EBV DNA positive but more than 40% of both stable and exacerbation COPD patients were EBV DNA positive. Thus, EBV infection is persistent during COPD, including disease exacerbation stage. According to another prospective cohort study, the presence of EBV DNA in sputum is corelating with bronchiectasis severity and exacerbations (Chen et al., 2020). Compared to controls, bronchiectasis patients exhibited a significant high detection rate of EBV DNA. Bronchiectasis patients with EBV DNA detected showed faster decline of lung function and shorter time to develop exacerbations. Thus, both studies demonstrated the association between EBV infection and the development of COPD.

In the murine model, MHV-68 infection enhanced bleomycin-induced fibrosis (Lok et al., 2002). Mice with both MHV-68 infection and bleomycin exposure exhibited more fibrosis when compared to those only MHV-68 infection or only exposed to bleomycin. MHV-68 and bleomycin together caused more collagen deposition and inflammation when compared to only bleomycin treated mice. Thus, MHV-68 promoted the development of fibrosis and contributed to an elevated level of fibrosis. In fluorescein isothiocyanate-induced pulmonary fibrosis, MHV-68 exacerbated fibrosis by increasing acute lung injury, collagen deposition in the lung and decreasing lung function (McMillan et al., 2008). Mechanistically, MHV-68 infection caused CCL2 and CCL12 chemokine production and subsequently

triggered fibrocyte recruitment, which potentially explained the augmentation of lung fibrosis.

1.4 Aim of the study

In a previous study, Sattler and colleagues in our group found that pulmonary exposure to CNP and DWCNT induced an increase of lytic virus protein expression in latently MHV-68 infected mouse lungs with a similar signature as acute infection, suggesting virus reactivation (Sattler et al., 2017). However, the cell types involved in reactivation and the underlying mechanisms were not yet resolved. Answering these questions would be very important for the identification of potential protective targets to interfere with ambient air pollution triggered virus reactivation and to finally prevent the development of related chronic lung diseases and their exacerbations.

Thus, in this thesis, we aimed to investigate the underlying mechanisms of NP-triggered MHV-68 reactivation, to identify the cell types involved in this process, and finally to inhibit and therapeutically target the responsible pathways.

For this purpose, we applied tissue optical clearing, light-sheet fluorescence microscopy and immunohistochemistry staining to identify the localization of virus reactivation induced by nanoparticle exposure.

Since MAPK signaling is involved in certain particle-cell interactions and plays important roles in herpesvirus infection and reactivation, we used a bone marrow derived macrophage *in vitro* model latently infected with MHV-68 (Ana-1/MHV-68 cells) to study the involvement of the MAPK signaling pathway in nanoparticle induced virus reactivation. Finally, we applied specific inhibitors to interfere with virus reactivation both *in vitro* and *in vivo*.

2. Material and Methods

2.1 Materials

2.1.1 Nanomaterials

Carbonaceous spherical nanoparticle (Carbon black, CNP, Printex 90; Degussa, Frankfurt, Germany), double-walled carbon nanotubes (DWCNT; NC2100; Nanocyl, Auvelais, Belgium) and MIN-U-SIL 5 (Silica; Berkeley, Springs, WV, US) were used in the project.

2.1.2 General Materials

Products	**Company**
Gloves	Kleenex Kimtech
Gloves	Nitril NextGen
Glass bottle & lid for NPs preparation	Carl Roth
Cell culture T75 flask	Greiner Bio-One
Cell pipette (10 µl, 20 µl, 100 µl, 1000 µl)	Eppendorf
Multi-pipette (100 µl, 300 µl)	Eppendorf
Tips (10 µl, 20 µl, 200 µl, 1000 µl)	Starlab
Tips with filters (10 µl, 20 µl, 200 µl, 1000 µl)	Biozol; Starlab
Pipette (5 ml, 10 ml, 25 ml, 50 ml)	Greiner Bio-One
Cell culture plate (6, 12, 24 & 96 well plate)	Greiner Bio-One
96-well plates for WST-1 & LDH assay	Greiner Bio-One
96-well plates for ELISA assay	Thermo Scientific
Black 96-well plates	Greiner Bio-One
Falcon tube (15 ml, 50 ml)	Corning Science
Microcentrifuge tube (1.5 ml, 2 ml)	Eppendorf
RNase-free microcentrifuge tube (0.5 ml, 1.5 ml)	Eppendorf
FACS tube (5 ml)	Eppendorf
70% Ethanol	Merck

2.1.3 Chemicals and reagents

(1) Commercial chemicals and reagents for NPs preparation and cell culture

Reagents and chemicals	Company	Product No.
Ultrapure water	Invitrogen	10977-049
Dulbecco's phosphate-buffered saline (DBPS)	Gibco	14190-094
RPMI medium 1640	Gibco	11835-063
Glasgow-MEM medium	PAN Biotech	P04-96500
L-Glutamine, 200mM (100x)	Gibco	25030-024
Non-essential amino acid (NEAA)	Gibco	11140-035
Fetal bovine serum (FBS)	Sigma	0001636679
Penicillin Streptomycin	Gibco	15140-122
0.25% Trypsin EDTA (1x)	Gibco	25200-114
Tryptose phosphate broth	Gibco	18050-039
0.4% Trypan Blue	Gibco	15250-061
Hygromycin B	Invitrogen	10687-010
Methyl cellulose	Merck	M0512

(2) Cell culture medium

Ana-1 cell line (Cox et al., 1989, Blasi et al., 1985) was cultured in RPMI 1640 medium supplemented with 15% FBS, 1% NEAA, 2 mM L-glutamine, 100 U/ml Penicillin and 100 µg/ml Streptomycin. Persistently MHV-68 latent infected Ana-1 cells (Ana-1/MHV-68 cells) were cultured in RPMI 1640 medium supplemented with 10% FBS, 2 mM L-glutamine, 100 U/ml Penicillin, 100 µg/ml Streptomycin and 5 µg/ml Hygromycin. BHK-21 cells (ATCC: CCL-10) were grown in Glasgow-MEM medium supplemented with 5% FBS, 5% tryptose phosphate broth, 2 mM L-glutamine, 100 U/mL Penicillin and 100 µg/mL Streptomycin. The overlay medium for plaque assay is prepared by dissolving sterile Methyl cellulose in BHK-21 culture medium.

(3) Reagents for WST-1 & LDH assay

Product	Product No.	Company

Cell proliferation Reagent WST-1	11644807001	Roche Diagnostics, Mannheim, Germany
Cytotoxicity Detection Kit (LDH)	11644793001	Roche Diagnostics, Mannheim, Germany

(4) Reagents for flow cytometry

FACS buffer: PBS containing 0.1% FBS

(5) Reagents for Western blot

Products	**Product No.**	**Company**
Sodium chloride (NaCl)	1.06404.1000	Merck KGaA, Darmstadt, Germany
Tris powder	4855.5	Carl Roth, Karlsruhe, Germany
10% SDS solution	A0676, 1000	AppliChem, Darmstadt, Germany
Triton X-100	A16046-AE	Thermo Fisher Scientific, Rockford, USA
Deoxycholate	D-6750	Merck KGaA, Darmstadt, Germany
Ethylenediaminetetraacetic acid (EDTA)	E9884	Merck KGaA, Darmstadt, Germany
10x Dulbecco's Phosphate Buffered Saline	56064C	SAFC Biosciences, Andover, UK
Tween® 20	1131K	MP Biomedicals, Eschwege, Germany
Glycine	3908.2	Carl Roth, Karlsruhe, Germany
β-Mercaptoethanol (β-ME)	63689	Merck KGaA, Darmstadt, Germany
Roti-Block	A151.1	Carl Roth, Karlsruhe, Germany
Protease and phosphatase inhibitor cocktail (100x)	78440	Thermo Fisher Scientific, Rockford, USA
BCA protein Assay Kit	23225	Thermo Fisher Scientific, Rockford, USA
Rotiphorese Gel 30%	3029.1	Carl Roth, Karlsruhe, Germany
Tetramethylethylenediamine (TEMED)	161-0801	Bio-Rad Laboratories, Hercules, California, USA
PVDF Transfer Membrane	88520;	Thermo Fisher Scientific, Rockford, USA
Ammonium persulphate	A7460-100G	Merck KGaA, Darmstadt, Germany

4x Laemmli buffer	161-0747	Bio-Rad Laboratories, Hercules, California, USA
Western Blot Stripping Buffer	46430	Thermo Fisher Scientific, Rockford, USA
ECL Western Blotting Detection Reagents	RPN2209	GE Healthcare, UK
SuperSignal West Femto Maximum Sensitivity Substrate	34095	Thermo Fisher Scientific, Rockford, USA

(6) Reagents for ROS detection

Products	**Product No.**	**Company**
2′,7′-Dichlorofluorescin diacetate (DCFH-DA)	D6883	Merck KGaA, Darmstadt, Germany
Dimethyl Sulfoxide (DMSO)	D4540	Merck KGaA, Darmstadt, Germany
30% hydrogen peroxide solution (H_2O_2)	1.07209.500	Merck KGaA, Darmstadt, Germany
N-acetylcysteine amide (NACA)	A0737	Merck KGaA, Darmstadt, Germany

(7) Reagents for RNA isolation, cDNA synthesis and qPCR

1) RNA isolation kit

NucleoSpin RNA Plus kit (740984.250) was purchased from MACHEREY-NAGEL.

2) cDNA synthesis reagents includes:

Reagents	**Company**
RNase-free H_2O without DEPC	Invitrogen, Waltham, MA, USA
Random Nonamers 0.1 mM	Sigma
5 x First Strand Buffer	Invitrogen, Waltham, MA, USA
10 x DTT 0.1 M	Invitrogen, Waltham, MA, USA
dNTP mix, 10 mM	Thermo Scientific, Vilnius, Lithuania
RNase-out 40 U/µl	Invitrogen, Waltham, MA, USA
Superscript II RT 200 U/µl	Invitrogen, Waltham, MA, USA

3) Reagents for qPCR includes:

Products	**Product No.**	**Company**
SybrGreen Master mix	04887352001	Roche Diagnostics, Mannheim, Germany
LightCycler® 480 Multiwell Plate 96	04729692001	Roche Diagnostics, Mannheim, Germany
Optically clear adhesive seal sheets	AB-1170	Thermo Fisher Scientific, Rockford, USA

4) Primer pairs (100 μM)

Gene name	**Forward primer (5'-3')**	**Reverse primer (5'-3')**
MHV-68 ORF50	GGAATTTCTCAGCGATGGCCTCT	CCTCTTTTGTTTCAGCAGAGACTCCA
MHV-68 ORF73	CTGGACTCCTCATCACCTT	TGTCTGAGCGTCTTCCAC
L8	CAGTGAATATCGGCAATGTTTTG	TTCACTCGAGTCTTCTTGGTCTC
HO-1	TTCTGGTATGGGCCTCACTGG	ACCTCGTGGAGACGCTTTACA
COX-2	CAACACCTGAGCGGTTAC	GTTCCAGGAGGATGGAGT
IL-1β	CAACCAACAAGTGTATTCTCCATG	GATCCACACTCTCCAGCTGCA
IL6	TAGTCCTTCCTACCCCAATTTCC	TTGGTCCTTAGCCACTCCTTC
TNF-a	CACCACGCTCTTCTGTCT	GGCTACAGGCTTGTCACTC
SAA3	GAAGCTGGTCAAGGGTCT	GTCAGCTCTTGAGTCCTCTG
NOS2	CCTGTGAGACCTTTGATG	CCTATATTGCTGTGGCTC
β-actin	TCCATCATGAAGTGTGACGT	GAGCAATGATCTTGATCTTCAT
HPRT	GTTGGATACAGGCCAGACTTTGT	CACAGGACTAGAACACCTGC

(8) Materials and reagents for BAL cells cytospin, IF staining & IHC staining

Reagents	**Product No.**	**Company**
4% Paraformaldehyde Solution	J19943	Thermo Fisher Scientific, Rockford, USA

Ammoniumchlorid	101145	Merck KGaA, Darmstadt, Germany
Bovine serum albumin	A2153	Merck KGaA, Darmstadt, Germany
Superfrost Plus Adhesion Microscope Slides	J1810AMNZ	Gerhard Menzel, Braunschweig, Germany
Xylene	CN 80.2	Carl Roth, Karlsruhe, Germany
Ethanol	1.06009	Merck KGaA, Darmstadt, Germany
Entellan mounting solution	1.07961	Merck KGaA, Darmstadt, Germany
HIER Citrate Buffer pH 6.0	ZUC028-500	Zytomed Systems, Berlin, Germany
HIER T-EDTA Buffer pH 9.0	ZUC029-500	Zytomed Systems, Berlin, Germany
Rodent Block M	RBM961	Biocare Medical, CA, USA
Vulcan Fast Red Chromogen kit2	FR805S	Biocare Medical, CA, USA
Rabbit on Rodent AP-Polymer	RMR625H	Biocare Medical, CA, USA
20 x TBS buffer	ZUC066-500	Zytomed Systems, Berlin, Germany
30% Hydrogen peroxide (H_2O_2)	1.07209	Merck KGaA, Darmstadt, Germany
Methanol	1.06009	Merck KGaA, Darmstadt, Germany
Hematoxylin solution	GHS232	Merck KGaA, Darmstadt, Germany
Normal goat serum	5425S	Cell Signaling Technology, Leiden, The Netherlands
Normal rabbit serum	10510	Invitrogen, Waltham, MA, USA
Goat Fab anti-Rabbit IgG (H+L)	111-007-003	Jackson ImmunoResearch, Ely, UK
Dako fluorescence mounting medium	S3023	Agilent Technologies, Glostrup, Denmark

(9) Materials and reagents for Light-sheet fluorescence microscopy (LSFM)

Reagents	**Product No.**	**Company**
Gelatin	24350.262	VWR, Milano, Italy
Saponin	47036	Merck KGaA, Darmstadt, Germany
Thimerosal	T8784	Merck KGaA, Darmstadt, Germany
Tetrahydrofuran (THF)	186562	Merck KGaA, Darmstadt, Germany

Dichloromethane (DCM)	270997	Merck KGaA, Darmstadt, Germany
Benzyl ether (DBE)	108014	Merck KGaA, Darmstadt, Germany

2.1.4 Equipment

Equipment	**Company**
Fine weight balance	Mettler-Toledo, Giessen, Germany
Weight balance	Sartorius, Goettingen, Germany
Sonication water bath	Bandelin, Berlin, Germany
Bioruptor Probe sonication	Diagenode SA, Seraing, Belgium
Ice machine	Buchner Labortechnik, Pfaffenhofen, Germany
Water bath	Lauda, Koenigshofen, Germany
Centrifugation	Eppendorf, Hamburg, Germany
Light microscope	ZEISS
Cell incubator	Thermo Fisher Scientific, Rockford, USA
Ventilation hood	Thermo Fisher Scientific, Rockford, USA
Tecan Reader	Tecan, Maennedorf, Switzerland
Fluorescent Tecan Reader	Tecan, Maennedorf, Switzerland
Shaker	Coulter Electronics, Luton, UK
Thermo Cycler	Eppendorf, Hamburg, Germany
Vortex mixer	Scientific Industries, Karlsruhe, Germany
Western blot system	Bio-Rad Laboratories, Hercules, California, USA
Western blot bands detection machine	Bio-Rad Laboratories, Hercules, California, USA
NanoDrop® ND-1000 spectrophotometer	Thermo Fisher Scientific, Rockford, USA
Light Cycler 480	Roche, Grenzach, Germany
BD FACSCanto™ II Flow Cytometer	BD Biosciences, San Jose, CA, USA
Olympus fluorescent microscope	Olympus, Japan

Shandon Cytospin3 cytocentrifuge	Shandon, PA
Decloaking chamber	Biocare Medical, CA, USA
Autoclave machine	Systec, Linden, Germany
Mirax Desk scanner	ZEISS

2.1.5 Animals

C57BL/6 mice used in the project were obtained from Charles River Laboratories (Sulzfeld, Germany). Later they were housed in individually ventilated cages (IVC).

2.1.6 Antibodies and related reagents

1. Polyclonal rabbit antiserum against MHV-68 lytic protein was used to label lytic virus proteins, which was described before (Steer et al., 2010).

2. Commercial antibodies

Antibody	**Company**	**Product No.**
Cleaved Caspase-3	Cell Signaling Technology	#9664
CD11b	Abcam	ab133357
CD11c	Cell Signaling Technology	#97585
p-p38 (Thr180/Tyr182)	Cell Signaling Technology	#4511
p38α/β	Santa Cruz Biotechnology	sc-7972
p-ERK1/2 (Thr202/Tyr204)	Cell Signaling Technology	#4370
p-MAPKAPK2 (Thr334)	Cell Signaling Technology	#3007
MAPKAPK2	Cell Signaling Technology	#3042
ERK1/2	Cell Signaling Technology	#4695
p-JNK (Thr183/Tyr185)	Cell Signaling Technology	#4668
JNK	Santa Cruz Biotechnology	sc-7345
p-c-Jun	Cell Signaling Technology	#9261
c-Jun	Cell Signaling Technology	#9165
β-actin	Sigma Aldrich	A3854

Anti-rabbit IgG	Cell Signaling Technology	#7074
Anti-mouse IgG	GE Healthcare	RPN4201

3. Fluorescence-labeled secondary antibody, DAPI and Phalloidin

Antibody	**Company**	**Product No.**
Goat anti-rabbit IgG (H+L), 488	Invitrogen	A11008
Goat anti-rabbit IgG (H+L), 555	Invitrogen	A21428
Goat anti-rabbit IgG (H+L), 647	Invitrogen	A21245
DAPI	Sigma Aldrich	D9564
Alexa Fluor 488 Phalloidin	Thermo Fisher scientific	A12379

4. Flow cytometry antibodies

Antibody	**Company**	**Product No.**
CD11b anti-human/mouse, PE	Miltenyi Biotech	130-113-235
CD11c anti-human/mouse, FITC	Miltenyi Biotech	130-110-837

2.2 Methods

2.2.1 Nanoparticles (NPs) preparation and treatment

3.0 mg CNP or DWCNT were weighted and dispersed with 3.0 ml ultrapure H_2O in a sterile glass tube to get a 1 mg/ml stock solution. 12 mg Silica was weighted and dispersed with 3 ml ultrapure H_2O in a sterile glass tube to get a 4 mg/ml stock solution. NPs dispersion was sonicated in an ice-cold water bath for 5 min followed by 30 seconds Bioruptor probe sonication (Diagenode, Liege, Belgium) at 30% power and continuous mode. NPs stock solution was vortex again before use.

For *in vitro* experiments, 50 µl NPs stock solution was diluted in 950 µl cell culture medium to reach a 50 µg/ml working concentration. To analyze the effect of NPs on Ana-1/MHV-68 cells, cells were exposed to 50 µg/ml CNP or DWCNT in culture medium. For immunofluorescence staining experiment, cells were seeded on cover slides in a 24-well plate and harvested after 24 h. ROS production was detected directly after treatment till 1 h. After 1 h NPs exposure, cells were

harvested and whole cell protein were extracted to investigated MAPK signaling. After 3 and 9 h, cells were harvested for RNA isolation followed by microarray analysis. After 24 h, cells were harvested for isolating RNA followed by performing qPCR. After 72 h, supernatant was collected for virus titer analysis by plaque assay.

For *in vivo* experiments, mice were instilled with 50 µg CNP, 0.1 µg LPS or equal amount sterile H_2O as sham control per mouse.

2.2.2 Cell culture

(1) Warm culture medium, DPBS and 0.25% Trypsin-EDTA in 37 °C for 30 min, bring them to proper temperature before start.

(2) Discard old supernatant by sucking with Pasteur pipette to a 50 ml Falcon tube. Rinse cells with 20 ml DPBS, shake the flask slightly and discard DPBS.

(3) Add 2 ml 0.25% Trypsin-EDTA, shake slightly and cover all the cells. Leave the flask in 37 °C incubator for 4 min till cells become roundish and detached from flask and form a white film.

(4) Add 18 ml medium to stop the reaction and mix them inside the flask. Transfer them into a 50 ml Falcon centrifuge tube and centrifuge 5 min at 1400 rpm.

(5) Afterwards, remove supernatant and resuspend cells with 5 ml fresh culture medium. Mix 10 µl suspension with 190 µl 0.2% Trypan blue solution, and calculate the cell number with bauer chamber under the light microscope.

(6) Inoculate $0.5*10^6$ cells for 20 ml medium per flask. Cells are split twice a week.

2.2.3 Cell viability assay (WST-1 assay)

(1) Seed cells in a 96-well plate at a density of 10,000 cells per well in 200 µl medium and add 200 µl PBS in samples surrounding wells. Seed blank wells with equal amount of medium without cells. Incubate at 37 °C for 24 h.

(2) Remove old medium and treat cells with 50 µg/ml CNP, 50 µg/ml DWCNT and 1 µg/ml LPS at final volume of 100 µl each well, incubate for 24 h.

(3) Take WST-1 reagent to RT before use. After 24 h of NPs exposure, add 10 µl of reagent to each well (including blank wells). Protect plate from light. Slightly

shake plate thoroughly for 1 minute to mix wells and incubate in 37 °C incubator for 1 h.

(4) After 1 h, take the supernatant to microcentrifuge tubes and centrifuge for 10 min at 14,000 rpm.

(5) Take 80 µl supernatant to a new plate and measure the absorbance of sample using a Tecan reader at wavelength of 440 nm.

(6) Subtract Optical Density (OD) value of blank from that of each of the samples. Normalize the viability to control and set control as 100% cell viability.

2.2.4 Cytotoxicity assay (LDH assay)

(1) Seed Ana-1 cells in a 24-well plate at a density of 100,000 cells each well in 1 ml full medium. Incubate at 37 °C for 24 h.

(2) Remove old medium and treat cells with 50 µg/ml CNP, 50 µg/ml DWCNT and 1 µg/ml LPS at final volume of 1 ml each well. Keep one well without treatment for high control preparation. Incubate plate for 24 h.

(3) After 24 h, take out supernatant to 1.5 ml microcentrifuge tubes. Take out medium from high control well and add 1 ml medium with 1% Triton X-100, lyse cells for 5 min. Transfer the 1 ml lysate to a microcentrifuge tube and centrifuge for 10 min at 14,000 rpm. Take supernatant without pellet to fresh tubes and keep them on ice or 4 °C for the following experiment.

(4) Set controls for the assay in a new 96-well plate

Add 100 µl medium without FBS into well as background control; add 95 µl medium without FBS and 5 µl lysate as high control.

(5) Add 70 µl medium without FBS to samples well and 30 µl sample supernatant.

(6) Prepare LDH working solution

Take catalyst bottle from -20 °C and reconstitute the lyophilisate in 1 ml ultrapure H_2O for 10 minutes. Mix thoroughly. Freshly prepare working solution by diluting catalyst 1:45 in dye solution. Avoid from light.

(7) Add 100 µl of working solution into each well and incubate for 15 min at RT. Protect from light.

(8) Add 50 µl stop solution and shake the plate for 10 s and immediately measure the absorbance of samples at wavelength of 492 nm.

(9) To determine the percentage cytotoxicity, subtract the OD value of background control from each sample, and calculate the average absorbance values of triplicates, the result is shown:

Cytotoxicity% = Sample average OD/(High control - background control)*100

2.2.5 Flow cytometry

(1) Cell preparation

Ana-1 cells were collected after cultivation and centrifuged at 400 g for 5 min to get a pellet. Then the pellet was washed with FACS buffer and centrifuged at 300 g for 10 min at 4 °C. Then the pellet was resuspended in a density of $10*10^6$ cells/ml in FACS buffer and transfer to FACS tubes.

(2) Antibody incubation

Cells were incubated with CD11b-PE, CD11c-FITC antibody (1:50 dilution) on ice for 15 min, protect cells from light. Afterwards, cells were washed with 1 ml FACS buffer and spun down at 300 g for 5 min at 4 °C. The supernatant was discard and cells were resuspended with 200 µl FACS buffer. Cells were ready for flow cytometry analysis.

(3) Flow cytometry analysis

Cells were acquired by FACScanto™ II flow cytometer and analyzed by FlowJo software (BD Biosciences, San Jose, CA, USA). Mean fluorescence Index (MFI) was used to show the intensity of CD11b or CD11c expression of the cells.

2.2.6 Western blot

(1) RIPA buffer preparation

	Final concentration	Stock concentration	Amount
NaCl	150 mM		0.877 g
Tris pH 7.2	10 mM	1000 mM	1 ml
SDS	0.1%	10%	1 ml
Triton X-100	1%	100%	1 ml

Deoxycholate	1%		1 g
EDTA	5 mM	500 mM	1 ml
ddH_2O			Fill up to 100 ml

(2) Wash buffer (PBST buffer)

Dissolve 10 x DPBS dry powder in 1 liter distilled water and sterile to get a 10 x DPBS stock solution. Dilute stock solution and add 0.1% Tween-20 to get PBST as washing buffer.

(3) Electrophoresis Buffer/Running Buffer (5 x Stock)

Take 15.1 g Tris powder, 94 g Glycine powder and 50 ml 10% SDS solution. Fill up to 1 liter with distilled water (dH_2O) to get a 5 x stock solution. Dilute stock solution with dH_2O to get 1x working solution.

(4) Transfer Buffer (10 x Stock)

Take 24.2 g Tris powder and 112 g Glycine powder. Fill up to 1 liter with dH_2O to get a 10 x stock solution. Dilute stock solution with dH_2O and add 200 ml methanol to get 1 l 1x working solution.

(5) 1.5M Tris-HCl & 0.5M Tris-HCl buffer

Take 90.855 g Tris powder and dissolve in 500 ml distilled water. Adjust pH to get 1.5M Tris-HCl buffer (pH = 8.8); Take 60.57 g Tris powder and dissolve in 500 ml distilled water. Adjust pH to get 0.5M Tris-HCl buffer (pH = 6.8).

(6) Laemmlin buffer

Mix 1 part of β-Mercaptoethanol and 9 part of 4x Laemmli buffer to get a 1 x working concentration of Laemmli buffer. For protein samples denaturation, dilute 3 part of protein sample with 1 part of Laemmli working buffer.

(7) Protein extraction

1) After NPs treatment, place the culture plate on ice, remove culture medium and wash cells with ice-cold PBS for 3 times. Aspirate PBS in the last wash step.

2) To prepare lysis buffer, add 10x protease and phosphatase inhibitor cocktail to RIPA buffer at 10 µl/ml. Mix thoroughly and add lysis buffer into each well. Remove cell lysate with cell scraper and transfer to a microcentrifuge tube. Leave lysate on ice for 15 min and vortex several times in between.

3) Set centrifugation machine to 4 °C before use. Load microcentrifuge tubes with cell lysate and remove cell debris by centrifugation at 14,000 rpm for 15 min.

4) Transfer the supernatant to a new microcentrifuge tube, keep them on ice for the following experiments.

(8) Protein concentration determination (BCA assay)

1) Prepare BSA standard by diluting Albumin stocks (2 mg/ml) to 0.5 mg/ml stock solution and make series dilutions as shown below:

Working solution (mg/ml)	0	0.025	0.05	0.1	0.2	0.3	0.4	0.5
Stock solution (µl)	0	4	8	16	32	48	64	80
PBS (µl)	80	76	72	64	48	32	16	0
Final volume (µl)	80	80	80	80	80	80	80	80

2) Add 20 µl of standard series dilution into 96-well plate. Add 2 µl protein samples and 18 µl PBS to have an equal volume of 20 µl. Always make triplicates for standard and samples.

3) Prepare BCA working solution by diluting Reagent A and Reagent B in 50:1. Add 200 µl working solution to each well and mix the plate thoroughly.

4) Incubate the plate in 37 °C incubator for 30 min. Measure absorbance at a wavelength of 562 nm. Determine the samples protein concentration.

(9) Gel & protein samples preparation

1) Constitution of glass plate

Take one thin and one thick glass plate and constitute them as the manufacture instruction.

2) Separating gel preparation

Separating gel (for 2 chambers 1.5mm)						
Gel concentration	7.5%	10%	12%	13%	14%	15%
H_2O	8.1ml	6.7ml	5.6ml	5.1ml	4.5ml	4.0ml
1.5M Tris-HCl	4.2ml	4.2ml	4.2ml	4.2ml	4.2ml	4.2ml
Acrylamid 30%	3.9ml	5.5ml	6.6ml	7.2ml	7.7ml	8.3ml
SDS 10%	165µl	165µl	165µl	165µl	165µl	165µl

TEMED	22µl	22µl	22µl	22µl	22µl	22µl
APS 25%	22µl	22µl	22µl	22µl	22µl	22µl

Add each reagent to a 50 ml Falcon tube, mix thoroughly and refill into the glass plate. After the refilling, add proper amount of ultrapure water to remove bubble between two glass plates. Allow the polymerization in RT for at least 45 to 60 min.

3) Stacking gel preparation

5% Stacking gel (for 2 chambers)		
Comb	1.5mm	0.75mm
H_2O	5.8 ml	1.95 ml
0.5M Tris-HCl	2.5 ml	0.63 ml
Acrylamid 30%	1.7 ml	0.43 ml
SDS 10%	100 µl	25 µl
TEMED	20 µl	5 µl
APS 25%	20 µl	5 µl

Add each reagent to a 50 ml Falcon tube, mix thoroughly and refill into the glass plate fully to avoid air bubble formation. Carefully insert the comb. Allow the gel polymerization in RT for at least 20 min.

4) Protein sample preparation for electrophoresis

a. After protein concentration determination, normalize all samples to the same concentration by diluting with PBS.

b. Take proper amount of protein samples, and dilute 3 part of sample with 1 part Laemmli working solution. Mix sample thoroughly.

c. Heat samples at 95 °C for 10 min. Keep samples on ice before loading into gel.

(10) Western blot

1) Protein samples loading into gel

After gel polymerization, constitute 2 gels and load 1x Running buffer in between. Remove the comb, remove debris of gel with pipette. Load equal amount of protein samples into gel well, add 6.5 µl and 2.5 µl Precision Plus Protein Western C Standard outside of protein samples.

2) Running gel

Run gels at 100 V for 10 min for stacking gel and then switch to 120 V, run 1 h for separating gel.

3) Blotting

a. Soak four black sponges and filter papers in transfer buffer. Soak PVDF membrane in methanol for 1 min for activation. Move PVDF membrane to transfer buffer.

b. After gel running, separate glass plates, cut gels and move to transfer buffer.

c. Make “sandwich” with a structure of (from bottom to top): Black holder, black sponges, filter paper, gel, membrane, filter paper, black sponges, white holder.

d. Constitute two “sandwich” as well as a cooling battery in the chamber. Start blotting with 100 V for at least 1 h, blotting time depends on different protein sizes.

4) Blocking

a. After blotting, take out the membrane and rinse in PBST solution for 1 min.

b. Prepare blocking solution by diluting 10 x Roti Block to 1x working solution with ultrapure water. Mix thoroughly.

c. Add 20 ml blocking solution and incubate membrane for 1 h at RT.

5) Primary antibodies incubation

Dilute primary antibodies to indicated concentration with blocking solution. Incubate membrane at 4 °C overnight.

6) Secondary antibody incubation

a. Wash membrane with PBST for 3 times, 10 min each.

b. Prepare proper secondary antibody in blocking solution. Incubate membrane at RT for 1 h.

7) Band detection

a. After incubation, wash membrane with PBST for 3 time, 5 min each.

b. Prepare detection solution by diluting ECL Prime Western Blotting Detection Reagent A and B in 1:1 ratio. Mix thoroughly. For weak antibodies, use super signal detection reagents.

c. Cover membrane with detection solution and incubate for 3 min at RT.

d. Place membrane into Bio-Rad detection machine and select program “Blot-Chemi” for band detection. Set proper exposure time. Use program “Blot-Chemi-High resolution” when applying super signal detection reagents.

e. Analyze the bands intensity and save images.

8) Membrane stripping and β-actin incubation

a. After targeted bands detection, wash blots to remove chemiluminescent substrate. Add 15 ml stripping buffer for each membrane and incubate for 13 min at RT. Discard stripping buffer, wash membrane with PBST for 3 times, 5 min each.

b. Block membrane again with blocking solution for 1 h at RT. Incubate with β-actin as loading control for 1 h at RT.

c. Wash again and repeat step “7)” to detect band.

2.2.7 RNA isolation, concentration determination & quantitative polymerase chain reaction (qPCR)

(1) RNA isolation from cells

Protocol was modified from: https://www.mn-net.com/de/nucleospin-rna-plus-mini-kit-for-rna-purification-with-dna-removal-column-740984.50?number=)

1) Homogenize and lyse sample

Seed cells in a 24-well plate and incubate for 24 h. After 24 h, remove the medium and treat cells with indicated treatments. After proper treatment time, transfer cell supernatant to a 1.5 ml microcentrifuge tube, add 350 µl lysis buffer (LBP) to each well, lyse cells for 10 min at RT. Centrifuge tube with supernatant at 6,000 rpm for 10 min. Transfer supernatant to a new microcentrifuge tube without disturbing the pellet. Mix the pellet with lysis buffer in each well.

2) Remove gDNA and filtrate lysate

After 10 min, place gDNA Removal Column in a Collection tube, add the homogenized cell lysate to the Column, centrifuge for 60 s at 11,000 g. Discard the Column and keep the flowthrough for the next step.

3) Adjust RNA binding condition

Add 100 µl Binding Solution (BS) to the flowthrough, mix the flowthrough by pipetting up and down several times.

4) Bind RNA

Transfer the whole lysate to the RNA Plus Column. Centrifuge for 60 s at 11,000 g.

5) Wash and dry silica membrane

1st time wash

After centrifuge, add 200 µl Wash buffer 1 (WB1) to each RNA Plus Column, centrifuge for 60 s at 11,000 x g. Discard the flowthrough.

2nd time wash

Add 600 µl Wash buffer 2 (WB2) to each RNA Plus Column, centrifuge for 60 s at 11,000 g. Discard the flowthrough.

3rd time wash

Add 250 µl WB2 to each RNA Plus Column, centrifuge for 120 s at 11,000 g to dry the membrane completely. Discard the flowthrough.

6) Elute RNA

Add 30 µl RNase-free H_2O and centrifuge for 60 s at 11,000 g. Again, add 30 µl RNase-free H_2O and centrifuge for 60 s at 11,000 g. The RNA is ready to measure the concentration.

(2) RNA concentration determination

Keep RNA samples as well as RNase-free H_2O on ice before determination with Nanodrop Spectrophotometers. Briefly, clean sample reader with KimWipe paper. Start the software “Nanodrop-ND” and turn to nuclei acid measurement. Load 1 µl RNase-free H_2O to initialize the system. After initialization, change measurement setting to RNA and click “blank”. Now the system is ready to measure RNA concentration. Remove H_2O on reader, load 1 µl RNA samples and click measure button. After reading is completed, record the concentration (ng/µl), A260/A280 as well as A260/A230 ratios. Wipe the reader with KimWipe and repeat measurement for all the RNA samples. A proper concentration and A260/A280 as well as A260/A230 ratios between 1.8 and 2.0 are required for the following experiments.

(3) cDNA synthesis

Pipette maximum of 1 µg total RNA in a PCR-clean tube, fill up to 10 µl with RNase-free H_2O if required. Add 1µl 0.1 mM Random Nonamers to each tube, mix thoroughly and centrifuge. Load samples to Thermo Cycler machine and select “denaturation” program with incubation at 70 °C for 5 min. Keep samples on ice for 5 min and then transfer to RT for 5 to 10 min.

In between, prepare Master Mix for cDNA synthesis:

Reagents	**Volume (for one sample)**
5x First Strand Buffer	4 µl
10x DTT (0.1 M)	2 µl
Superscript II RT (200 U/µl)	1 µl
RNase Inhibitor (40 U/µl)	1 µl
20x 4dNTP mix (10 mM)	1 µl
In total	9 µl

Add 9 µl Master Mix to each sample, mix thoroughly and centrifuge. Place samples in Thermo Cycler and start “cDNA synthesis” program. Samples are incubated at 42 °C for 1 h followed with incubation at 70 °C for 15 min. After incubation, centrifugate samples and dilute the 20 µl 1:5 with RNase-free H_2O to get a final 100 µl volume. cDNA samples can be stored in -20 °C.

(5) qPCR and data analysis

1) Thaw cDNA samples, RNase-free H_2O, primer pairs (100 µM) and SybrGreen Master Mix and keep on ice before use.

2) Prepare primer mix by diluting forward and reverse primer pair with RNase-free H_2O to reach a final 10 µM concentration. The primer mix is ready to use.

3) The constitution of Master mix for one gene in each well is:

Reagents	**Volume (µl)**
RNase-free H_2O	2.4
SybrGreen Master mix (2 x concentration)	5.0
Primer mix	0.6

In total	8.0

4) Prepare proper amount of Master Mix for each gene. For one gene, make replicates for every sample.

5) Add 8.0 µl Master Mix into each well. Load 2 µl cDNA samples to reach a final 10 µl in each well. For each gene, internal calibrator is also set and 2 µl mix of random cDNA belonging to the same set was loaded. No template control (NTC) is always included to load 2 µl RNase-free H_2O instead of cDNA samples.

6) Cover plates with transparent sealing tightly. Centrifuge the plate at 1,500 rpm for 2 min at RT. Protect plate from light.

7) Place the plate into Light Cycler 480 machine and run with the following setting:

initial enzyme activation (one cycle at 50°C for 2 min and 95 °C for 15 min), 40 cycles amplification (95 °C for 15 s, 60 °C for 1 min).

8) The fold change in expression was shown as $2^{-\Delta\Delta Ct}$, where $\Delta Ct = Ct_{\text{target gene}} - Ct_{\text{housekeeping gene}}$, and $\Delta\Delta Ct$ reflects ΔCt of each treatment normalized to control. Thus, the mean value for control was 1 and value for treatment was shown as the fold change compared to control. Results of three independent experiments were shown.

2.2.8 Transcriptomic study with Microarray and GSEA analysis

(1) Total RNA isolation

See RNA isolation (2.2.7).

(2) Microarray analysis

RNA quality was assessed with the Agilent 2100 Bioanalyzer and only high quality RNA (RNA integrity number; RIN > 7) was used for microarray analysis. Total RNA was amplified using the GeneChip WT PLUS Reagent Kit (Thermo Fisher Scientific, Waltham, USA). Amplified cDNA was hybridized on Mouse Clariom S arrays (Thermo Fisher Scientific, Waltham, USA). Staining and scanning (GeneChip Scanner 3000 7G; Thermo Fisher Scientific, Waltham, USA) was done according to manufacturer's instructions.

The Transcriptome Analysis Console (TAC; version 4.0.1.36; Thermo Fisher Scientific, Waltham, USA) was used for quality control and to obtain annotated normalized SST-RMA gene-level data.

Statistical analysis were performed using R (v4.0.4). Genewise testing for differential expression was performed by the limma t-test and regulated gene sets were defined by raw $P < 0.05$ or by using the Benjamini-Hochberg multiple testing correction (FDR < 10%). To reduce background, gene sets were filtered using DABG $P < 0.05$ in more than half of the samples in at least one group per comparison. PCAs were done in R. Pathway analysis were generated using QIAGEN's Ingenuity Pathway Analysis (IPA®, QIAGEN Redwood City, www.qiagen.com/ingenuity) by Fisher's Exact Test p-values.

(3) Bioinformatic analysis

Gene set enrichment analysis (GESA) was performed by GSEA_4.1.0 software (Broad Institute, Cambridge, MA, USA). Heatmaps were generated with R software (version 4.0.4; pheatmap package).

2.2.9 Reactive oxygen species (ROS) detection

Principle

2′,7′-Dichlorofluorescin diacetate (DCFH-DA) dye was used to detect intracellular ROS level. 2′,7′-Dichlorofluorescin diacetate is a cell-permeable non-fluorescent probe. Upon oxidation, the probe is de-esterified intracellularly and turns to highly fluorescent 2′,7′-dichlorofluorescein. The fluorescent intensity reflects intracellular level.

Procedure

(1) Add 2.052 ml DMSO to 50 mg 2',7'-Dichlorofluorescin diacetate powder, mix thoroughly to make 50 mM stock solution. Aliquot 10 µl/vial and store in -20 °C.

(2) Seed cells into 96-well plate at a density of 10,000 cells/well in 200 µl medium. Incubate in 37 °C incubator for 24 h.

(3) After 24 h, prepare DCFH-DA working solution by diluting in culture medium to get a final concentration of 30 µM. Remove old medium in each well, add 50 µl medium with DCFH-DA to each well and incubate at 37 °C incubator for 30 min. To investigate the effect of ROS scavenger (N-acetylcysteine amide, NACA)

on ROS production, 5 mM NACA was added together with DCFH-DA and incubate for 30 min.

(4) After 30 min, cells were challenged with CNP (50 µg/ml), DWCNT (50 µg/ml) or H_2O_2 (10 mM). Immediately after treatment, measure the fluorescence intensity with excitation and emission at 485 nm and 535 nm, respectively. Set this intensity as baseline. Measure fluorescence again at 10, 30 & 60 min after treatment.

2.2.10 Virus titer determination - Plaque assay

Plaque assay was performed in BHK-21 cells treated with supernatant collected from NPs or LPS exposed Ana-1/MHV-68 cells after 72 h.

(1) Baby Hamster Kidney Fibroblasts (BHK-21 cells) cultivation

BHK-21 cells were grown in Glasgow-MEM supplemented with 5% FBS, 5% tryptose phosphate broth, 2 mM L-glutamine, 100 U/mL Penicillin and 100 µg/mL Streptomycin.

(2) Seed BHK-21 cells in 24-well plates and culture in 37 °C for 24 h.

(3) Series dilution for virus titer determination

1) Prepare 5 ml tubes for series dilution, take 6 tubes for each Ana-1/MHV-68 cells supernatant sample, add 900 µl medium into each tube.

2) Thaw NPs or LPS treated Ana-1/MHV-68 cells supernatant from -80 °C, vortex thoroughly. Take 100 µl supernatant and add to the first tube with 900 µl medium, vortex thoroughly. Take 100 µl solution from the first tube to the second tube with 900 µl medium, vortex thoroughly. Continue the series dilution till the sixth tube, which contains 1000 µl solution in total, vortex thoroughly. Thus, the series dilution has been made from 10^{-1} to 10^{-6}. Repeat the series dilution for all samples.

3) Remove the medium of prepared BHK-21 cells, add 900 µl series dilution solution to each well. Pipette from 10^{-6} dilution to 10^{-1} dilution. Finish all wells. Incubate plates in 37 °C for 90 min.

(4) Overlay medium change

Aspirate medium, carefully add 2 ml overlay medium to each well, Pipette from 10^{-6} dilution to 10^{-1} dilution. Finish all wells. Incubate plates in 37 °C incubator for 5 days.

(5) Crystal Violet staining

After 5 days, aspirate overlay medium, add 300 µl Crystal Violet staining solution into each well, fix and stain for 15 min. Invert the plate to remove the solution in each well, slightly wash each well with running tap water. Dry the plate in RT for at least 1 day.

(6) Plaques counting and titer determination

Count plaques under the microscope, virus titer is calculated as:

N plaque * 1.1 (*input factor*) * dilution = number pfu/ml

N: counted plaque number

Input factor = 1/ inoculum value = 1/0.9 ≈ 1.1

Inoculum value 900 µl /1000 µl = 0.9

2.2.11 Immunofluorescence (immunocytochemistry) staining

1. Reagents preparation

Quenching solution (50 mM NH_4Cl): dilute 300 µl 1 M NH_4Cl in 5.7 ml DPBS.

Blocking solution: dilute 1% Triton X-100 and 5% BSA in DPBS.

2. Experimental procedure

(1) Place sterile cover slides in a 24-well plate. Seed Ana-1 cells or Ana-1/MHV-68 cells at a density of 10,000 cells/well in medium, culture in 37 °C incubator for 24 h. Treat cells with designed treatment for proper time.

(2) After treatment, remove the medium, fix cells with 300 µl 4% PFA solution for 15 min at RT. Discard solution, wash cells with PBS for 2 times, 5 min each.

(3) Add 500 µl 50 mM NH_4Cl solution and quench free aldehyde groups of cells for 10 min. Add 500 µl blocking solution to permeabilize and block cells for 1 h at RT.

(4) Dilute primary antibody with blocking solution. After blocking, discard blocking solution and incubate cells with primary antibody at 4 °C overnight.

(5) Discard the primary antibody, wash cells with PBS for 2 times, each time 5 min. Dilute secondary antibody (Goat anti-Rabbit AlexaFlour 555, 1:1000), Phalloidin 488 (1:150) with blocking solution. Add 300 µl to each well and incubate for 1 h at RT. Protect plate from light.

(6) Dilute DAPI 1:1000 in PBS. Discard secondary antibody, add 300 µl DAPI solution to each well and incubate for 10 min at RT. Protect plate from light.

(7) Discard the solution, wash cells with PBS for 3 times, each time 5 min.

(8) Add one drop DAKO mounting medium onto microscope slide, take the cover slide out from culture plate and place on microscope slide. Keep mounting medium in between. Slightly press to remove air bubbles.

(9) Dry slides in RT for at least 1 h and store in 4 °C. Protect slides from light.

2.2.12 Animal experiments

C57BL/6 mice were anesthetized with midazolam/medetomidine/fentanyl (MMF) and infected i.n. with 5×10^4 PFU MHV-68. After 28 days, mice were instilled with either 50 µg CNP, 0.1 µg LPS or equal amount sterile H_2O as sham control per mouse as described previously. For p38 inhibitor experiment, 30 mg/kg p38 inhibitor (SB203580; Merck, Darmstadt, Germany) were administrated by intraperitoneal injection (i.p.) per mouse 1 h before instillation. After 24 h, lung tissue were harvested either for protein, RNA and DNA isolation or fixed with 4% Paraformaldehyde (PFA) solution for histological analysis. Bronchoalveolar lavage (BAL) fluid and cells were also collected for inflammatory cells profiles, RNA isolation and cytokine measurement as described before. All animal experiments were in compliance with protocols approved by the local Animal Care and Use Committee (District Government of Upper Bavaria; permit numbers: 55 2-1-54-2532-67-2015).

2.2.13 BAL cells cytospin & characterization

After 24 h of CNP instillation, mice were sacrificed, Bronchoalveolar lavage was performed by cannulating the trachea and infusing the lungs six times with 1.0 ml PBS without calcium and magnesium, as described previously (Sattler et al., 2017). The first two times lavage were collected separately and pelleted down at 425 g for 20 min at 4 °C to separate fluids for cytokine detection. The pellet was

also collected with the rest lavage to finally get all cells in pellet. The pellets were suspended in RPMI 1640 medium containing 10% FBS, total living cell number was counted with 0.2% trypan blue solution and 30,000 cells were used for each cytospin and two cytospin slides were generated from each mouse. Two cytospin slides from each group were performed with May-Grünwald Giemsa staining followed by macrophages, neutrophils and lymphocytes number counting. The rest cytospin slides were used for immunofluorescence staining.

2.2.14 Immunohistochemistry (IHC) staining

1. Reagents preparation

TBS wash buffer: Dilute TRIS Wash Buffer (20x; Zytomed Systems, Berlin, Germany) with distilled H_2O to get 1 x TBS buffer.

2. Experimental procedure

Before staining, incubate slices at 60 °C incubator for at least 1 h to remove the surrounding parafilm.

(1) Deparaffinization/Rehydration

Incubate slides in Xylene for 5 min, repeat incubation in new Xylene for another 5 min. Then incubate slides in 100% Ethanol for two times, 90%, 80% and 70% Ethanol for one time, 1 min each time. Rinse slides into distilled H_2O for 1 min.

(2) Peroxidase blocking

Prepare 1.8% H_2O_2-Methanol solution freshly by mixing 6 ml H_2O_2, 80 ml Methanol and 14 ml distilled H_2O. Incubate slides for 20 min at RT to block peroxidase. Rinse slides with distilled H_2O after incubation.

(3) Epitope Retrieval

1) Prepare Retrieval solution in bracket.

Use HIER Citrate Buffer pH 6.0 or HIER T-EDTA Buffer pH 9.0 depending on different antibodies. Dilute 10 ml buffer to 90 ml distilled H_2O and mix thoroughly.

2) Heat-Induced Epitope Retrieval (HIER) procedure

Add 500 ml distilled H_2O inside decloaking chamber, place all the slides inside rack and place rack into decloaking chamber. Close the lid and start program. Slides are heated at 125 °C for 30 s then are heated at 90 °C for 10 s. Bring slides

to RT to cool down for 10 min. After 10 min, gradually cool down slides with 1 x TBS solution by adding and pouring 5 to 6 times.

(4) Blocking

Add distilled H_2O into a black staining chamber to keep a proper humidity inside. Move slides into glass slides staining rack, wash with TBS for 2 times, 2 min each time. Draw an intact circle with DAKO Histology pen, keep inside chamber until the circle get solid. Wash slides with TBS again. Place all the sides inside the staining chamber, add 1 or 2 drop of blocking solution (Rodent Block M). Incubate for at least 30 min at RT.

(5) Primary antibody incubation

After 30 min, wash slides with TBS for 2 min. Dilute primary antibody with Antibody diluent (AD) solution. Add 100 µl onto each sample, incubate at 4 °C overnight.

(6) Secondary antibody incubation

Wash slides with TBS for 3 times. Add 1 drop of Rabbit on Rodent AP-Polymer, Incubate in RT for 30 min. After incubation, wash slides with TBS for 3 times, 2 min each time.

(7) Vulcan Fast Red Chromogen incubation

Mix 2.5 ml Vulcan Fast Red Buffer and one drop of 'Vulcan Fast Red Chromogen', freshly prepare solution before use. Protect from light. Place slides into chamber, add 100 µl solution and incubate in RT between 6 and 12 min. After incubation, stop reaction with distilled H_2O.

(8) Counterstaining with Hematoxylin

Stain slides in Hematoxylin for 2 s then rinse in distilled H_2O. Incubate slides in tap water for 1 min then distilled H_2O for 5 min.

(9) Slides drying and xylene incubation

Place all the sides on 60 °C dryer for 15 to 30 min to dry slides. Incubate slides in Xylene for 2 times, 5 min each time.

(10) Mounting

Take 24*50 mm cover slides, place one drop Entellan mounting solution onside, cover on the tissue, press a little bit to remove bubbles. Remove extra entellan between slides. Dry sides at least 1 h under the hood.

(11) Imaging and quantification

Images were taken with Olympus BX-51 light microscope (Olympus, Hamburg, Germany). Design-based stereology was used to analyze IHC slides using Olympus microscope equipped with a computer-assisted stereological toolbox (newCAST, Visiopharm) running Visiopharm Integrator System (VIS) software (v.6.0.0.1765).

2.2.15 Immunofluorescence (IF) staining and ZEISS scanning

1. Reagents preparation

Blocking solution: 5% goat serum in PBS containing 0.3% Triton X-100

Antibody diluent (AD) solution: 1% BSA in PBS containing 0.3% Triton X-100

PBST: 0.1% Tween-20 in PBS

2. Experimental procedure

Before staining, incubate slices at 60 °C incubator for at least 1 h to remove the surrounding parafilm.

(1) Deparaffinization/Rehydration

The same as IHC staining.

(2) Epitope Retrieval

The same as IHC staining.

(3) Blocking

Add distilled H_2O into a black staining chamber to keep a proper humidity inside. Move slides into glass slides staining rack, wash with PBST for 2 times, 2 min each time. Draw an intact circle with DAKO Histology pen, keep inside chamber until the circle get solid. Wash all the slides with PBST again. Place all the sides inside the staining chamber, add 100 µl blocking solution. Incubate for 1 h at RT.

(4) Primary antibody incubation

After 1 h, wash slides with PBST solution for 5 min. Check the integrate of circle. Dilute primary antibody with AD solution. Add 100 µl to each sample, incubate at 4 °C overnight.

(5) Secondary antibody incubation

Wash slides with PBST for 3 times. Add 100 µl fluorescence-labeled secondary antibody and incubate in RT for 1 h. After incubation, wash slides with PBST for 3 times, 5 min each time.

(6) 2nd time blocking (for double labeling primary antibodies from the same host species)

After washing, incubate slides with 100 µl normal rabbit serum blocking solution for 1 h at RT.

(7) Surface blocking of immunoglobulins for double labeling primary antibodies from the same host species

Wash slides with PBST for 3 times. Dilute unconjugated Rabbit Fab fragment in blocking solution (1:45 dilution) and incubate for 1 h at RT.

(8) 2nd Primary antibody incubation

Wash slides with PBST for 3 times. Dilute primary antibody in AD solution and add 100 µl to each sample, incubate at 4 °C overnight.

(9) Secondary antibody & DAPI incubation

Wash slides with PBST for 3 times, 5 min each time. Dilute fluorescence secondary antibody, DAPI & Phalloidin 488 in AD solution, add 100 µl to each sample, incubate for 1 h at RT. After incubation, wash slides with PBST for 3 times, 5 min each time.

(10) Mounting

Mount slides with DAKO medium, remove bubbles if necessary. Dry slides at least 1 h at RT avoiding from light and store at 4 °C.

(11) Imaging

Images were obtained either by LEICA confocal fluorescence microscope (SP5-II, Leica, Wetzlar, Germany) for high resolution images or Zeiss Axio Scan.Z1

(Carl Zeiss, Jena, Germany) for slices scanning. Later analysis were performed with ZEN Blue 2.3 software.

2.2.16 Light-sheet fluorescence microscopy (LSFM) with 3DISCO tissue clearing protocol

1. Reagents preparation

PBSGT solution: 0.2% Gelatin, 0.5% Triton X-100 and 0.01% Thimerosal in PBS. Filter solution with 0.22 µm filter.

PBST solution: 0.5% Triton X-100 and 0.01% Thimerosal in PBS.

2. Experimental procedure

(1) Lung tissue perfusion

Mouse lungs were perfused and fixed with 4% PFA at 4°C overnight. Discard solution and change to PBS for two times, then the tissue can be stored in PBS for following experiments.

(2) Dehydration

When lungs are not well perfused, dehydrate samples in freshly prepared 50%, 80% and 100% Methanol/PBS series for 1 h each at RT. Then incubate samples in 100% Methanol for 1 h. Afterwards, samples can be stored in Methanol at 4 °C.

(3) Bleaching

Bleach the sample with ice cold 6% H_2O_2-Methanol solution overnight at 4°C. Then wash in 100% Methanol for 2 times at RT, 1 h each time.

(4) Rehydration

Rehydrate samples in freshly prepared 80%, 50% and 0% Methanol/PBS series, for 1 h each at RT.

(5) Blocking and permeabilization

Incubate samples in PBSGT for 3 days with rotation at RT.

(6) Primary antibody incubation

Dilute primary antibody in PBSGT + 0.1% saponin (10 µg/mL) and incubate samples for 7 days at RT. After incubation, discard antibody, wash samples with PBST for 6 times at RT, 1 h each time.

(7) Secondary antibody incubation

Dilute secondary antibody in PBSGT+ 0.1% saponin (10 µg/mL), filter with 0.22 µm filter to avoid precipitates. Incubate samples for 3 days at RT. Protect samples from light. After incubation, discard antibody, wash samples with PBST for 6 times at RT, 1 h each time.

(8) Optical Clearing

1) Incubate samples in 50% Tetrahydrofuran in H_2O overnight at RT. In the second day, further incubate samples in 50%, 80% and 100% Tetrahydrofuran in H_2O, 1 h each time. Then incubate samples in 100% Tetrahydrofuran overnight. Incubate one more time in fresh 100% Tetrahydrofuran for 1 h at RT.

2) Incubate samples in Dichloromethane (DCM) for 20 - 40 min.

3) Finally incubate samples in Benzyl ether (DBE) for at least 4 h before imaging.

(9) Imaging

Images was taken with UltraMicroscope II (Miltenyi Biotec, Bergisch Gladbach, Germany)

2.2.17 Statistical analysis

All values were shown as mean ± SD and analyzed by either Student's *t* test or one-way ANOVA using the GraphPad Prism software, v9.0 (GraphPad Software, Inc., San Diego, CA, USA). "*" was used to show significant difference, * $P < 0.05$, ** $P < 0.01$. Statistical analysis of transcriptomic study was shown in the part of "Transcriptomic study by microarray analysis".

3. Results

3.1 Characterizations of nanoparticles (NPs)

CNP, DWCNT as well as Min-U-Sil 5 (Quartz) particles were used in the study.

Carbon black or carbonaceous nanoparticle (CNP) is a soot-like nanoparticle, with a diameter of 14 nm. Brunauer–Emmett–Teller (BET) analysis revealed the CNP surface area of 272 m^2/g. When CNP is dispersed in sterile ultrapure H_2O and cell culture medium, there is aggregation formation and reachs a diameter between 140 and 170 nm analyzed by Dynamic light scattering (DLS) measurement. Polydispersity Index (PdI) is between 0.1 and 0.2, which reflects a stable dispersion in H_2O and medium.

Double walled carbon nanotubes (DWCNT) is an engineered nanomaterial with a fiber shape similar to asbestos. DWCNT is 10 nm in diameter and 1000 nm in length with BET of 660 m^2/g. DWCNT also forms aggregations when dispersed in sterile ultrapure H_2O as well as cell culture medium. The dynamic diameter is 1800 to 3200 nm accompanied with high PdI (0.4-0.6). Compared to CNP, DWCNT is less stable in cell culture condition and results in faster sedimentation. This allows more interaction between NPs and cells.

Min-U-Sil 5 (Silica; Quartz) showed a median diameter of 1.7 µm declared on the datasheet from the manufacturer.

Table 3.1 Characterization of NPs in the study

Nanoparticles	**Name**	**Acronym**	**Particle Size[a] (nm)**	**BET[b] (m^2/g)**
Carbon black	Printex 90	CNP	14	272
Double walled carbon nanotubes	DWCNT	DWCNT	10*1000	660

a Particle Size: primary particle size, not considering agglomerate formation

b BET: Brunauer-Emmett-Teller (BET) surface area analysis of particle surface area based on nitrogen adsorption.

3.2 Nanoparticles exposure triggered MHV-68 reactivation localized to CD11b+ macrophage-like infiltrates

3.2.1 Nanoparticle exposure triggered MHV-68 reactivation

1. The overview of lytic virus protein expression during MHV-68 acute infection, latency and reactivation by light-sheet fluorescence microscopy (LSFM)

In a previous study, Sattler and colleagues in our group found that both CNP and DWCNT exposure induced an increase of MHV-68 lytic virus protein expression by immunohistochemistry staining in mouse lungs which suggested MHV-68 reactivation (Sattler et al., 2017). Here, we used the 3DISCO tissue optically clearing method, and stained whole lung lobes with anti-MHV-68 serum followed by light-sheet fluorescence microscopy (LSFM) imaging to get an overview of MHV-68 lytic virus protein expression and localization at a whole lung scale after different treatments. Virus acute infection, latent infection as well as reactivation induced by nanoparticles exposure were included for analysis.

Lung morphology was taken from tissue autofluorescence (AF) using excitation and emission wavelength of 470 and 535 nm, respectively. Staining of MHV-68 lytic protein was obtained using excitation and emission wavelength of 640 and 690 nm, respectively. Scanning of images were used to reconstitute 3D structure of lungs.

Briefly, C57BL/6 mice were intranasally infected with MHV-68 for 28 days to establish latency. At day 28, mice were instilled with either CNP (50 µg), LPS (0.1 mg; positive control) or equal volume of H_2O (sham control). After 24 h, mouse lungs were harvested and fixed with 4% PFA for the following experiments. “acute infection” (6 days post MHV-68 intranasally infection), “latently infection” (28 days post MHV-68 infection with subsequent 24 h H_2O instillation) and “reactivation” induced by CNP or LPS (28 days post MHV-68 infection with subsequent 24 h CNP or LPS instillation) were included for imaging. 24 h of LPS instillation was used as a positive control.

First, examples of mouse right lung inferior lobes before and after tissue clearing were shown in **Fig. 3.1** to represent the efficiency of optical clearing. Lung lobes of “latency” and “acute infection” turn white after perfusion (left) whereas dark

nanoparticles still deposit in tissue in CNP exposed lungs (middle). Lung lobe exhibits transparent after optically clearing (right) and thus allows a deep imaging performance as well as good reconstruction of 3D morphology.

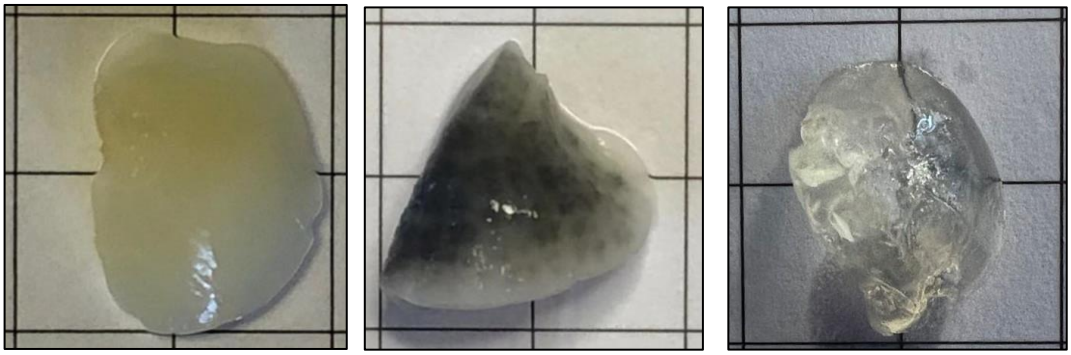

Figure 3.1 The morphology of perfused mouse lung lobes before and after tissue optically clearing.

Mice lungs were perfused and fixed with 4% PFA at 4°C overnight. Lungs were washed in PBS, then lobes were cut and stored in PBS. Representative images of perfused lung lobe of latently infected mouse (left), perfused lung lobe of latently infected mouse exposed to CNP for 24 h (middle) and perfused lung lobe of latently infected mouse after tissue clearing (right) are shown. Each square of background is 0.5 * 0.5 cm.

Then, anti-MHV-68 serum staining was performed to show lytic virus protein expression in MHV-68 acute infection, latent infection as well as reactivation induced by CNP and LPS. Since lung tissue exhibits high AF, lung morphology was generated by AF without further staining. As depicted in **Fig. 3.2a**, a clear structure of lung lobes was imaged and shown (left side). Importantly, there was a dramatic increase of MHV-68 lytic virus protein expressed in mouse lung 6 days after infection. Infection predominantly occurs in bronchial epithelium regions and indicates an epithelial damage. A vertical snapshot image (right side) also showed that MHV-68 infected predominately in epithelium. There is generally low lytic virus protein stained in latency mice instilled with H_2O as a negative control (**Fig. 3.2b**). Furthermore, 24 h after CNP exposure during latency triggered an increase of MHV-68 lytic virus protein expression which confirmed MHV-68 reactivation. LPS caused a higher level of MHV-68 reactivation compared to CNP. And compared to acute infection, there are only mild expression of lytic protein in lung, demonstrating a relative lower virus activity during virus reactivation.

Thus, LSFM provides us an overview of MHV-68 lytic virus protein expression and localization in mouse model and confirms pulmonary exposure CNP triggered MHV-68 reactivation.

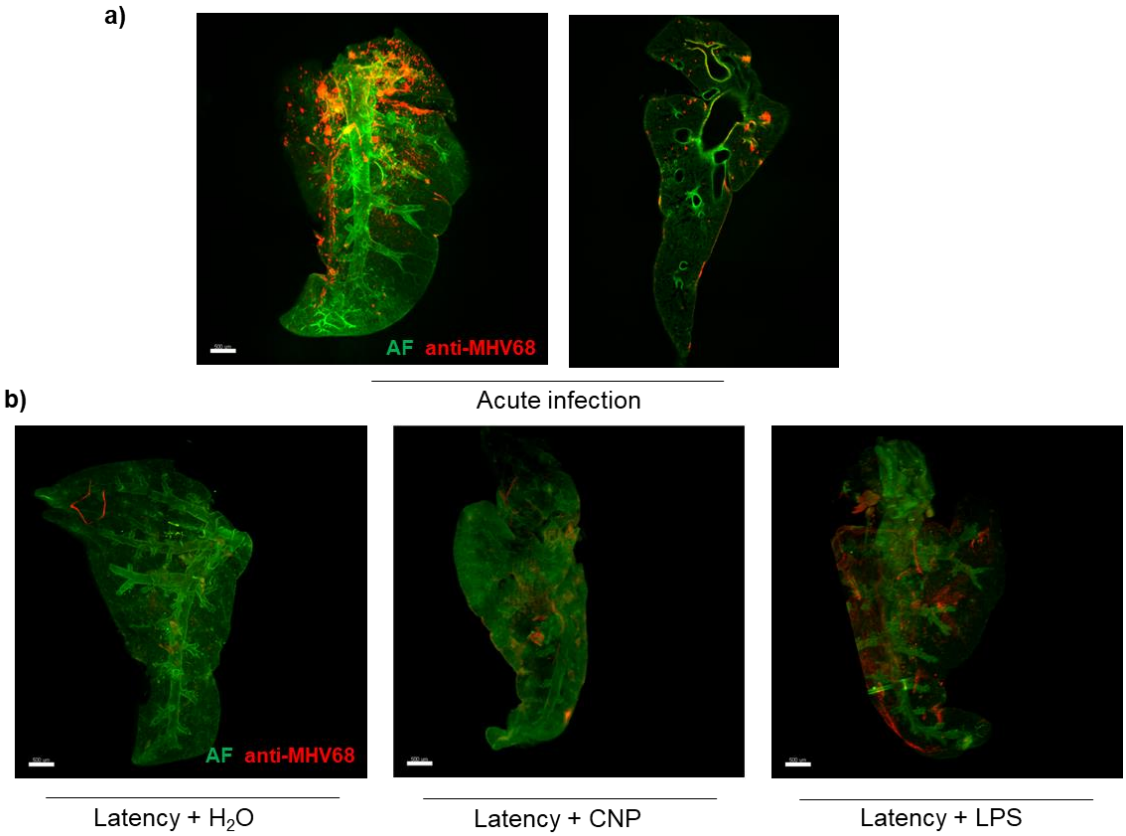

Figure 3.2 Light-sheet fluorescence microscopy (LSFM) showing an overview of MHV-68 acute infection, latency and reactivation induced by CNP and LPS.

Mouse lungs were perfused and fixed with 4% PFA. Lung lobes were cut and incubated with anti-MHV-68 rabbit serum followed by fluorescence-labeled secondary antibody and shown in red. Autofluorescence (AF) generated in green represents lung lobe structure. Optically clearing was performed and images were taken with Light-sheet fluorescence microscope (LSFM) and reconstituted with Imaris software (Version 9.3.1). **a.** An overview of MHV-68 lytic protein expression in acute infected mouse (infection after 6 d) as well as vertical snapshot image was shown. **b.** An overview of MHV-68 lytic virus protein expression in life cycle stage of latency, reactivation induced by CNP (50 µg, 24 h) and LPS (positive control; 0.1 µg, 24 h) in mouse lung lobes. Magnification: 0.63 x, scale bar: vertical snapshot image, 1000 µm; rest images, 500 µm.

2. Distribution and quantification of MHV-68 reactivation induced by CNP

To obtain detailed information of localization, lung tissue were also harvested to obtain paraffin-embedded tissue slides to investigate the distribution of MHV-68 infection and reactivation. Similarly, a dramatic increase of lytic virus protein was observed after 6 days of MHV-68 infection and predominantly occurs in epithelial

regions as well as single macrophage-like cells. There is still spontaneous reactivation occurring in latency phase with less cells exhibiting lytic protein expression. Subsequently CNP or LPS exposure for 24 h reactivated latent virus and triggered a significant increase of lytic protein expression (**Fig. 3.3a**). The percentage of lytic protein expressed cells quantification demonstrated the reactivation induced by CNP as well as LPS (**Fig. 3.3b**). The results also indicated that MHV-68 reactivation mainly occurred in lung peribronchiolar areas exhibiting cell infiltrations.

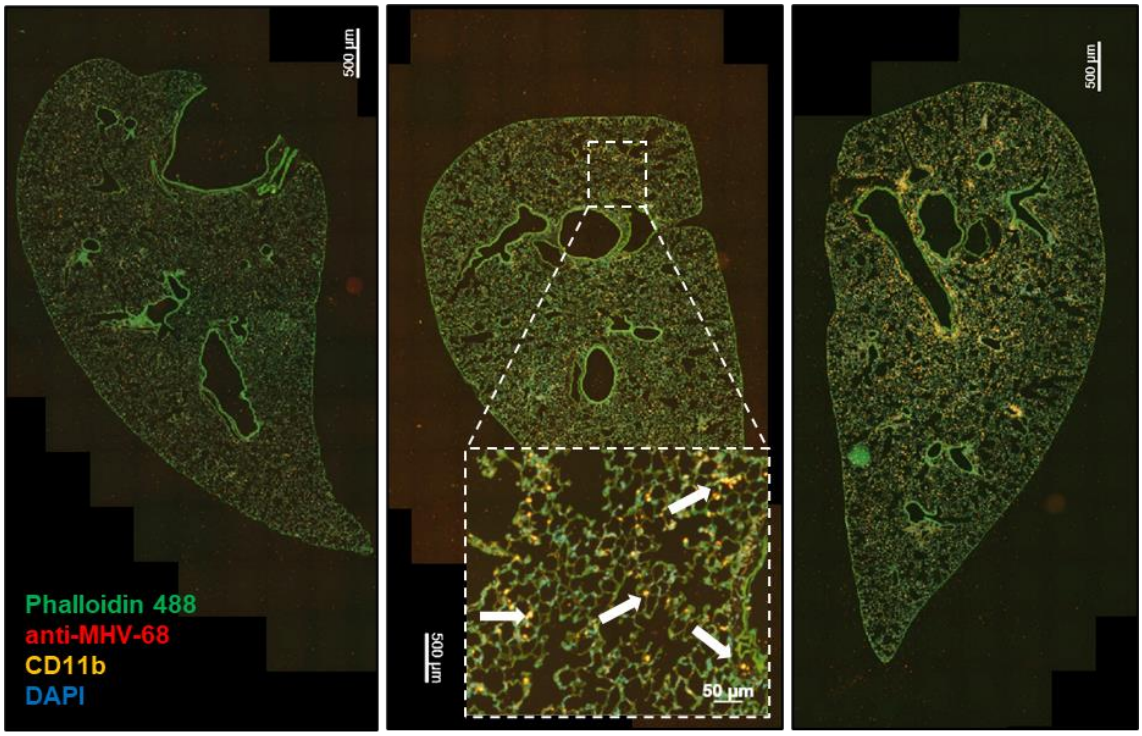

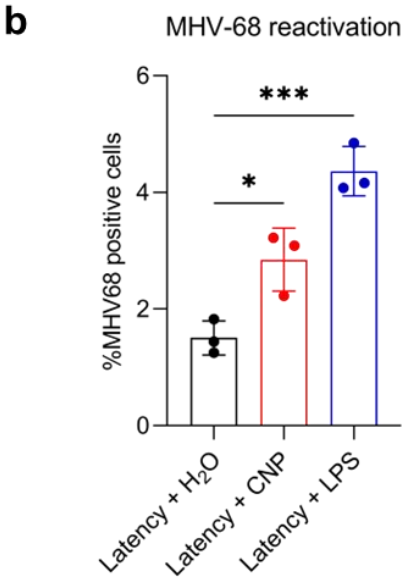

Figure 3.3 The distribution and quantification of MHV-68 reactivation induced by pulmonary CNP exposure.

Mouse lung slides (3 µm) were stained with anti-MHV-68 rabbit serum and fluorescence labeled secondary antibody, DAPI and Phalloidin 488 staining represented cell nuclei and cell morphology, respectively. Slides were scanned with Zeiss Axio Scan.Z1 fluorescent microscope (ZEISS, Germany) and analyzed with ZEN Blue 2.3 software. a. Scanned slides showed the expression and localization of MHV-68 lytic proteins in different groups, including acute infection ("Acute infection"), latency ("Latency + H_2O") as well as reactivation ("Latency + CNP" and "Latency + LPS"). b. Quantification of percentage of MHV-68 antiserum positive staining cells in lung slides. 3 mice from each group were included for analysis. One-way ANOVA as well as post Tukey's multiple comparisons test were used. * $P < 0.05$, **** $P < 0.0001$.

3.2.2 The localization of MHV-68 reactivation triggered by NPs is mainly in CD11b+ infiltrating cells

In the previous study, immunohistochemistry (IHC) staining revealed that CNP induced the increase of lytic virus protein expression in mouse lungs indicating MHV-68 reactivation (Sattler et al., 2017). Again from **Fig. 3.3**, MHV-68 reactivation mainly occurred in lung peribronchiolar areas and is likely to occur in mononuclear cells. Here, to understand the localization, we performed anti-MHV-68 immunofluorescence double staining together with the macrophage markers CD11b and CD11c.

CD11b, or integrin alpha M, belongs to integrin family and predominately expressed in monocytes and granulocytes. In lung tissue, A high expression of CD11b is mainly in the recruited macrophages originally from monocytes or bone marrow or interstitial macrophages. CD11c, also named Integrin alpha X, is a type I transmembrane protein mainly expressed on dendritic cells, interstitial macrophages and tissue resident macrophages. The co-expression of CD11c, Siglec F and F4/80 identified resident alveolar macrophages. Thus, here we use CD11b and CD11c unambiguously as markers of macrophages, with resident alveolar macrophages representing CD11c positive but not CD11b and recruited macrophages exhibiting CD11b positive but CD11c negative to investigate the localization of MHV-68 reactivation induced by CNP (Misharin et al., 2013, Moldobaeva et al., 2018, Cass et al., 2021, Janssen et al., 2011).

1. MHV-68 reactivation triggered by CNP mainly localized to CD11b+ infiltrating macrophages in mouse lungs

As shown in **Fig. 3.4a**, pulmonary CNP exposure triggered MHV-68 lytic virus protein expression mainly in CD11b positive cells and similar result was also found in LPS exposed mice lungs, which demonstrated the main involvement of infiltrating macrophage-like cells in MHV-68 reactivation.

We further quantified the CD11b expressing cell number in different conditions. We found that there was a moderate increase of CD11b positive cells (but not significant) after MHV-68 acute infection and it remained a comparable number in latency compared to non-infected control (**Fig. 3.4b**). However upon CNP exposure, there was a 60% increase in the number of CD11b positive cells in lung tissue, whereas a significant increase of CD11b positive cells triggered by LPS (**Fig. 3.4b**). To confirm CD11b positive cells are the main MHV-68 reactivation cells, we found that more than 60% CD11b positive cells are exhibiting MHV-68 reactivation (**Fig. 3.4c**), no matter spontaneous reactivation during latency or reactivation induced by CNP and LPS exposure.

As a marker of monocytes, CCR2 was used to perform double staining with CD11b to further investigate the localization of MHV-68 reactivation. As shown in **Fig. 3.4e**, very little colocalization of CD11b and CCR2 was observed after CNP exposure. Accompanied with former results, monocytes are not main MHV-68 reactivation cell types.

Thus, CNP treatment induced an increase of CD11b cells in infiltrating areas of mouse lungs, CNP triggered MHV-68 reactivation mainly localizes in CD11b cells.

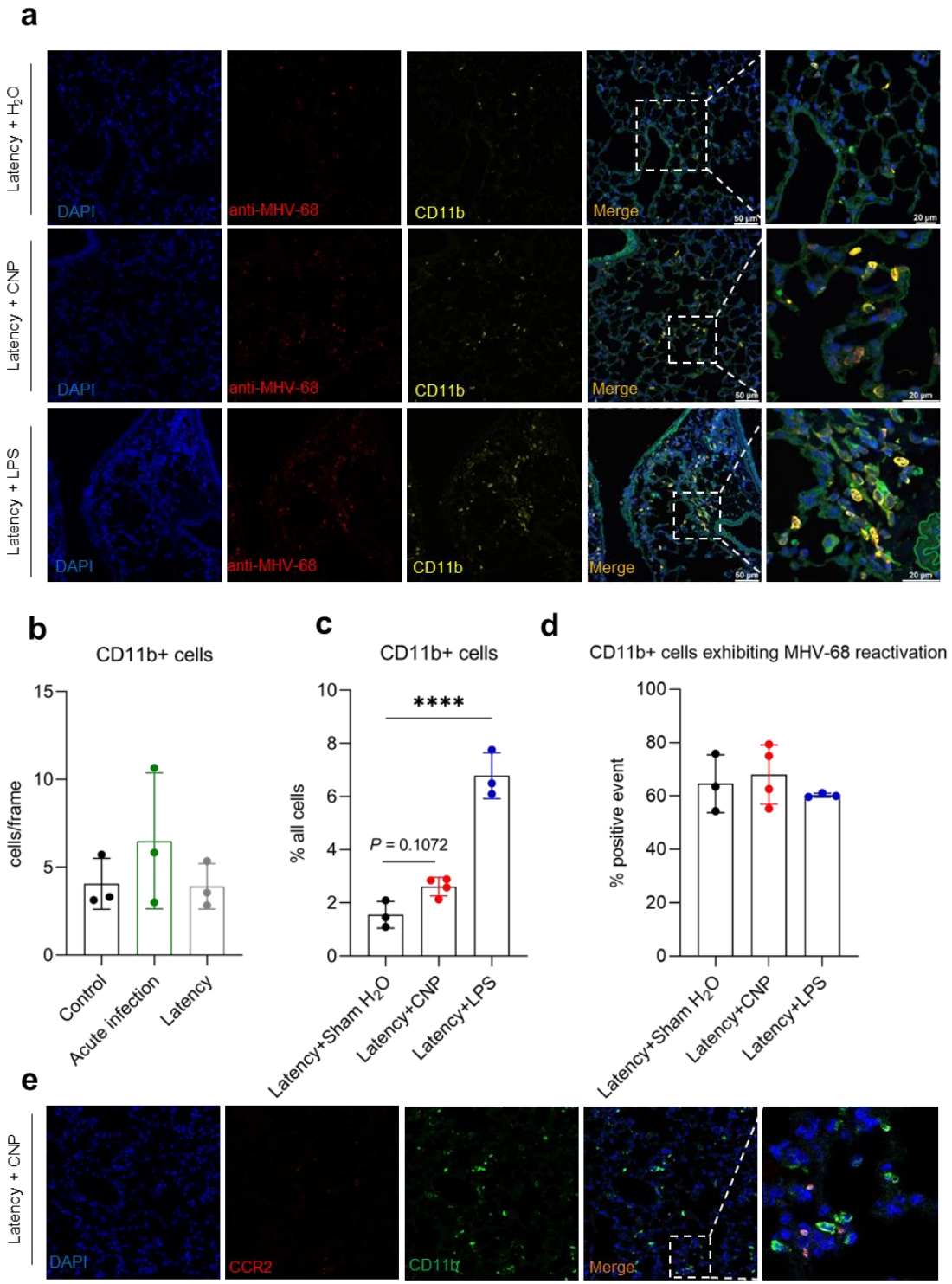

Figure 3.4 The localization of MHV-68 lytic virus protein expression in CD11b positive cells in mouse lungs exposed to CNP.

Mouse lung slides (3 μm) were stained with anti-MHV-68 serum (red), CD11b antibody (yellow) as well as DAPI (blue) by immunofluorescence double staining. Images with magnification of 40 x were taken with Leica confocal microscope, Representative images of each channel as well as merge images were shown in **a**. Scale bar: 50 μm (20 μm in enlarged images). Samples from 3 mice of each group were included for staining and representative images were shown. CD11b

positive cells were quantified during control, acute infection (MHV-68 infection after 6 days) and latency (MHV-68 infection after 28 days and exposed to H_2O for 24 h) as well as CNP and LPS exposed, data were shown in **b & c**. The percentage of CD11b+ cells exhibiting MHV-68 reactivation was shown in **d**. A double staining of CCR2 (red) and CD11b (green) in group "Latency + CNP 24 h" was shown. One-way ANOVA as well as post Tukey's multiple comparisons test were used. **** $P < 0.0001$.

2. MHV-68 reactivation triggered by CNP rarely localized to CD11c+ resident cells

Furthermore, we performed anti-MHV-68 immunofluorescence double staining together with CD11c in mouse lung slides to verify the localization of MHV-68 lytic virus protein expression in tissue resident alveolar macrophages in air space. As shown in **Fig. 3.5**, CD11c positive cells mainly localized in alveolar regions demonstrating the majority of alveolar macrophages. However, they rarely exhibit the appearance of MHV-68 lytic virus protein staining. Similar results were also found in LPS exposed mice. Thus, alveolar macrophages are not main target cells of MHV-68 reactivation triggered by CNP.

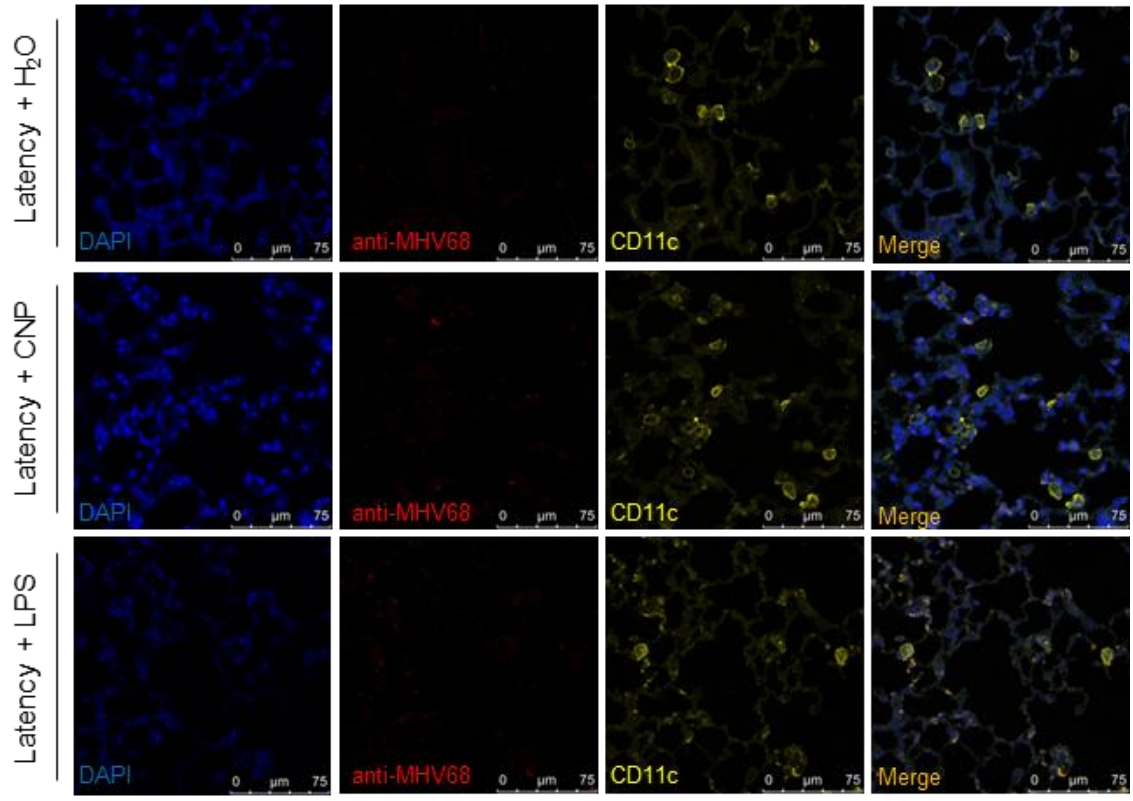

Figure 3.5 The localization of MHV-68 lytic virus protein expression in CD11c positive cells in mouse lungs exposed to CNP.

Mouse lung slides (3 µm) were stained with anti-MHV-68 serum (red), CD11c antibody (yellow) as well as DAPI (blue) by immunofluorescence double staining. Images with magnification of 40 x were taken with Leica confocal microscope, Representative images of each channel as well as merge images were shown. Scale bar, 75 µm. Samples from 3 mice of each group were included for staining and representative images were shown.

3. Alveolar macrophages but not recruited macrophages are main macrophages in bronchoalveolar lavage (BAL) cells but hardly showed MHV-68 reactivation

To further confirm the localization of MHV-68 reactivation induced by pulmonary CNP exposure, we investigated the composition of CD11b and CD11c positive cells in bronchoalveolar lavage (BAL) cells.

Mouse lungs were lavage followed by BAL cells harvest and counting after 24 h CNP or LPS exposure. Cytospins with 30,000 cells were generated to perform either Giemsa staining or immunofluorescence staining. Giemsa staining were firstly conducted to differentiate different types of cells. As shown in **Fig. 3.6a**, both CNP and LPS instillation triggered an increase of total BAL cells in mice compared to control. CNP instillation did not cause macrophages number alteration whereas LPS instillation significantly reduced macrophages in BAL fluid (BALF) (**Fig. 3.6b**). Besides, both CNP and LPS instillation caused an increase of neutrophils in BALF which suggested an pro-inflammatory response in lungs. However, no change of lymphocytes were observed in different treatments.

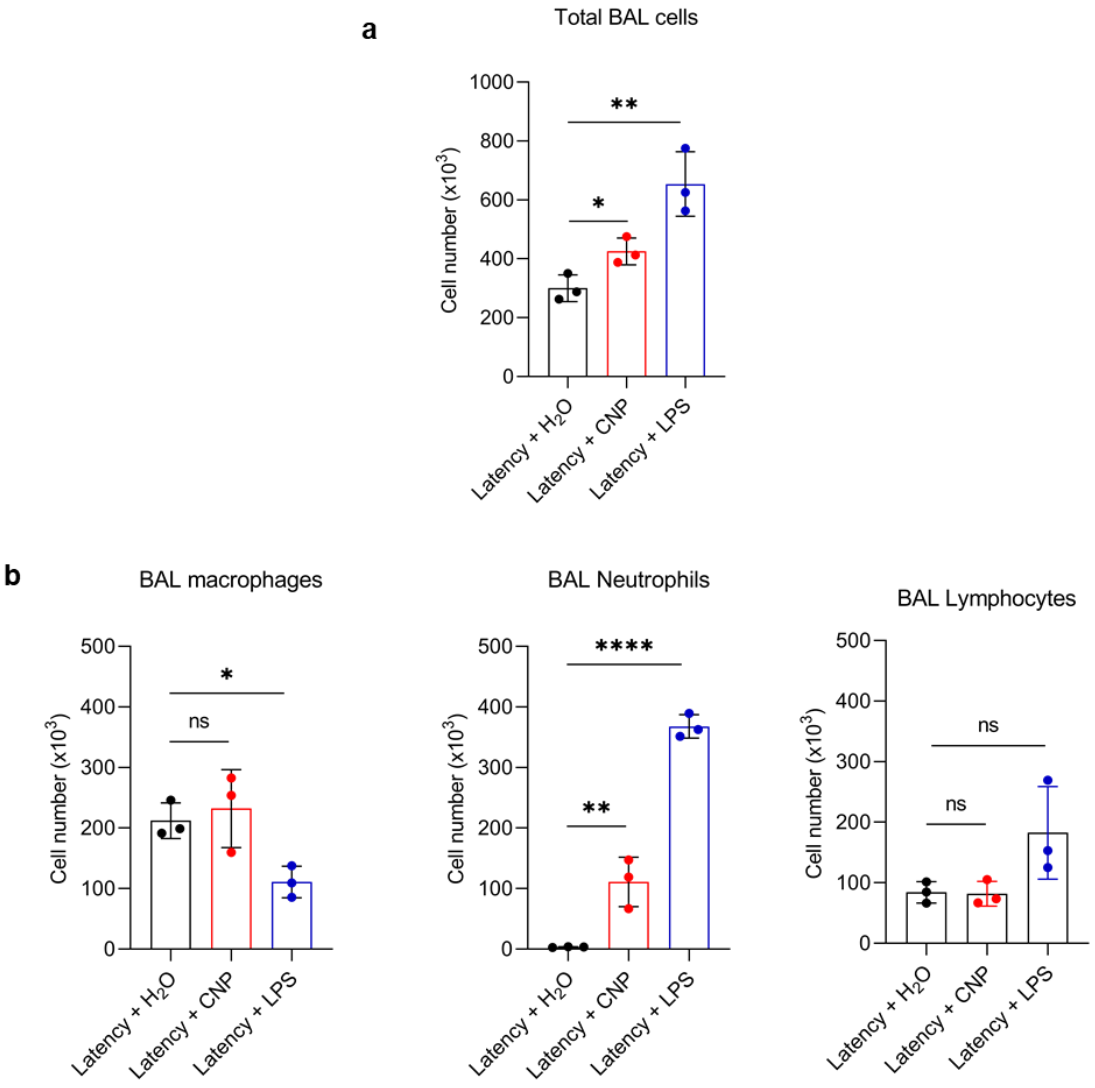

Figure 3.6 Bronchoalveolar lavage (BAL) cells number and cell differentiations.

a. Total BAL cells were harvested and counted, total cell number was shown. **b.** Cytospins were performed with 30,000 cells followed by Giemsa staining and macrophages, neutrophils and lymphocytes differentiations. 3 mice from each group were included for analysis. One-way ANOVA as well as post Tukey's multiple comparisons test were used. * $P < 0.05$, ** $P < 0.01$, **** $P < 0.0001$.

Next, to investigate whether there are MHV-68 reactivation in BAL macrophages, we performed anti-MHV-68 immunofluorescence double staining together with CD11b or CD11c in cytospin slides. As shown in **Fig. 3.7**, cytospin slides from 24 h CNP instilled mouse showed a majority of CD11c positive cells demonstrating a main source of alveolar macrophages after lavage. Besides, there are similar amount of CD11c positive cells in CNP instilled mouse compared to control mouse (sham H_2O control). However, less CD11c positive cells were observed

in cytospins from LPS instilled mouse, reflecting a decrease of alveolar macrophages upon LPS exposure. These findings fit to the BAL cell differentiations by Giemsa staining showed in **Fig. 3.6**. anti-MHV-68 serum staining showed that there is an equal level of lytic protein expression in CNP and LPS exposed mice compared to negative control. Thus, alveolar macrophages from alveolar regions remain the major components of BAL macrophages after lavage upon CNP exposure and there are no significant MHV-68 reactivation occurrence.

As shown before, CNP and LPS instillation caused an increase of neutrophils in BALF. According to DAPI staining, we were able to distinguish neutrophils by their polymorphonuclear morphology (**Fig. 3.7**). Here we found an increase of polymorphonuclear cells in CNP exposed mice. LPS exposure even triggered a dramatic increase of these cells. However, no MHV-68 reactivation were observed in either CNP or LPS instilled mice. Thus, both CNP and LPS caused an increase of neutrophils in BALF but they were not involved in MHV-68 reactivation.

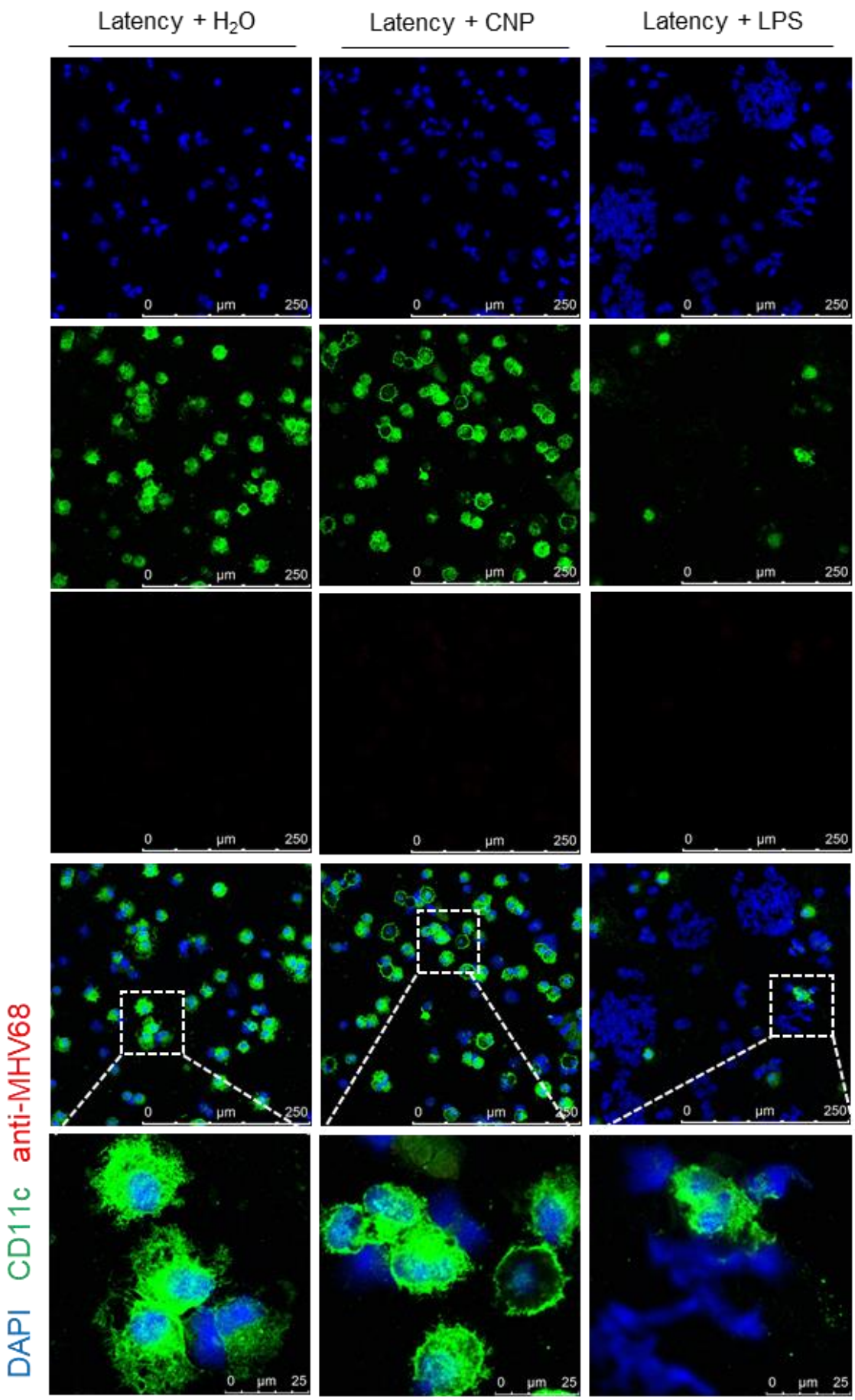
Latency + H_2O
Latency + CNP
Latency + LPS
DAPI
CD11c
anti-MHV68
0 µm 250
0 µm 25

Figure 3.7 A major source of alveolar macrophages in BAL macrophages but showed no MHV-68 reactivation upon CNP exposure.

BAL cells cytopsin slides were fixed with 4% PFA and stained with anti-MHV-68 serum (red), CD11c (green) as well as DAPI (blue). Images were taken with Confocal fluorescence microscope (Leica, TSC-SP5-II, Germany) to show detailed localization of MHV-68 reactivation. Scale bar: 250 µm (25 µm for enlarged images).

Next, the performance of MHV-68 immunofluorescence double staining with CD11b showed that there are rarely less amount of CD11b positive cells in BAL cells even those cells exhibit MHV-68 lytic protein expression (**Fig. 3.8**). Our findings demonstrated that infiltrating macrophages which showed MHV-68 reactivation are not localized in alveolar regions after 24 h of CNP or LPS exposure.

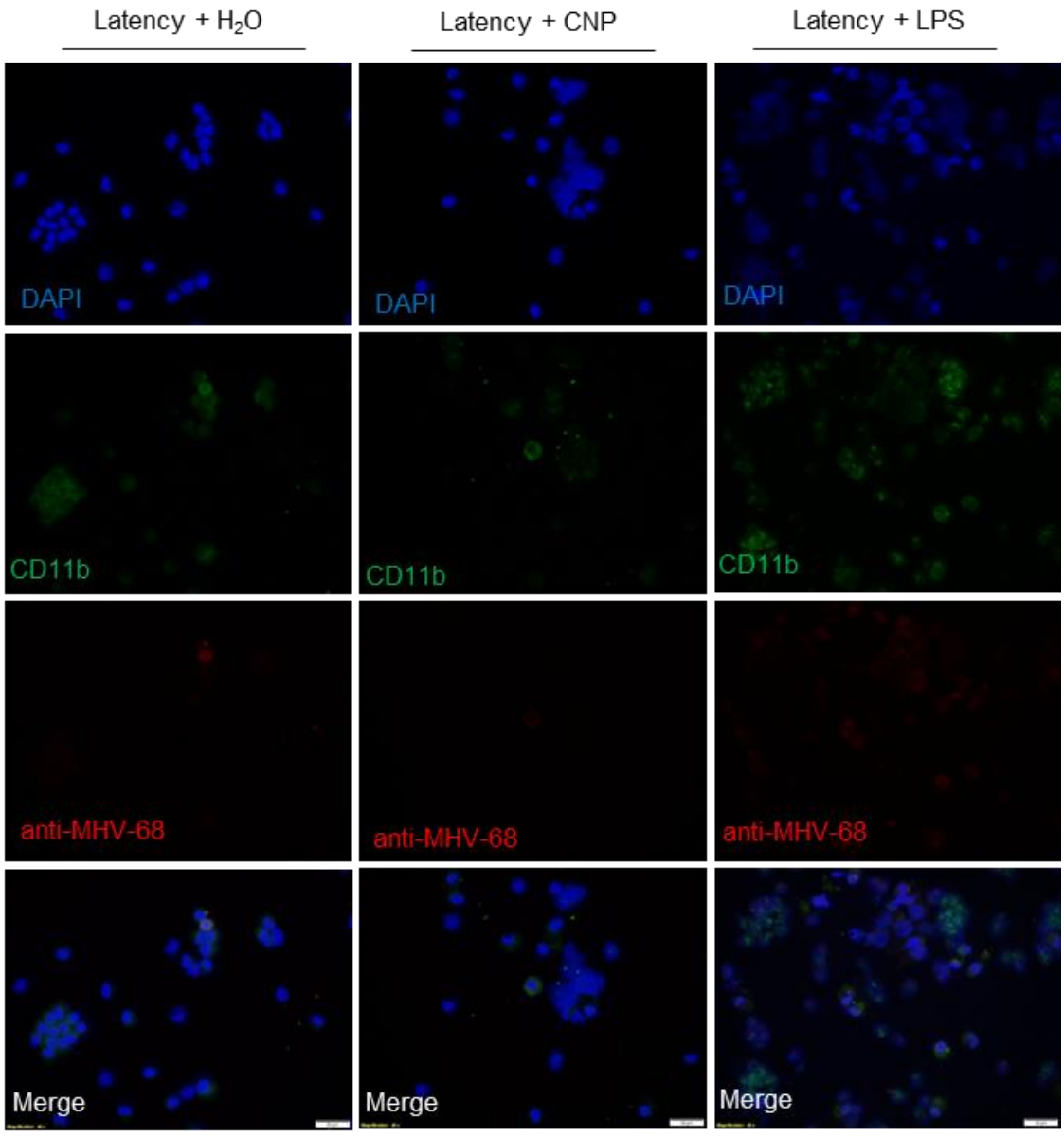

Figure 3.8 BAL cells staining hardly showed the appearance of CD11b positive cells exhibiting MHV-68 reactivation upon CNP exposure.

BAL cells cytopsin slides were fixed with 4% PFA and stained with anti-MHV-68 serum (red), CD11b (green) as well as DAPI (blue). Images were taken with Olympus BX-51 fluorescence microscope (Olympus, Hamburg, Germany) to show detailed localization of MHV-68 reactivation. Scale bar: 20 µm.

Taken together, MHV-68 reactivation triggered by pulmonary CNP after 24 h predominantly localizes in CD11b positive infiltrating macrophages in lung tissues but not alveolar regions. MHV-68 reactivation rarely localizes in CD11c positive resident alveolar macrophages in air space. These findings provide information to select and establish proper *in vitro* models and proceed further mechanism studies.

3.3 *In vitro* mechanism study of MHV-68 reactivation triggered by NPs exposure

3.3.1 Murine BMDM Ana-1 cells as an *in vitro* model for MHV-68 reactivation investigation

As shown *in vivo*, NPs exposure reactivates latent MHV-68 and mainly localizes in CD11b positive infiltrating macrophage-like cells in the lung. However, the mechanism underlying MHV-68 reactivation induced by NPs exposure still remains unclear.

First, an *in vitro* model mimicking main reactivation cell type is needed. Murine bone marrow derived macrophages (BMDM) Ana-1 cell line was established from bone marrow cells of C57BL/6 (H-2^b) mice infected with J2 recombinant retrovirus for immortalization (Cox et al., 1989). Here, we investigated the surface marker expression of CD11b and CD11c with flow cytometry in Ana-1 cells. As shown in **Fig. 3.9**, we found that more than 90% of Ana-1 cells are expressing CD11b but less than 5% cells expressing CD11c, which provides an *in vitro* model representative for infiltrating macrophages in lung to study the mechanism underlying MHV-68 reactivation triggered by NPs.

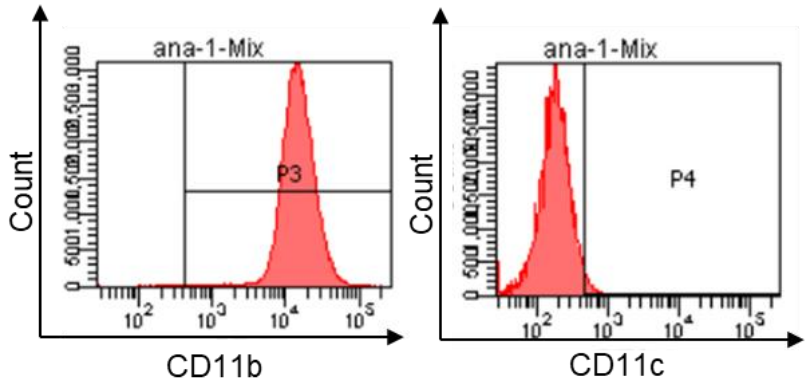

Figure 3.9 The expression of CD11b and CD11c in Ana-1 cells investigated by flow cytometry.

Ana-1 cells were either stained with CD11b or CD11c. Cells were incubated with CD11b-PE, CD11c-FITC antibody (1:50 dilution) on ice for 15 min, protect cells from light. Cells were acquired by FACScanto™ II flow cytometer and analyzed by FlowJo software (BD Biosciences, San Jose, CA, USA). Mean fluorescence Index (MFI) was used to show the intensity of CD11b or CD11c expression of the cells. Three independent experiments were conducted and one representative blot was shown.

3.3.2 NPs exposure triggered MHV-68 reactivation *in vitro*

To study MHV-68 reactivation, the establishment of "MHV-68 latency" *in vitro* model is needed. MHV-68 persistently latent infected Ana-1 cells (Ana-1/MHV-68 cells) were established before (Sattler et al., 2017) and used for following *in vitro* studies.

1. CNP and DWCNT induced Ana-1 cells viability decrease in a dose-dependent manner

Here, except for carbonaceous nanoparticles (CNP), we also included engineered double walled carbon nanotubes (DWCNT) in the study. To find a proper concentration, a dose-dependent cell viability alterations of two NPs were investigated including 12.5, 25, 50, 100, 200 and 400 µg/ml. Ana-1 cells treated with equal amount of medium was used as negative control. After 24 h, WST-1 assay was performed. As depicted in **Fig. 3.10**, both CNP and DWCNT induced a dose-dependent decrease of cell viability. At dose of 50 µg/ml, CNP and DWCNT induced 15% and 40% viability decrease respectively compared to control. With this dose, no severe cytotoxicity was observed and thus used for the following experiments.

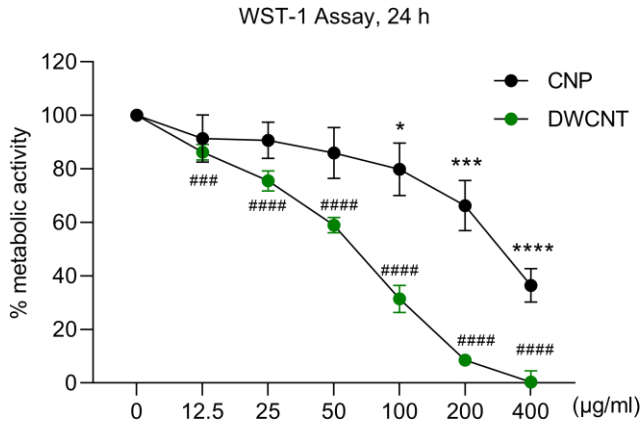

Figure 3.10 Ana-1 cell viability alteration induced by CNP and DWCNT.

Ana-1 cells were exposed to 12.5, 25, 50, 100, 200 and 400 μg/ml CNP or DWCNT, equal amount of medium was included as negative control. Cell viability was determined after 24 h by WST-1 assay. Three independent experiments were performed and included for statistical analysis. One-way ANOVA followed by Tukey's multiple comparisons test was used for statistical analysis. "*" and "#" indicates statistically significant difference between "CNP" and "DWCNT" with "control". $^{*}P < 0.05$, $^{**}P < 0.01$, $^{***}P < 0.001$, $^{****}P < 0.0001$. $^{\#}P < 0.05$, $^{\#\#}P < 0.01$, $^{\#\#\#}P < 0.001$, $^{\#\#\#\#}P < 0.0001$.

LPS (1 μg/ml) was used as a positive control to investigate MHV-68 reactivation in the *in vitro* study. Thus, we also investigated the effect of LPS on Ana-1 cells viability. As shown in **Fig. 3.11**, LPS at dose of 1 μg/ml did not trigger significant alteration of cell viability after 24 h.

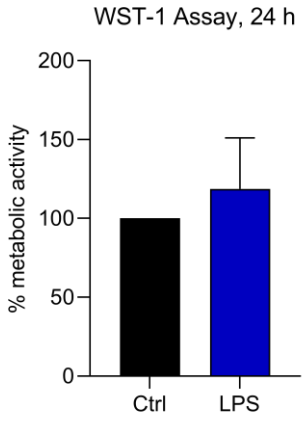

Figure 3.11 Ana-1 cell viability alteration induced by LPS.

Ana-1 cells were exposed to 1 μg/ml LPS, equal amount of medium was included as negative control. Cell viability was investigated with WST-1 assay after 24 h exposure. Three independent experiments were performed and included for statistical analysis. Data was analyzed by Student's t test and no difference was found in between.

2. CNP and DWCNT upregulated MHV-68 lytic viral gene expression and triggered virus titer increase *in vitro*

To study MHV-68 reactivation *in vitro*, Ana-1/MHV-68 cells were treated with CNP and DWCNT. LPS was used as a positive control. Cells were harvested to isolate RNA and investigate the kinetics of viral gene expression at different time points by qPCR. After 72 h, cell supernatant was collected and used to determine the infectious virus titer performed by Plaque assay. For viral gene expression determination, Open Reading Frame 50 (ORF50, expressed in the lytic phase of virus life cycle), Open Reading Frame 73 (ORF73, continuously expressed in all phases of virus life cycle) were detected and 60S ribosomal protein L8 (L8) was used as a housekeeping gene. Fold change of ORF50 and ORF73 was analyzed and the ratio of ORF50/ORF73 was shown to represent lytic viral gene expression. Here, the kinetics of viral gene expression was shown in **Fig. 3.12a**.

We found that both CNP and DWCNT upregulated lytic viral gene and the peak of viral gene upregulation appeared at 24 h post NPs exposure. In contrast, LPS triggered a stronger and faster lytic viral gene expression upregulation compared to NPs. The peak of lytic viral gene upregulation induced by LPS was 12 h but the lytic gene remained highly expression up to 72 h. Combining NPs and LPS exposure, 24 h time point will be used for the following experiments to investigate lytic viral gene expression.

In the other hand, plaque assay is a well-established method to quantify the infectious doses which reflects virus concentration. By infecting monolayer BHK-21 cells with supernatant from CNP, DWCNT or LPS treated Ana-1/MHV-68 cells after 72 h, the number of plaque forming units (pfu) was determined. As shown in **Fig. 3.12b**, plaque assay indicated that CNP and DWCNT triggered a significant increase of infectious virus titer. Similarly to lytic gene expression, LPS also triggered a higher infectious virus titer compared to NPs.

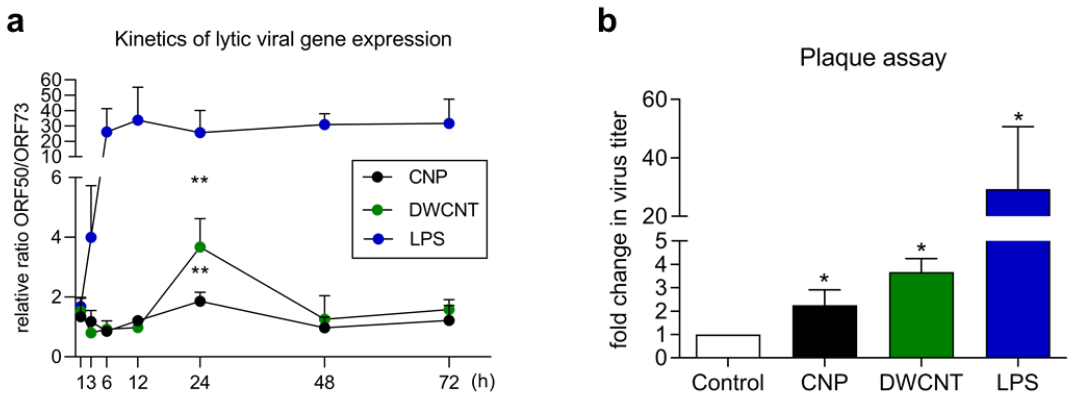

Figure 3.12 Nanoparticle exposure triggered the increase of lytic viral gene expression as well as infectious virus titer.

a. Kinetics of viral genes expression triggered by CNP and DWCNT at 50 μg/ml after 24 h in Ana-1/MHV-68 cells were performed by qPCR. LPS (1 μg/ml) was used as a positive control. Open Reading Frame 50 (ORF50, expressed in the lytic phase of virus life cycle), Open Reading Frame 73 (ORF73, continuously expressed in all phases of virus life cycle) were detected and 60S ribosomal protein L8 (L8) was used as a housekeeping gene. Fold change of ORF50 and ORF73 was analyzed and the ratio of ORF50/ORF73 was shown to represent viral gene expression. **b.** Plaque assay result performed from 72 h CNP and DWCNT (50 μg/ml) exposed Ana-1/MHV-68 cell supernatant, LPS (1 μg/ml) was used as a positive control. Student *t* test was used for statistical analysis. In all groups, N=3. * $P < 0.05$, ** $P < 0.01$.

3. CNP and DWCNT induced MHV-68 lytic virus protein expression *in vitro*

Furthermore, we also investigated whether CNP and DWCNT induced MHV-68 lytic protein expression in Ana-1/MHV-68 cells. Ana-1/MHV-68 cells were treated with CNP, DWCNT (50 μg/ml) and LPS (1 μg/ml). After 24 h, cells were fixed and stained with MHV-68 antiserum. As shown in **Fig. 3.13**, similarly to LPS, both CNP and DWCNT induced the increase of MHV-68 lytic virus protein expression.

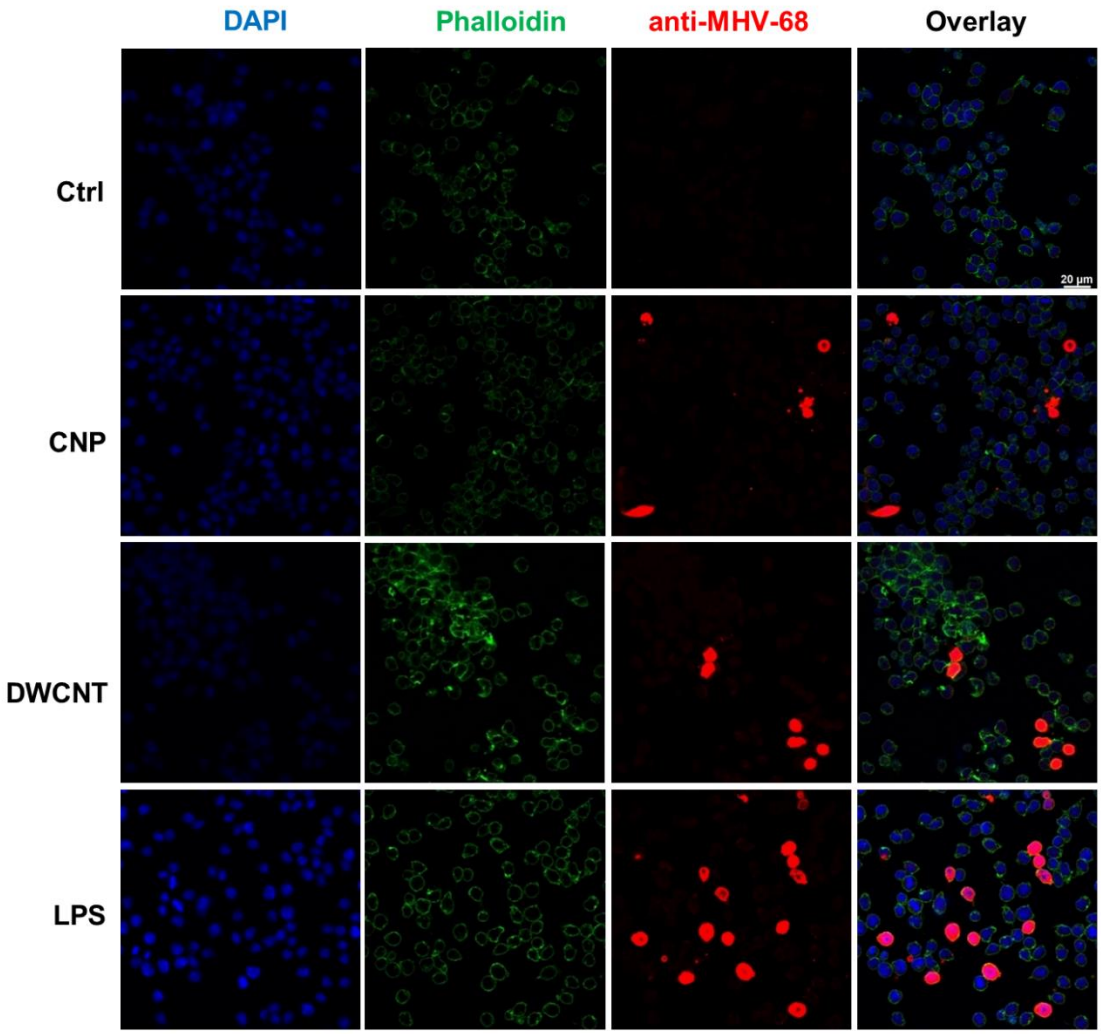

Figure 3.13 NPs exposure triggered MHV-68 lytic virus protein expression in Ana-1/MHV-68 cells.

Anti-MHV-68 serum immunofluorescence staining revealed lytic virus protein expression in Ana-1/MHV68 cells induced by CNP and DWCNT at 50 µg/ml after 24 h. Ana-1/MHV68 cells were harvested and fixed with 4% PFA after 24 h exposed to CNP and DNWCT, LPS (1 µg/ml) was used as a positive control. Anti-MHV-68 serum (red) staining represents lytic virus protein expression, DAPI (blue) and Phalloidin (green) staining represent nuclei and cell structure, respectively. Scale bar: 20 µm.

Taken together, CNP and DWCNT exposure triggered the upregulation of lytic viral gene expression, lytic virus protein expression as well as the increase of infectious virus titer, which all together confirmed MHV-68 reactivation induced by nanoparticle exposure *in vitro*.

3.3.3 CNP and DWCNT activated MAPK signaling pathway in Ana-1/MHV-68 cells

Up to now, we proved that CNP and DWCNT exposure triggered gammaherpesvirus reactivation both *in vitro* and *in vivo*. However, the underlying mechanism is still unclear.

MAPK signaling pathway is often described as pathways related to gammaherpesvirus infection and reactivation. In the other hand, MAPK signaling pathway can be activated by certain nanoparticle-cell interactions and contributes to pro-inflammatory responses.

Thus, we investigated whether CNP and DWCNT exposure activated MAPK signaling pathway and was involved in MHV-68 reactivation in the context of CNP and DWCNT exposure.

1. Silica particles were used as a positive control to activate MAPK signaling in Ana-1 cells

To investigate the MAPK signaling activation in Ana-1 cells, a positive control is needed. Fritsch-Decker and colleagues reported that engineered amorphous silica nanoparticles (nanosilica) activated MAPK signaling in RAW264.7 cells in early time points (Fritsch-Decker et al., 2018). Thus, we ought to investigate whether silica particle also activate MAPK signaling in Ana-1 cells and provide us a particle positive control.

MIN-U-SIL 5 Silica particles (Quartz) were used in the study. Quartz dust has been proved to cause severe and permanent lung inflammation and damage. Studies also found that Quartz causes Silicosis and cancer.

First, we studied the dose-response of Quartz on Ana-1 cells viability to determine proper concentration for the following experiments. As shown in **Fig. 3.14**, WST-1 assay revealed that Quartz triggered a dose-dependent decrease of cell viability in Ana-1 cells after 24 h exposure. In between, 50 µg/ml and 100 µg/ml Quartz caused 25% to 50% cell viability decline. As published by Fritsch-Decker et al., nanosilica activated MAPK signaling pathway at both concentrations (50 µg/ml and 100 µg/ml) and triggered higher level of kinase phosphorylation upon 100 µg/ml treatment (Fritsch-Decker et al., 2018). Taken together, Quartz at 100

µg/ml (Q100) was further used to investigate the MAPK signaling pathway activation in Ana-1 cells.

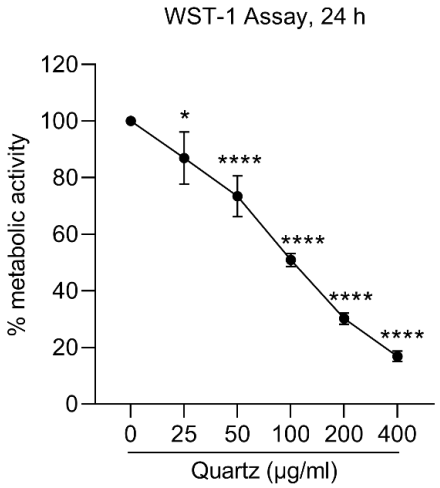

Figure 3.14 Dose-dependent cell viability alteration of Ana-1 cells exposed to quartz after 24 h.

Ana-1 cells were treated with Quartz (0, 25, 50, 100, 200 and 400 µg/ml). Cell viability was measured by WST-1 assay after 24 h. Negative control was normalized to 100% and the viability of Quartz treatments are the relative change compared to control. Four independent experiments were performed and included for statistical analysis. One-way ANOVA followed by Tukey's multiple comparisons test was used for statistical analysis. * $P < 0.05$, **** $P < 0.0001$.

Then, Ana-1 cells were exposed to 100 µg/ml Quartz (Q100) or equal amount of H_2O as negative control. Cells were harvested after 0.5, 1, 2, 4 and 6 h. Whole cell protein was extracted, phosphorylated and total protein of p38, ERK as well as JNK were detected by western blot. A ratio of phosphorylated/total protein band intensity was shown to represent the level of phosphorylation of each kinase. As shown in **Fig. 3.15**, p38 and JNK was phosphorylated by Q100 in a time-dependent manner in Ana-1 cells. p38 phosphorylation peaked at 6 h whereas JNK phosphorylation peaked at 4 h post Q100 exposure. However, ERK was faster phosphorylated compared to p38 and JNK, with significant induction after 30 min and 1 h exposure. Thus, Quartz at 100 µg/ml (Q100) activated MAPK signaling in Ana-1 cells.

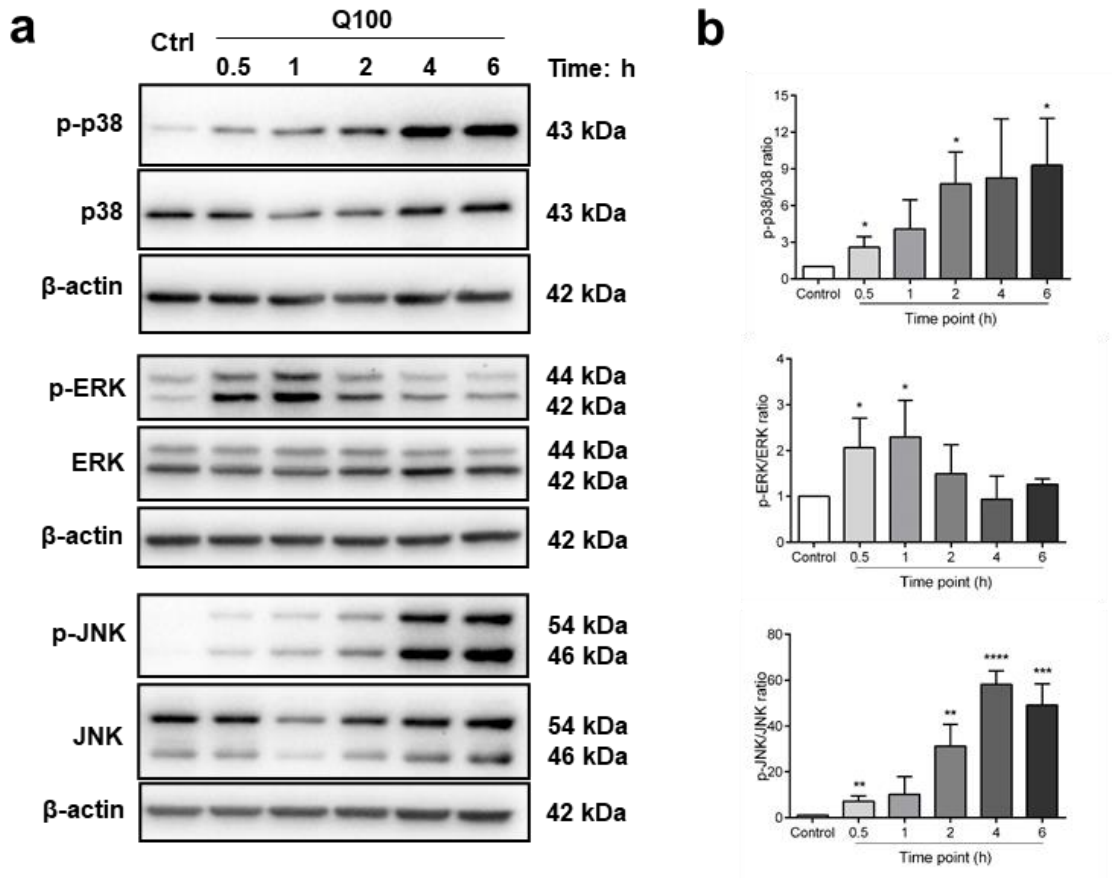

Figure 3.15 Quartz (Q100) activated MAPK signaling pathway in Ana-1 cells.

p38, ERK and JNK phosphorylation as well as total protein expression were investigated by western blot. β-actin was used as loading control. Representative blots were shown in **a**. Three independent experiments were performed and included for statistical analysis. Quantification of phosphorylation and total protein ratio was shown in **b**. Data was analyzed by Student's *t* test, "*" indicates statistically significant difference between "Q100" and "control". *: $P < 0.05$, **: $P < 0.01$, ***: $P < 0.001$, ****: $P < 0.0001$.

2. CNP and DWCNT activated MAPK signaling in Ana-1/MHV-68 cells

Later on, we investigated whether CNP and DWCNT at 50 μg/ml also activated MAPK signaling in Ana-1/MHV-68 cells. Cells were exposed to 50 μg/ml CNP or DWCNT, cells were harvested after 0.5, 1, 2, 4, 6 h. Whole cell protein was extracted, phosphorylated and total protein of p38, ERK as well as JNK were detected by western blot.

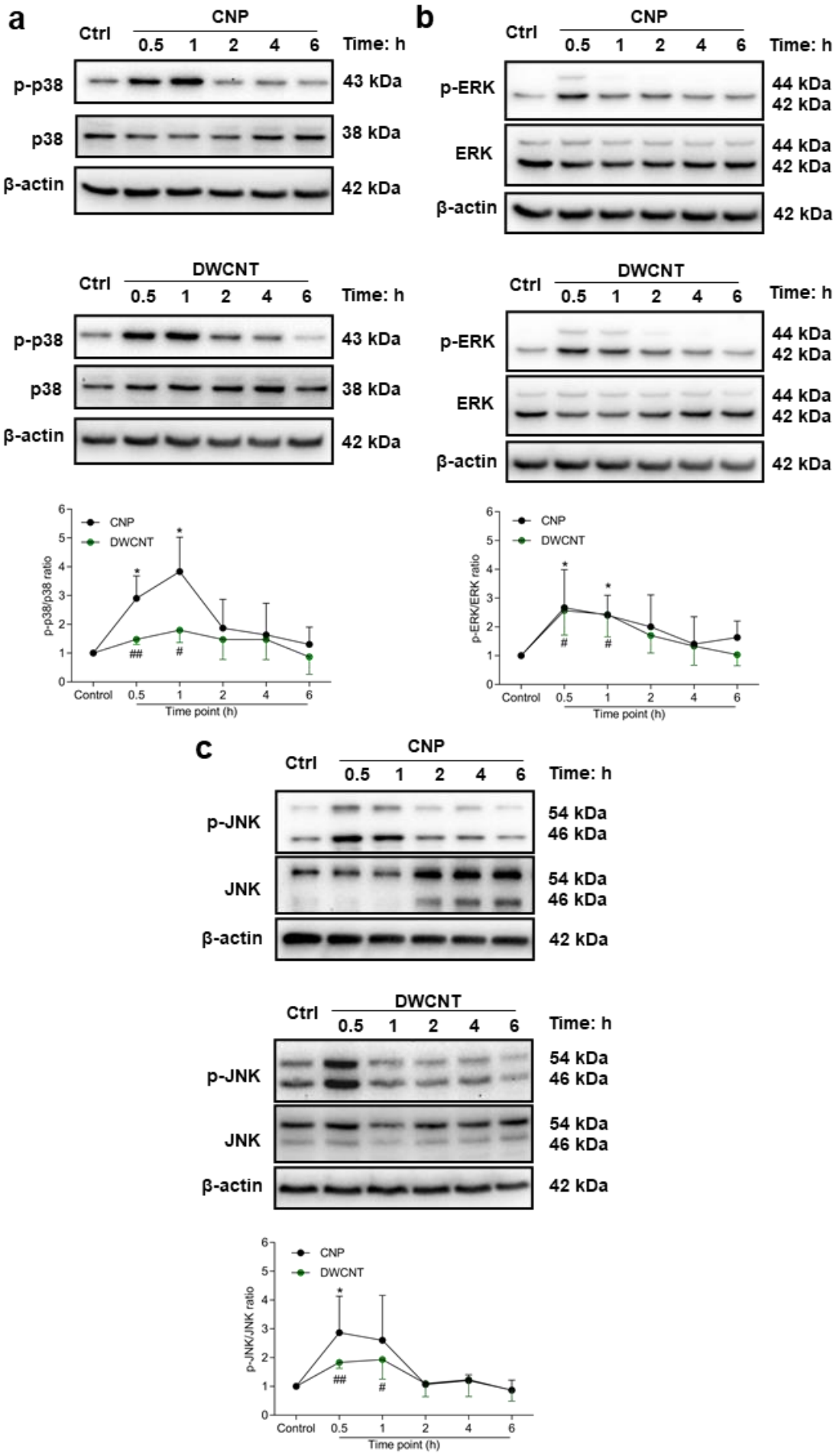
a
Ctrl
CNP
0.5 1 2 4 6
Time: h
p-p38
p38
β-actin
43 kDa
38 kDa
42 kDa
DWCNT
b
p-ERK
ERK
44 kDa
42 kDa
p-p38/p38 ratio
p-ERK/ERK ratio
Control
Time point (h)
c
p-JNK
JNK
54 kDa
46 kDa
p-JNK/JNK ratio

Figure 3.16 CNP and DWCNT activated MAPK signaling in early time points in Ana-1/MHV-68 cells.

Cells were treated with CNP (50 μg/ml), DWCNT (50 μg/ml) or equal amount of medium as control. Whole cell protein was extracted after 0.5, 1, 2, 4 and 6 h after exposure. Both phosphorylation and total protein expression of p38, ERK as well as JNK were detected. β-actin was used as loading control. A ratio of phosphorylated/total protein intensity was used to represent the level of phosphorylation. Three or four independent experiments were performed and included for statistical analysis. Representative blots and quantification results for p38 (**a**), ERK (**b**) and JNK (**c**) MAPK were shown here. Data was analyzed by Student's t test, "*" indicates statistically significant difference between "CNP" and "Control (Ctrl)" whereas "#" indicates statistically significant difference between "DWCNT" and "Control (Ctrl)". *: $P < 0.05$, #: $P < 0.05$, ##: $P < 0.01$.

We found that, CNP and DWCNT also triggered p38, ERK as well as JNK phosphorylation in Ana-1/MHV-68 cells. ERK was faster phosphorylated with significant induction after 30 min and 1 h after exposure. However, compared to quartz, p38 and JNK are faster phosphorylated with a significant induction after 30 min and 1 h. Representative blots and quantification results were shown in **Fig. 3.16**.

Taken together, both CNP and DWCNT activated MAPK signaling pathway in Ana-1/MHV-68 cells in early exposure time.

3.3.4 No characteristically pro-inflammatory polarization of macrophages by NPs exposure

1. Transcriptomic changes upon NPs exposure in Ana-1/MHV-68 cells

It is widely reported that MAPK signaling induction triggers downstream transcriptomic activation and contribute to pro-inflammatory response. Thus, we ought to investigate whether CNP and DWCNT triggered MAPK signaling alters transcriptomic activation which further contributes to MHV-68 reactivation.

Since both CNP and DWCNT induce significant p38, ERK and JNK phosphorylation after 30 min and 1 h, we isolated RNA from Ana-1/MHV-68 cells after 3 and 9 h CNP (50 μg/ml) and DWCNT (50 μg/ml) exposure and performed Affymetrix Microarray analysis. RNA isolated from LPS (1μg/ml) treated cells was used as a positive control.

In **Fig. 3.17a**, top upregulated and downregulated genes triggered by CNP and DWCNT at 3 and 9 h were shown in heatmap. To our surprise, there are less

amount of genes that were up-/down-regulated more than 2 folds, both NPs induced a mild alteration of transcriptomic activation. Next, we performed GSEA to investigate the underlying signaling activation. As shown in **Fig. 3.17b** & **c**, “TNFα signaling via NF-κB” is significantly activated by CNP and DWCNT after 9 h. There is the same signature of “TNFα signaling via NF-κB” activation for both NPs at 3 h after exposure (data not shown). A list of genes in the hallmark of signaling activation is shown in **Table 3.2**.

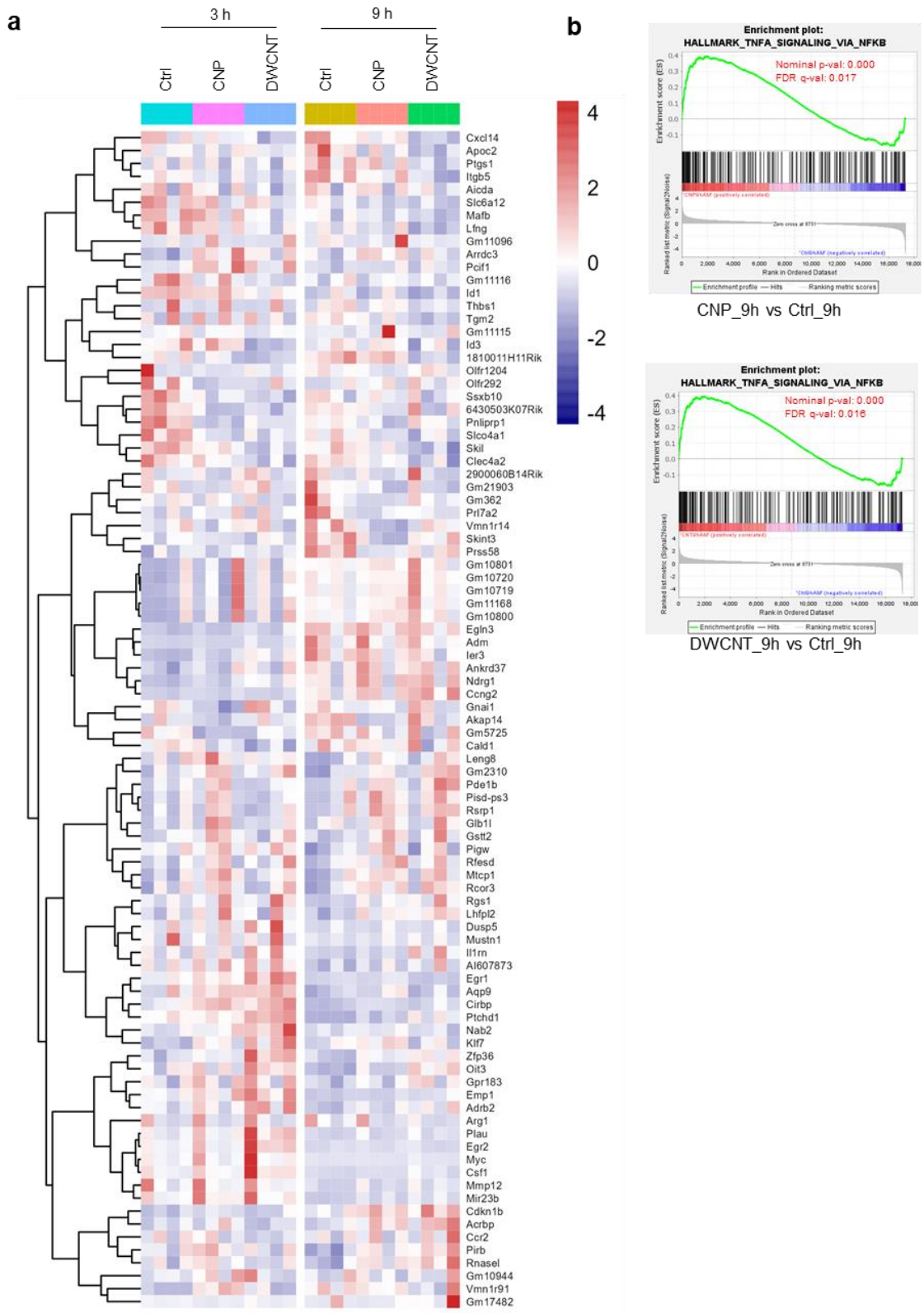

Figure 3.17 Transcriptomic study of Ana-1/MHV-68 cells treated with NPs with Affymetrix Microarray and GSEA analysis.

Ana-1/MHV-68 cells were exposed to CNP (50 µg/ml), DWCNT (50 µg/ml), LPS (1µg/ml) or equal amount of medium as control. Whole cell RNA was isolated after 3 and 9 h. RNAs with concentration more than 100 ng/µl, 260/280 ratio between 2.0 and 2.2 were later used for

microarray. RNA integrity number (RIN) value was more than 7 indicating good integrity of RNA. A list of top 50 upregulated and downregulated genes were sorted and heatmap was generated with R software (v4.0.4)and shown in **a**. GSEA analysis was performed to investigate the hallmark of activated signaling. Enrichment plots of "TNFα signaling via NF-κB" activation triggered by CNP and DWCNT after 9h were shown in **b** and **c**.

Table 3.2 Top regulated genes upon TNFa Signaling activation induced by CNP and DWCNT

No.	SYMBOL	TITLE	RANK IN GENE LIST	RANK METRIC SCORE	RUNNING ES	CORE ENRICHMENT
1	MYC	MYC proto-oncogene, bHLH transcription factor	0	3.72262764	0.031370264	Yes
2	CCL2	C-C motif chemokine ligand 2	1	3.672533989	0.062318392	Yes
3	CSF1	colony stimulating factor 1	8	2.859089136	0.08606113	Yes
4	TNF	tumor necrosis factor	14	2.499105215	0.10682873	Yes
5	PLAU	plasminogen activator, urokinase	17	2.444320679	0.12730995	Yes
6	EGR1	early growth response 1	21	2.175572634	0.14546803	Yes
7	PTGER4	prostaglandin E receptor 4	47	1.619469047	0.15765445	Yes
8	CEBPD	CCAAT enhancer binding protein delta	48	1.61574614	0.1712702	Yes
9	IL7R	interleukin 7 receptor	50	1.592536211	0.18463194	Yes
10	DUSP5	dual specificity phosphatase 5	51	1.586559892	0.19800176	Yes
11	SERPINB8	serpin family B member 8	54	1.574585676	0.21115379	Yes
12	MAP2K3	mitogen-activated protein kinase kinase 3	69	1.536373496	0.22328268	Yes
13	PLAUR	plasminogen activator, urokinase receptor	95	1.416049838	0.2337549	Yes
14	BCL6	BCL6 transcription repressor	118	1.333537698	0.24370709	Yes
15	CCND1	cyclin D1	137	1.275913119	0.2534074	Yes
16	EGR2	early growth response 2	144	1.260162592	0.2636761	Yes
17	GPR183	G protein-coupled receptor 183	162	1.201536179	0.27280807	Yes
18	LITAF	lipopolysaccharide induced TNF factor	167	1.191399932	0.28261417	Yes
19	ETS2	ETS proto-oncogene 2, transcription factor	170	1.188235283	0.29251048	Yes
20	DUSP2	dual specificity phosphatase 2	178	1.177777767	0.3020265	Yes
21	IER2	immediate early response 2	192	1.143011928	0.31089902	Yes
22	PHLDA1	pleckstrin homology like domain family A member 1	196	1.136363626	0.32029977	Yes
23	KLF2	Kruppel like factor 2	199	1.127321005	0.32968274	Yes
24	SQSTM1	sequestosome 1	204	1.119483352	0.33888283	Yes
25	JAG1	jagged canonical Notch ligand 1	216	1.105675101	0.34755754	Yes
26	FOSL1	FOS like 1, AP-1 transcription factor subunit	229	1.086261988	0.35601026	Yes
27	EHD1	EH domain containing 1	237	1.07996428	0.36470202	Yes
28	RHOB	ras homolog family member B	268	1.043360472	0.37174147	Yes
29	ATP2B1	ATPase plasma membrane Ca2+ transporting 1	269	1.042428732	0.38052592	Yes
30	IL6ST	interleukin 6 signal transducer	270	1.04203701	0.38930708	Yes
31	SGK1	serum/glucocorticoid regulated kinase 1	280	1.025200486	0.3974205	Yes
32	FOS	Fos proto-oncogene, AP-1 transcription factor subunit	306	1	0.40438673	Yes
33	TRAF1	TNF receptor associated factor 1	328	0.98173517	0.4114327	Yes

34	ID2	inhibitor of DNA binding 2	331	0.98083657	0.4195813	Yes
35	JUNB	JunB proto-oncogene, AP-1 transcription factor subunit	352	0.960183024	0.4265041	Yes
36	RCAN1	regulator of calcineurin 1	390	0.921165407	0.43210486	Yes
37	DUSP4	dual specificity phosphatase 4	412	0.893266618	0.43840533	Yes
38	PFKFB3	6-phosphofructo-2-kinase/fructose-2,6-biphosphatase 3	450	0.859429359	0.44348583	Yes
39	B4GALT1	beta-1,4-galactosyltransferase 1	469	0.845949769	0.44956285	Yes
40	ABCA1	ATP binding cassette subfamily A member 1	473	0.842696607	0.4564889	Yes
41	PLK2	polo like kinase 2	500	0.828265131	0.4619495	Yes
42	CEBPB	CCAAT enhancer binding protein beta	677	0.743944645	0.45793527	Yes
43	PLEK	pleckstrin	696	0.734387338	0.46307218	Yes
44	TRIB1	tribbles pseudokinase 1	711	0.729166687	0.4683988	Yes
45	IER5	immediate early response 5	713	0.72859025	0.47448015	Yes
46	CD44	CD44 molecule	835	0.686947048	0.47319916	Yes
47	JUN	Jun proto-oncogene, AP-1 transcription factor subunit	877	0.674888909	0.47649086	Yes
48	ZC3H12A	zinc finger CCCH-type containing 12A	879	0.674418628	0.4821157	Yes

2. The effect of CNP and DWCNT exposure on classical pro-inflammatory genes expression

Then we investigated whether CNP and DWCNT exposure triggered a pro-inflammatory response. A cluster of classical pro-inflammation genes were sorted and showed in the heatmap in **Fig. 3.18**. After 3 h exposed to LPS, there are significant Cxcl10, Cxcl2, Tnf, Ptgs2, Il1b and Il6 upregulation. Meanwhile, COX-2, Cxcl1, Cxcl5, Saa3 as well as Lcn2 are upregulated 9 h post LPS exposure. However, no these relative genes were upregulated upon CNP and DWCNT exposure either 3 or 9 h after exposure.

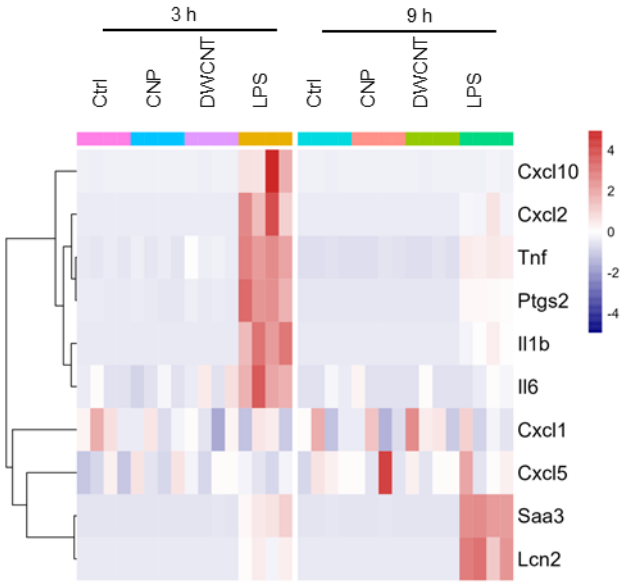

Figure 3.18 Cluster of classical genes related to pro-inflammatory response induced by CNP, DWCNT and LPS.

Classical genes related to pro-inflammatory responses were sorted in dataset and heatmap was generated with R software (pheatmap package) to visualize gene expression. Ctrl, CNP, CNT and LPS represent treatment of “Control”, “CNP (50 μg/ml)”, “DWCNT (50 μg/ml)” and “LPS (1 μg/ml)” to Ana-1/MHV-68 cells. Both gene data from 3 and 9 h exposure were generated. Four independent experiments were performed and included for analysis.

Compared to CNP and DWCNT, LPS showed a strong response and there are a number of genes upregulated after 3 and 9 h exposure. Top upregulated and downregulated genes were shown in heatmap (**Fig. 3.19a**). We also found signature of general higher level gene expressions at 3 h compared to 9 h. Next, volcano plots (**Fig. 3.19b**) showed the most upregulated genes by LPS at two time points, including Cxcl2, Il1b, Il6, Saa3, Lcn2, Nos2, which are widely reported to be involved in pro-inflammatory responses.

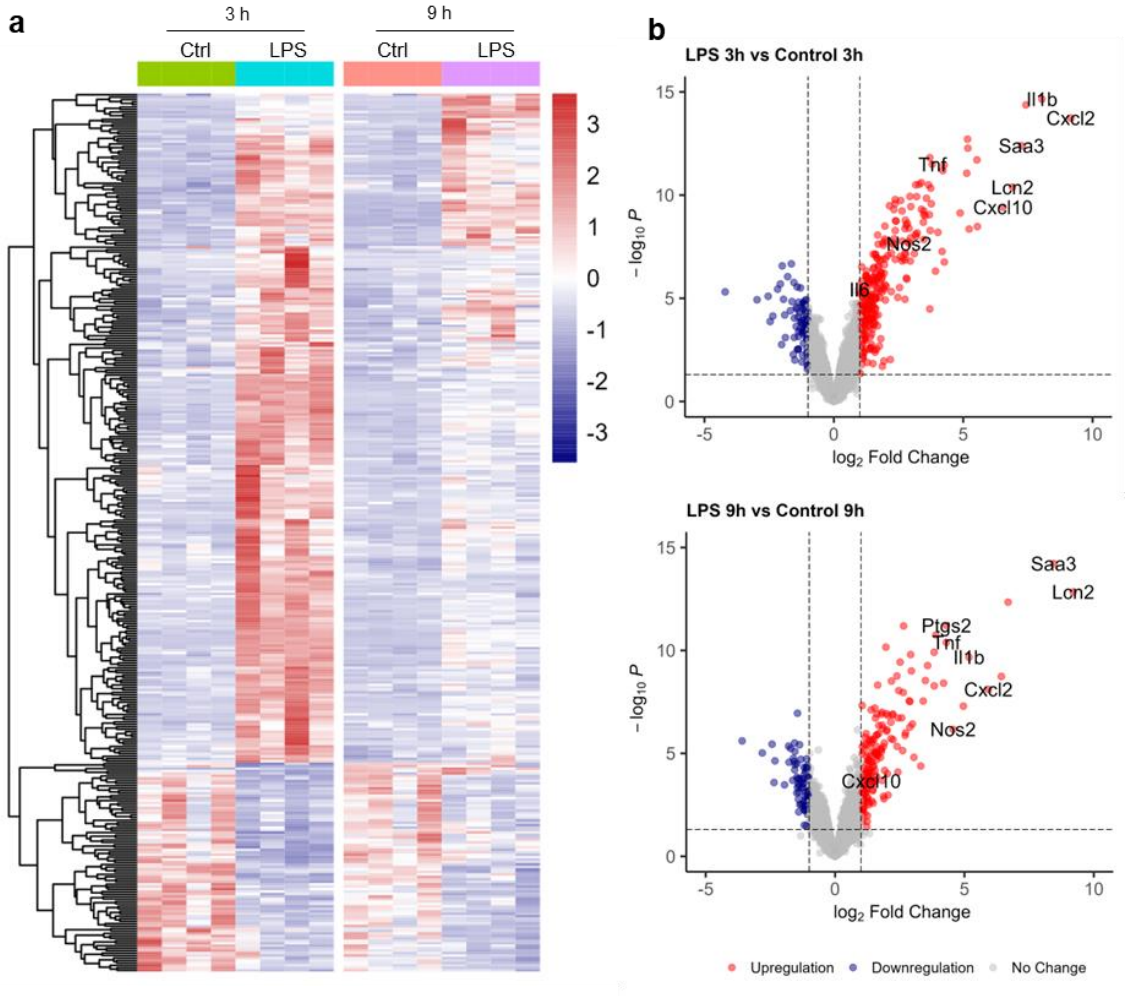

Figure 3.19 Transcriptomic study of Ana-1/MHV-68 cells exposed to LPS with Affymetrix Microarray analysis.

a. A list of top upregulated and top downregulated genes induced by LPS after 3 and 9 h exposure were sorted and heatmap was generated with R. **b**. Volcano plots were generated with R software to show the top regulated genes after LPS exposure at 3 & 9 h.

We next confirmed some of those genes expression by qPCR and data were shown in **Fig. 3.20**. Similar to microarray results, both NPs did not trigger Saa3, Il1b, Il6, Nos2 and Ptgs2 upregulation at 1, 3, 6 and 12 h post exposure, whereas strong inductions by LPS treatment were observed.

Thus, CNP and DWCNT exposure did not trigger characteristically pro-inflammatory polarization of macrophages *in vitro.*

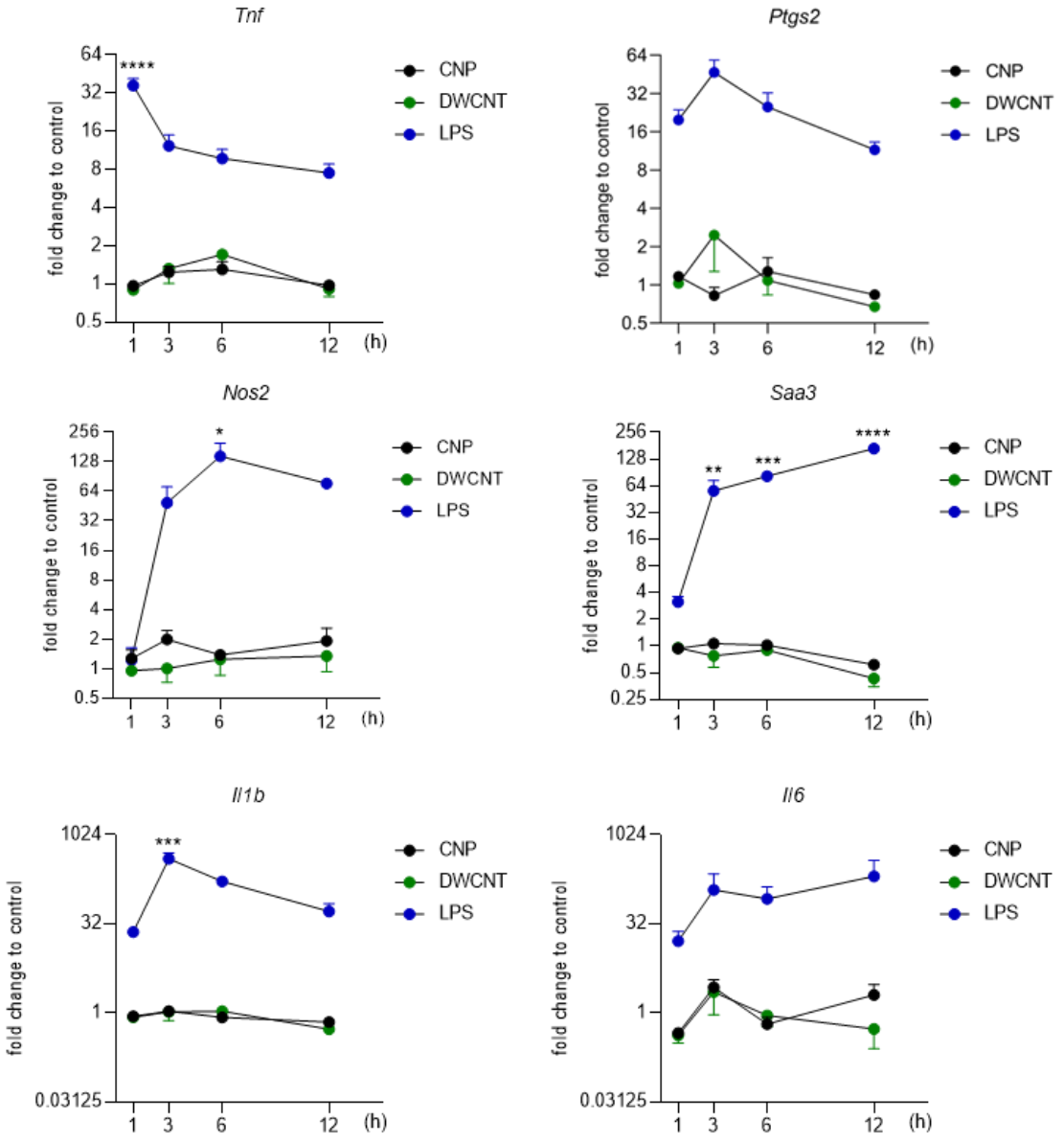

Figure 3.20 Classical pro-inflammatory genes expression confirmation performed by qPCR.

Ana-1/MHV-68 cells were exposed to CNP (50 μg/ml), DWCNT (50 μg/ml), LPS (1 μg/ml) or equal amount of medium as control. Whole cell RNA was isolated after 1, 3, 6, 12 h. cDNA was synthesized, Saa3, Il1b, Nos2, Il6, Tnf and Ptgs2 was detected by qPCR. Hprt was used as a housekeeping gene. Results were shown as fold change normalized to control. Four or five independent experiments were performed and included for statistical analysis. One-way ANOVA as well as post Tukey's multiple comparisons test were used. * $P < 0.05$, ** $P < 0.01$, *** $P < 0.001$, **** $P < 0.0001$.

3.3.5 p38 inhibition by SB203580 efficiently inhibits p38 MAPK signaling pathway and attenuates MHV-68 reactivation induced by CNP

Currently, we found that both CNP and DWCNT induced MAPK signaling pathway activation in Ana-1/MHV-68 cells. Then the association of MAPK activation with MHV-68 reactivation induced by NPs needs further investigation.

Here, we applied p38, ERK and JNK specific inhibitors to investigate whether the abolishment of MAPK signaling attenuated MHV-68 lytic viral gene expression as well as infectious virus titer. A schematic representation was shown in **Fig. 3.21**. Briefly, cells were treated with specific inhibitors 30 min prior to CNP (50 μg/ml), DWCNT (50 μg/ml) or LPS (1μg/ml), equal amount of medium treated to cells was included as control. Whole cell protein was extracted after 1 h to investigate phosphorylation and total protein expression of three kinases. RNA was isolated after 24 h to detect viral gene expression and plaque assay was performed with supernatants collected after 72 h.

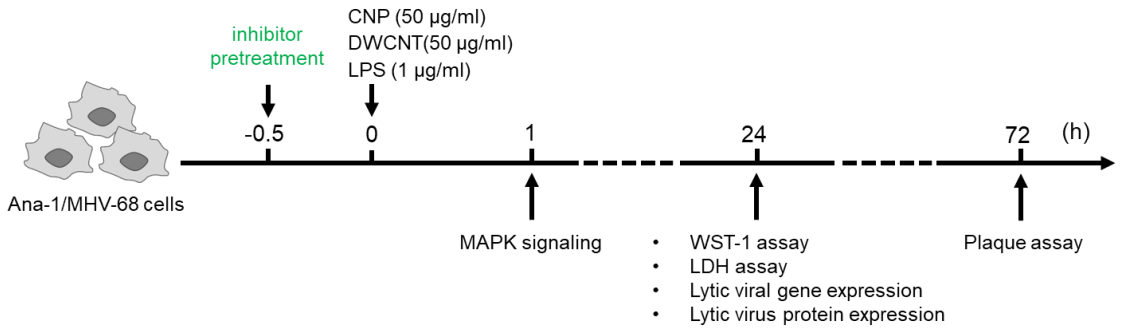

Figure 3.21 Schematic representation of study on the effect of inhibitor pretreatment on MHV-68 reactivation induced by NPs.

Cells were treated with specific inhibitors 30 min prior to CNP (50 μg/ml), DWCNT (50 μg/ml) or LPS (1μg/ml) treatment, equal amount of medium treated to cells was included as control. Whole cell protein was extracted after 1 h to study phosphorylation and total protein expression of three

kinases. RNA was isolated after 24 h to detect viral gene expression and plaque assay was performed with supernatants collected after 72 h.

SB203580, a selective p38 inhibitor, has been widely used to block the activation of MAPKAPK-2, which is the p38 MAPK downstream target.

First, we investigated whether the application of p38 inhibitor brings further toxic effects to Ana-1/MHV-68 cells performed by WST-1 and LDH assay. As shown in **Fig. 3.22 a & b**, CNP and DWCNT at dose of 50 µg/ml exhibited similar cell viability decrease as we showed before but no significant LDH release. Cells either treated with the highest concentration of p38 inhibitor (10 µM) alone or together with CNP, DWCNT or LPS treatment showed no further cell viability alteration and LDH release. Thus, p38 inhibitor at current concentration was not toxic to Ana-1/MHV-68 cells.

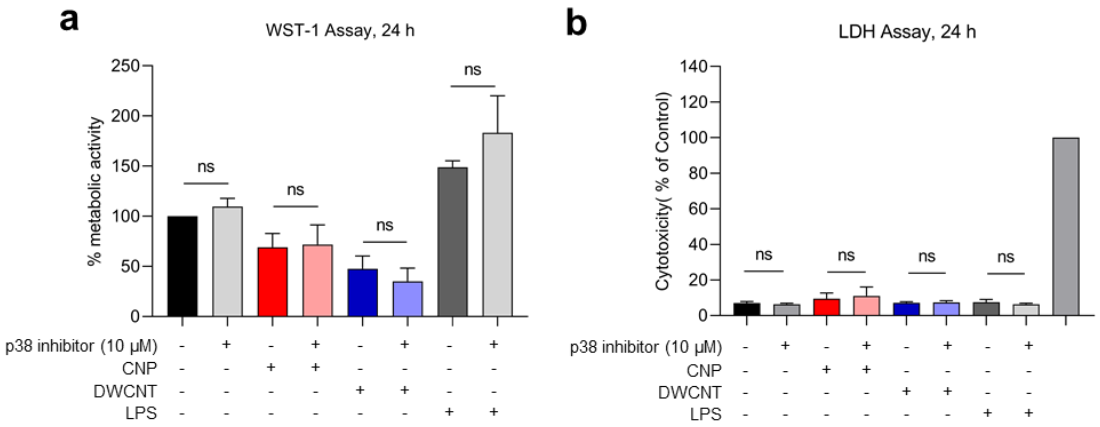

Figure 3.22 The toxic effect of p38 inhibitor to Ana-1/MHV-68 cells after 24 h.

WST-1 assay (**a**) and LDH assay (**b**) was performed to investigate cell viability change and cytotoxicity, respectively. p38 inhibitor (10 µM) was pretreated to cells 30 min prior to NPs (50 µg/ml) or LPS (1 µg/ml) treatment. Equal amount of medium treated to cells was included as control. After 24 h, supernatant was collected to perform LDH assay whereas cells were left to perform WST-1 assay. For LDH assay, 1% Triton X-100 lysed cells in medium was used as a positive control for LDH release. Three independent experiments were performed and included for statistical analysis. Student *t* test was made between each treatment with or without p38 inhibitor pretreatment. “ns”, no significance.

Next, we pretreated Ana-1/MHV-68 cells with p38 inhibitor to investigate the role on p38 as well as MAPKAPK2 phosphorylation. p38 inhibitor with three different concentrations (0.6, 1 & 10 µM) showed no effect to inhibit p38 phosphorylation, data was shown in **Fig. 3.23a**. However, MAPKAPK2, the downstream target of

p38 MAPK, was less phosphorylated when cells were pretreated with p38 inhibitor (10 μM) compared to relevant CNP, DWCNT or LPS treatment (**Fig. 3.23**), demonstrating an effective inhibition of p38 inhibitor on p38 MAPK signaling.

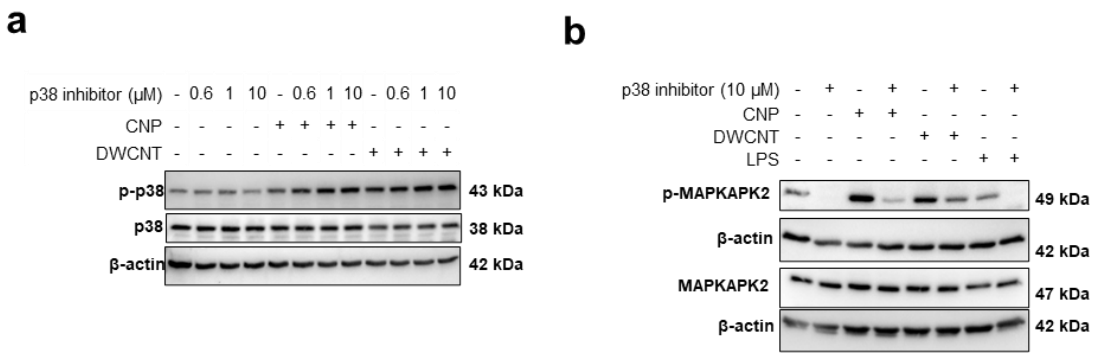

Figure 3.23 p38 inhibitor blocked MAPKAPK2 phosphorylation induced by NPs.

Cells were pretreated with p38 inhibitor 30 min prior to NPs (50 μg/ml) or LPS (1 μg/ml) treatment. Equal amount of medium treated to cells was included as control. Whole cell protein was extracted after 1 h to investigate phosphorylation and total protein expression by western blot. p38 inhibitor with only 10 μM was used to investigate MAPKAPK2 expression. β-actin was used as loading control. **a**. the effect of p38 inhibitor (0.6, 1 & 10 μM) on p38 phosphorylation and total protein expression induced by NPs or LPS. **b**. the effect of p38 inhibitor (10 μM) on MAPKAPK2 phosphorylation and total protein expression induced by NPs or LPS. Three independent experiments were performed and representative blots were shown here.

Next, to investigate whether p38 MAPK signaling activation contributes to herpesvirus reactivation, lytic viral gene expression and infectious virus titer were detected after p38 inhibitor pretreatment and NPs exposure. Results were shown in **Fig. 3.24**. Consistently with our former findings, CNP and DWCNT at 50 μg/ml triggered a significant increase of lytic viral gene expression. p38 inhibition sufficiently blocked CNP and LPS but not DWCNT induced lytic viral gene upregulation. Similar effect of p38 inhibition was also found in infectious virus titer attenuation of CNP and LPS groups but not DWCNT.

Thus, CNP but DWCNT induced herpesvirus reactivation is depending on p38 MAPK signaling pathway activation.

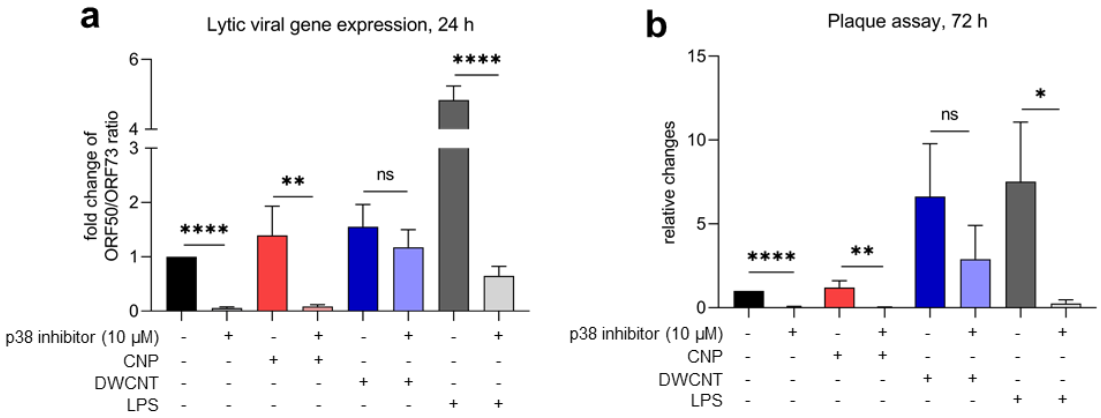

Figure 3.24 Effect of p38 MAPK inhibition on lytic viral gene expression and infectious virus titer.

Ana-1/MHV-68 cells were pretreated with p38 inhibitor (10 μM) 30 min prior to NPs (50 μg/ml) or LPS (1 μg/ml) treatment. Equal amount of medium treated to cells was included as control. RNA was isolated after 24 h to investigate ORF50 and ORF73 gene expression by qPCR, L8 was used as housekeeping genes. Fold changes of genes were calculated and the ratio of ORF50 to ORF73 was shown to represent lytic viral gene expression level. Plaque assay was performed to investigate the infectious virus titer change with supernatant collected after 72 h. Four independent experiments were performed and included for statistical analysis. Student *t* test was made between each treatment with or without p38 inhibitor pretreatment. "*", $P < 0.05$; "**", $P < 0.01$; "***", $P < 0.001$; "****", $P < 0.0001$; "ns", no significance.

3.3.6 ERK inhibitor pretreatment failed to block MHV-68 reactivation induced by NPs exposure

Similarly, we next investigated the contribution of ERK MAPK signaling in herpesvirus reactivation induced by NPs exposure. ERK specific inhibitor (PD98059) was used in the study.

First, the toxic effect of ERK inhibitor on Ana-1/MHV-68 cells was studies. We found that ERK inhibitor at 50 μM reduced cell viability but did not trigger LDH release (**Fig. 3.25**).

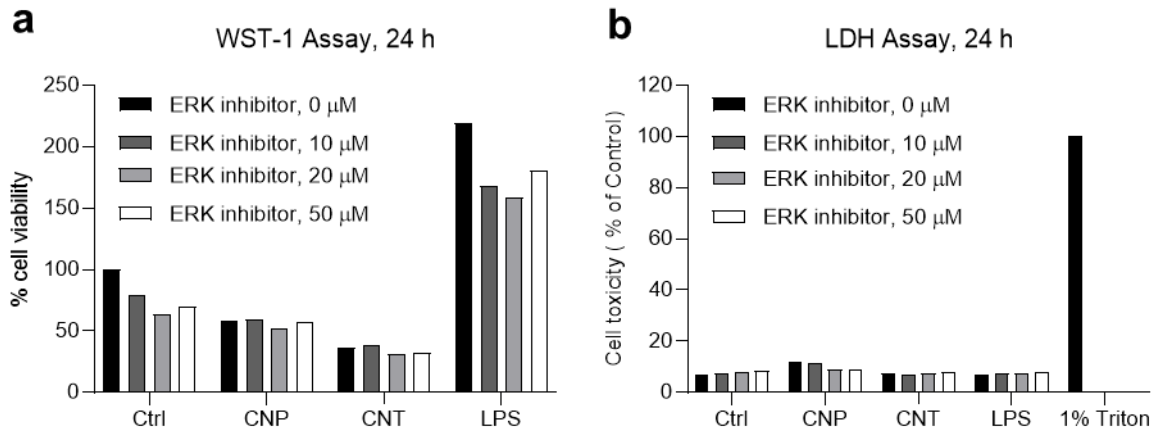

Figure 3.25 Cytotoxicity of ERK inhibitors to Ana-1/MHV-68 cells performed by WST-1 and LDH assay.

Ana-1/MHV-68 cells were pretreated with ERK inhibitor (PD95059, 50 μM) 30 min prior to NPs (50 μg/ml) or LPS (1 μg/ml) treatment. Equal amount of medium treated to cells was included as control. After 24 h, supernatant was collected to perform LDH assay whereas cells were left to perform WST-1 assay. For LDH assay, 1% Triton X-100 lysed cells in medium was used as a positive control for LDH release. Three independent experiments were performed and included for statistical analysis. One-way ANOVA as well as post Tukey's multiple comparisons test were used. * $P < 0.05$.

Next, whether ERK inhibitor pretreatment can abolish ERK phosphorylation was studied. As shown in Figure 3.26, ERK inhibitor reduced the basal level of ERK phosphorylation, the upregulation of ERK phosphorylation induced by CNP and DWCNT exposure was also inhibited.

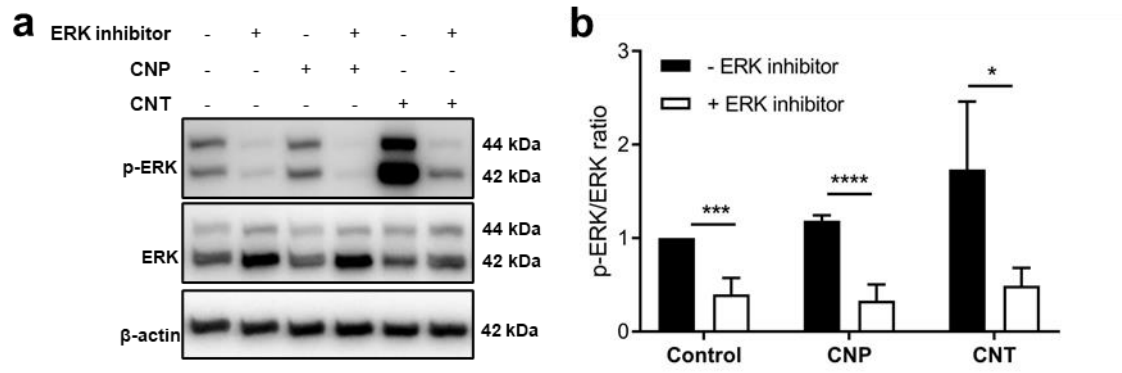

Figure 3.26 ERK inhibition abolished ERK phosphorylation induced by NPs.

Ana-1/MHV-68 cells were pretreated with ERK inhibitor (PD98059, 50 μM) 30 min prior to NPs (50 μg/ml) treatment. Equal amount of medium treated to cells was included as control. Whole cell protein was extracted after 1 h to investigate ERK phosphorylation

and total protein expression by western blot. β-actin was used as loading control. Three independent experiments were performed and representative blots were shown here.

Next, to investigate whether the abolishment of ERK signaling contribute to herpesvirus reactivation, lytic viral gene expression and infectious virus titer alteration was studied. To our surprise, ERK signaling inhibition triggered even stronger upregulation of lytic viral gene as well as elevated infectious virus titer in all treatments including the ERK inhibitor treatment alone, which suggested a further elevated herpesvirus reactivation. Results were shown in **Fig. 3.27**.

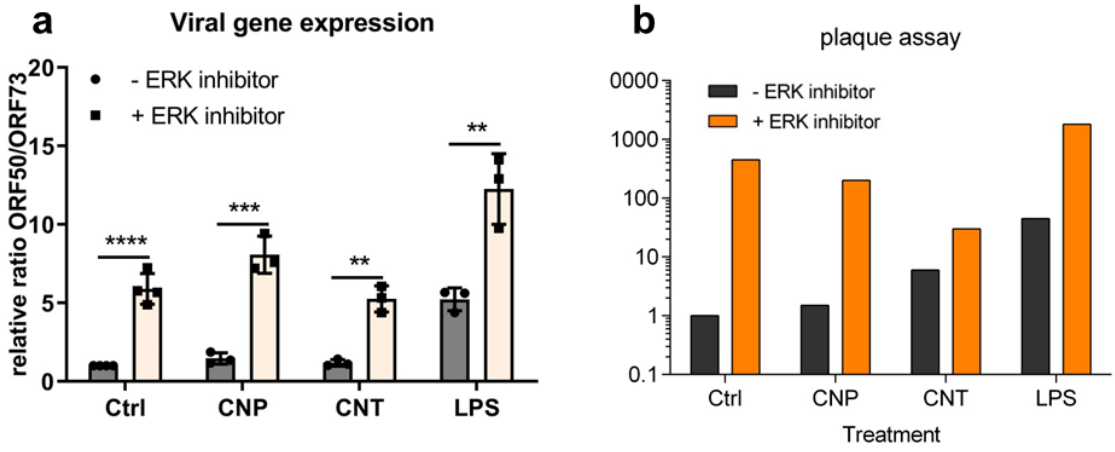

Figure 3.27 ERK inhibitor pretreatment triggered stronger MHV-68 reactivation induced by NPs and LPS.

Ana-1/MHV-68 cells were pretreated with ERK inhibitor (PD98059, 50 μM) 30 min prior to NPs (50 μg/ml) or LPS (1 μg/ml) treatment. Equal amount of medium treated to cells was included as control. RNA was isolated after 24 h to investigate ORF50 and ORF73 gene expression by qPCR, L8 was used as housekeeping genes. Fold changes of genes were calculated and the ratio of ORF50 to ORF73 was shown to represent lytic viral gene expression level. Plaque assay was performed to investigate the infectious virus titer change with supernatant collected after 72 h. Four independent experiments were performed and included for statistical analysis. Student *t* test was made between each treatment with or without ERK inhibitor pretreatment. "*", $P < 0.05$; "**", $P < 0.01$; "***", $P < 0.001$; "****", $P < 0.0001$; "ns", no significance.

Since ERK inhibition reduced cell viability, next we investigated whether the stronger reactivation induced by ERK inhibition was related to cell death.

It has been proved that ERK inhibitor induce apoptosis. We stained Ana-1/MHV-68 cells with claved-caspase3, a key event in apoptosis, to see whether ERK inhibition activate apoptosis. We found that CNP at 50 μg/ml has no effect on cleaved-caspase 3 expression but ERK treatment or together with CNP significantly upregulated cleaved-caspase 3 (**Fig. 3.28**). The result demonstrated the occurrence of apoptosis induced by ERK inhibition.

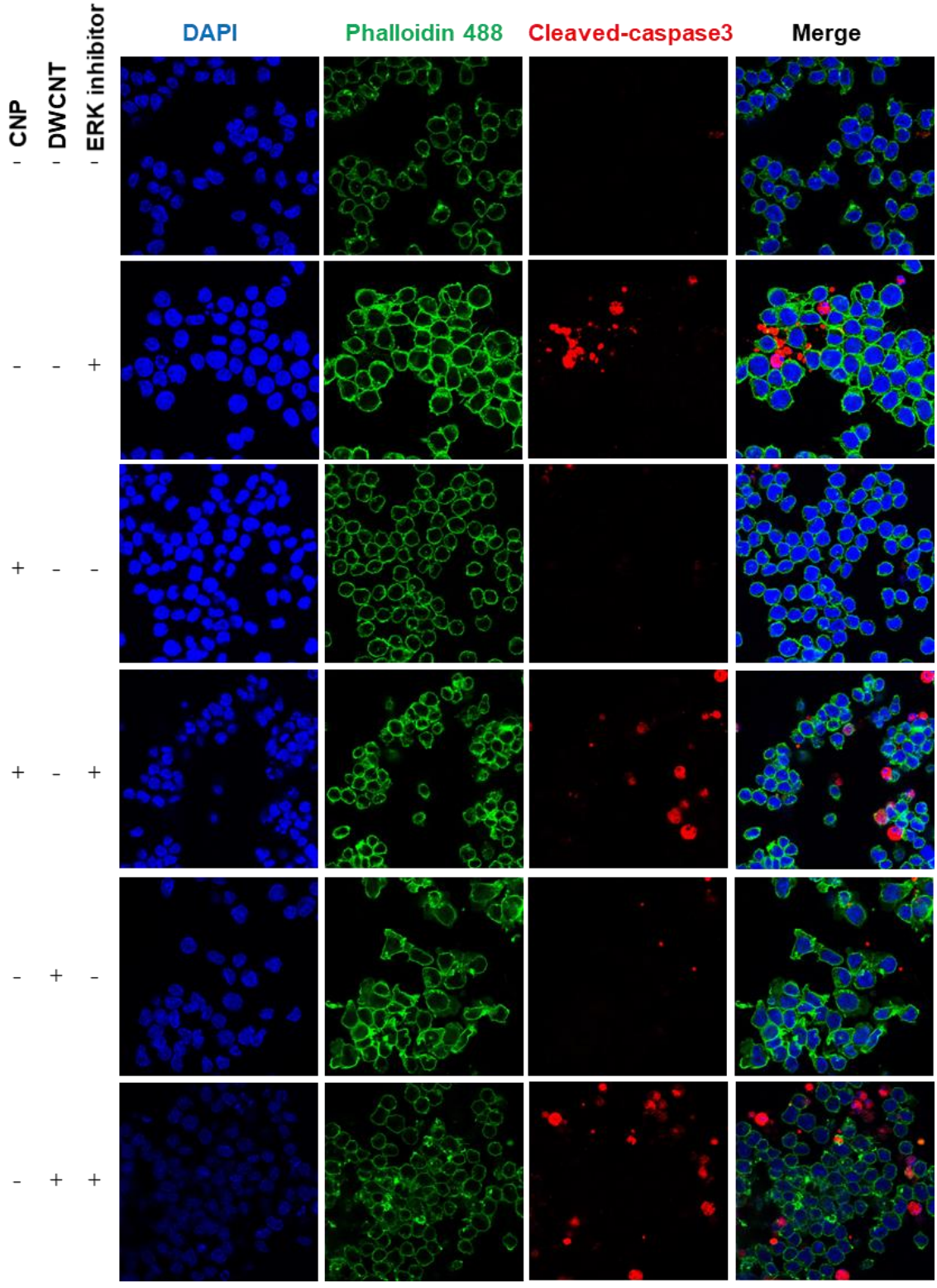

Figure 3.28 ERK inhibition triggered apoptosis in Ana-1/MHV-68 cells.

Ana-1/MHV68 cells were pretreated with ERK inhibitor (PD98059, 50 μM) 30 min prior to NPs (50 μg/ml) treatment. Equal amount of medium treated to cells was included as control. Cells were fixed and stained with cleaved-caspase 3 (red), Phalloidin 488 (green) and DAPI (blue) after 24 h. Representative images were shown.

We also tried to use low concentration of ERK inhibitor, but we also see ERK inhibition triggered higher lytic viral gene expression (**Fig. 3.29**).

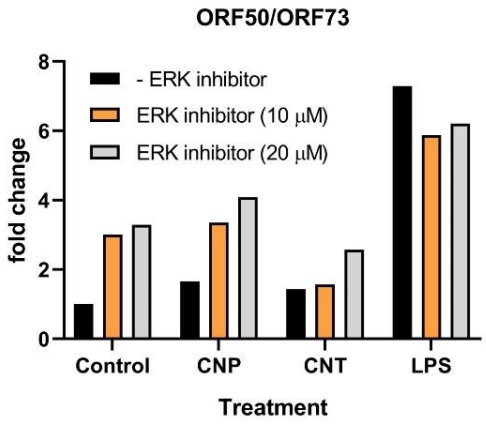

Figure 3.29 ERK inhibitor in lower concentration still triggered MHV-68 lytic viral gene upregulation.

Ana-1/MHV-68 cells were pretreated with ERK inhibitor (PD98059, 10, 20 μM) 30 min prior to NPs (50 μg/ml) or LPS (1 μg/ml) treatment. Equal amount of medium treated to cells was included as control. RNA was isolated after 24 h to investigate ORF50 and ORF73 gene expression by qPCR, L8 was used as housekeeping genes. Fold changes of genes were calculated and the ratio of ORF50 to ORF73 was shown to represent lytic viral gene expression level.

Taken together, ERK MAPK signaling contributed not to MHV-68 reactivation induced by NPs but played an important role in the maintenance of latency in Ana-1/MHV-68 cells.

3.3.7 JNK inhibitor pretreatment failed to block MHV-68 reactivation induced by NPs exposure

Here, JNK specific inhibitors were used to investigate the contribution of JNK MAPK signaling to herpesvirus reactivation.

First, we found that JNK inhibitor showed no further significant toxic effect to Ana-1/MHV-68 cells either treated alone or together with NPs as well as LPS treatment (**Fig. 3.30**).

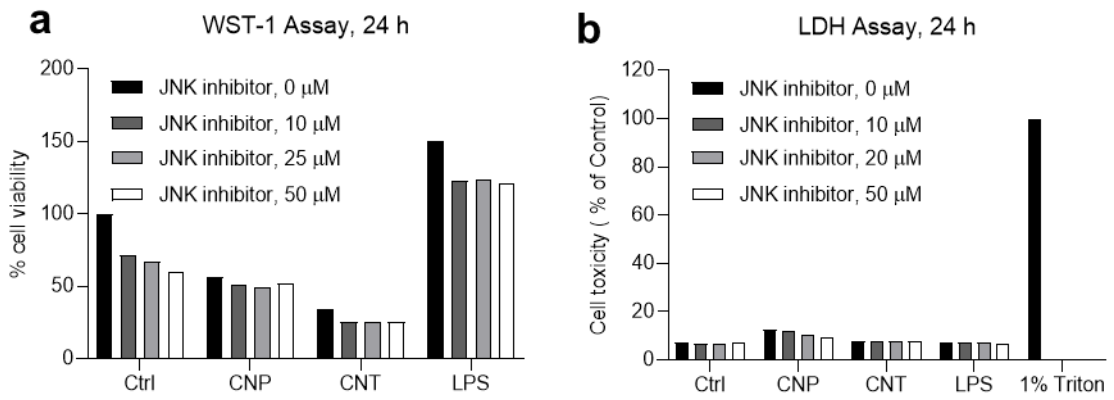

Figure 3.30 Cytotoxicity of JNK inhibitors treatment to Ana-1/MHV-68 cells.

Ana-1/MHV-68 cells were pretreated with JNK inhibitor (10, 25 and 50 μM) 30 min prior to NPs (50 μg/ml) or LPS (1 μg/ml) treatment. Equal amount of medium treated to cells was included as control. After 24 h, supernatant was collected to perform LDH assay whereas cells were left to perform WST-1 assay. For LDH assay, 1% Triton X-100 lysed cells in medium was used as a positive control for LDH release. Three independent experiments were performed and included for statistical analysis. One-way ANOVA as well as post Tukey's multiple comparisons test were used.

Next, the effect of JNK inhibition on the phosphorylation of JNK as well as downstream target c-Jun was investigated. As shown in **Fig. 3.31**, there was not a significant inhibition of JNK inhibition on JNK but c-Jun phosphorylation triggered by both CNP and DWCNT. JNK inhibitor at dose of 50 μM exhibited the strongest effect and was further used to study the involvement of JNK MAPK in herpesvirus reactivation induced by NPs exposure.

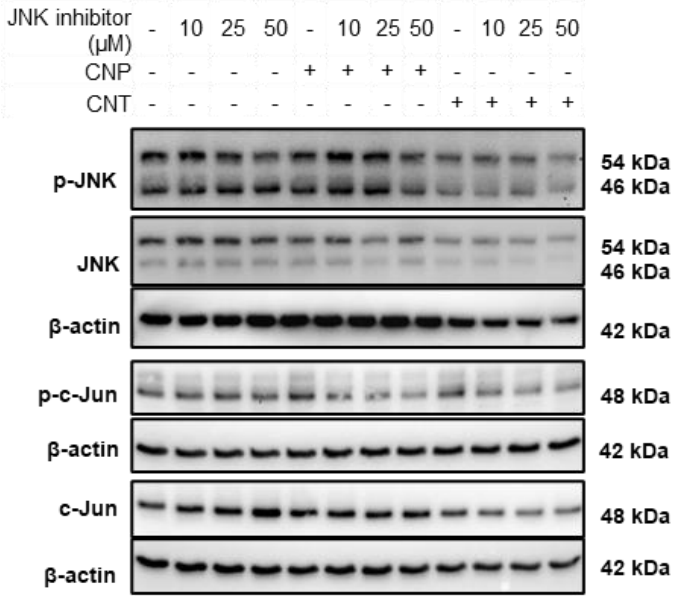

Figure 3.31 The role of JNK inhibition on JNK and c-Jun phosphorylation.

Ana-1/MHV-68 cells were pretreated with JNK inhibitor (10, 25 and 50 μM) 30 min prior to NPs or LPS treatment. Equal amount of medium treated to cells was included as control. Whole cell protein was extracted after 1 h to investigate ERK phosphorylation and total protein expression by western blot. β-actin was used as loading control. Three independent experiments were performed and representative blots were shown here.

Then, we investigated whether JNK MAPK signaling also contributes to herpesvirus reactivation induced by NPs exposure. We found that JNK inhibitor pretreatment induced equal level or even higher lytic viral gene expression and infectious virus titer **(Fig. 3.32**). Together treated with NPs or LPS, similar effects were found.

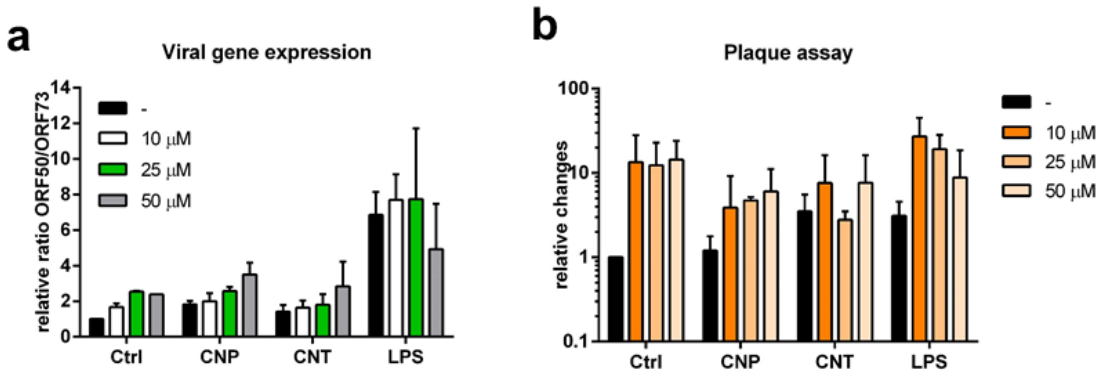

Figure 3.32 MHV-68 reactivation induced by NPs exposure is not depending on JNK MAPK signaling.

Ana-1/MHV-68 cells were pretreated with JNK inhibitor (10, 25 and 50 μM) 30 min prior to NPs or LPS treatment. Equal amount of medium treated to cells was included as control. RNA was isolated after 24 h to investigate ORF50 and ORF73 gene expression by qPCR, L8 was used as housekeeping genes. Fold changes of genes were calculated and the ratio of ORF50 to ORF73 was shown to represent lytic viral gene expression level. Plaque assay was performed to investigate the infectious virus titer change with supernatant collected after 72 h. Four independent experiments were performed and included for statistical analysis.

Taken together, JNK MAPK signaling less likely contributed to herpesvirus reactivation induced by NPs exposure but was potentially involved in latency maintenance.

3.3.8 NPs triggered intracellular ROS production and N-acetylcysteine amide (NACA) efficiently scavenged ROS but does not block MHV-68 reactivation

Nanoparticles are widely reported to trigger ROS production which contributes to pro-inflammatory response, cell damage and development of diseases. Furthermore, ROS production has also been proved to initiate MAPK signaling activation as well as herpesvirus reactivation. N-acetylcysteine amide (NACA), a specific scavenger of ROS, serves as an antioxidant to reduce oxidative stress. Thus, in the study, we used NACA to study the role of oxidative stress in herpesvirus reactivation induced by NPs exposure in Ana-1/MHV-68 cells.

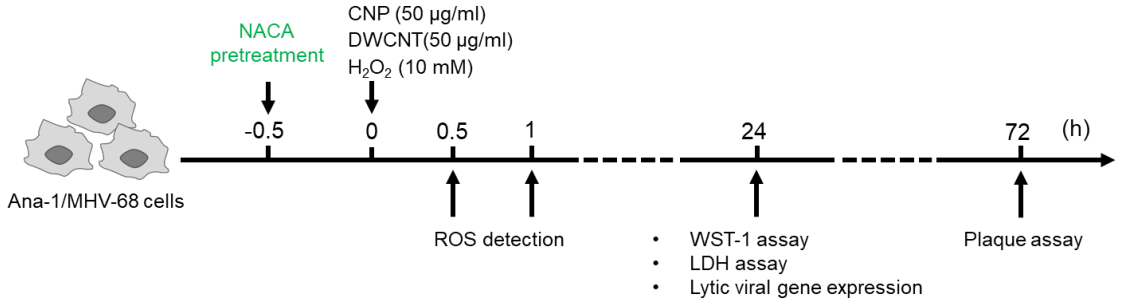

Figure 3.33 Schematic representation of study on the effect of NACA pretreatment on MHV-68 reactivation induced by NPs.

For *in vitro* experiments, Cells were pretreated with NACA (5 mM) for 30 min prior to CNP (50 μg/ml), DWCNT(50 μg/ml) treatment, H_2O_2 (10 mM) was used as a positive control to evaluate intracellular ROS production. ROS was measured by Dichloro-dihydro-fluorescein diacetate (DCFH-DA) assay after 30 min and 1 h NPs exposure. WST-1 assay and LDH assay were performed to investigate the additional toxic effect of NACA to cells based on NPs exposure after 24 h. To study the involvement of ROS in MHV-68 reactivation induced by NPs exposure, NACA pretreatment on lytic viral gene expression as well as infectious virus titer alteration were investigated.

First, we investigated whether NACA triggered an additional toxic effect to Ana-/MHV-68 cells. As shown in **Fig. 3.34**, pretreatment of NACA (5 mM) did not bring further cell viability alteration upon CNP and DWCNT exposure. Meanwhile, no additional LDH release was detected after 24 h. Thus, NACA at dose of 5 mM showed no toxic effect to Ana-1/MHV-68 cells and was suitable for the following experiments.

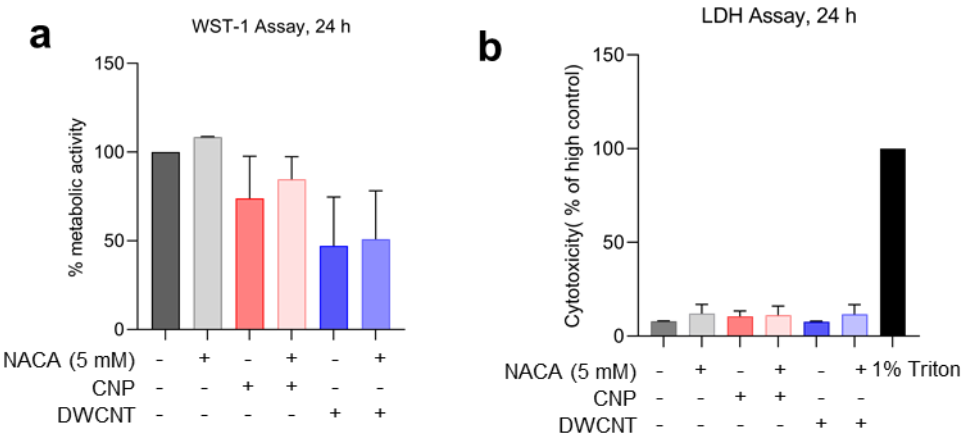

Figure 3.34 The cytotoxicity of NACA to Ana-1/MHV-68 cells.

Ana-1/MHV-68 cells were pretreated with NACA (5 mM) 30 min prior to NPs (50 μg/ml) or LPS (1 μg/ml) treatment. Equal amount of medium treated to cells was included as control. After 24 h, supernatant was collected to perform LDH assay whereas cells were left to perform WST-1 assay. For LDH assay, 1% Triton X-100 lysed cells in medium was used as a positive control for LDH release. Two independent experiments were performed and included for comparison.

Next, whether NPs exposure triggered intracellular ROS production was detected with DCFH-DA probe and the potential effect of NACA on ROS production was investigated. H_2O_2 (10 mM) was used as a positive control. As shown in **Fig. 3.35**, both CNP and DWCNT triggered a significant increase of ROS production up to 1 h after exposure. Pretreatment of NACA significantly abolished ROS produced by NPs treatment.

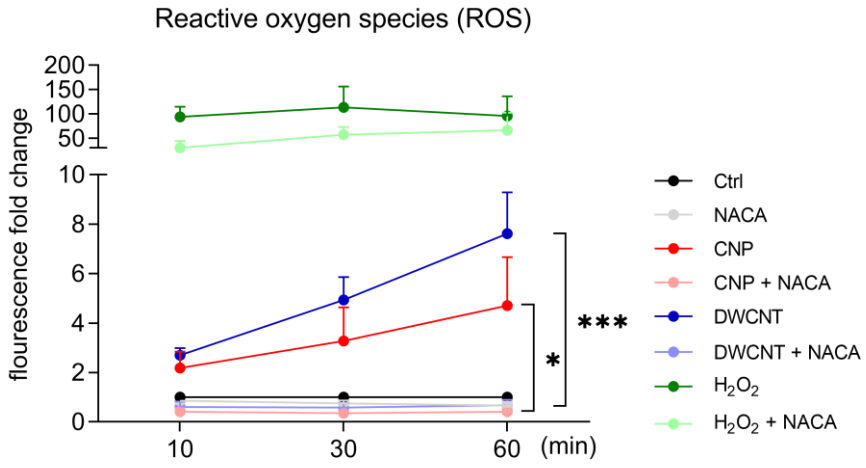

Figure 3.35 CNP and DWCNT triggered intracellular ROS production.

Ana-1/MHV-68 cells were pretreated with NACA (5 mM) 30 min prior to NPs (50 μg/ml) or H_2O_2 (10 mM) treatment. Equal amount of medium treated to cells was included as control. DCFH-DA (15 μM) was added together with NACA. The fluorescence was measured 10, 30 and 60 min after

NPs or H_2O_2 exposure with microplate reader with excitation and emission wavelength at 485 nm and 535 nm. The level of ROS induced by NPs and H_2O_2 as well as the effect of NACA on ROS production was shown. To quantify the effect of NACA on ROS, area under curve (AUC) of NPs treatment with or without NACA treatment was calculated, Student *t* test was used for statistical analysis. The effect of NACA on Hmox-1 expression was analyzed by Student *t* test. "*" $P < 0.05$; "**" $P < 0.01$; "***" $P < 0.001$.

Next, we investigated whether the production of ROS contributed to herpesvirus reactivation induced by CNP and DWCNT exposure. Here we found that, the pretreatment of NACA failed to downregulated the lytic viral gene expression induced by CNP and DWCNT exposure (**Fig. 3.36a**). NACA also showed no effect on blocking infectious virus titer (**Fig. 3.36b**).

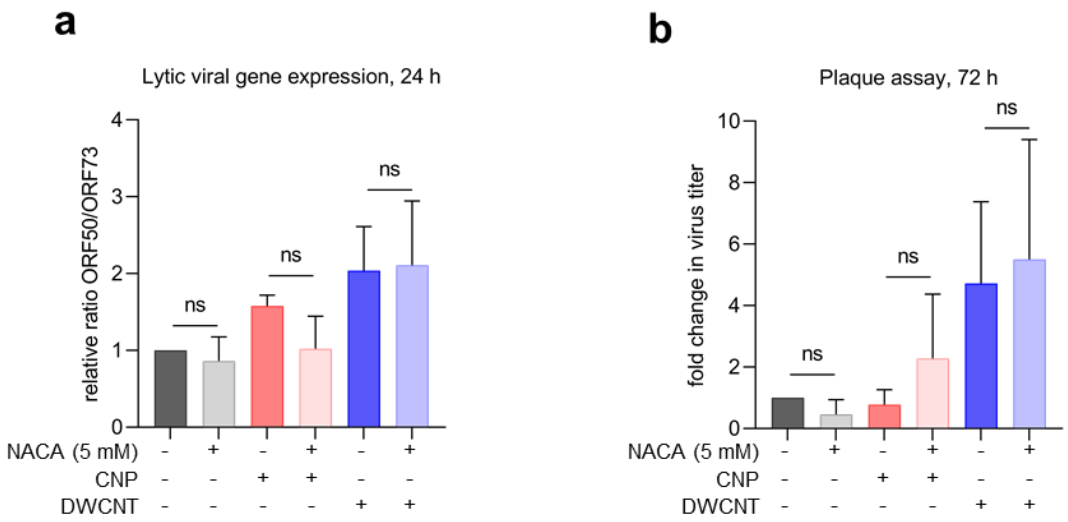

Figure 3.36 NACA failed to block MHV-68 reactivation induced by NPs exposure.

Ana-1/MHV-68 cells were pretreated with NACA (5 mM) 30 min prior to NPs (50 μg/ml) treatment. Equal amount of medium treated to cells was included as control. RNA was isolated after 24 h to investigate ORF50 and ORF73 gene expression by qPCR, L8 was used as housekeeping genes. **a.** Fold changes of genes were calculated and the ratio of ORF50 to ORF73 was shown to represent lytic viral gene expression level. **b.** Plaque assay was performed to investigate the infectious virus titer change with supernatant collected after 72 h. Three independent experiments were performed and included for statistical analysis with Student *t* test. ns, no significance.

Thus, ROS production during oxidative stress was not contributing to herpesvirus reactivation induced by NPs exposure.

3.4 *In vivo* application of p38 inhibitor attenuated MHV-68 reactivation induced by CNP

3.4.1 Animal experiments

Former findings in this study revealed that CNP exposure triggered MHV-68 reactivation depending on p38 MAPK signaling pathway *in vitro*.

Next we would like to translate our *in vitro* findings to *in vivo*, to investigate whether p38 MAPK signaling inhibition also contributes to herpesvirus reactivation induced by CNP in mice. This might be a protective target to the exacerbations of chronic lung diseases related to herpesvirus reactivation.

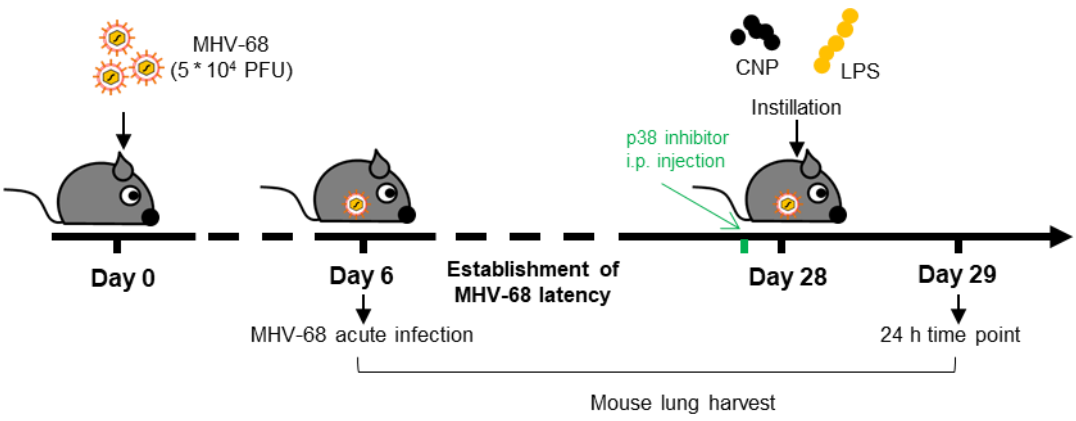

Figure 3.37 Schematic representation of animal experiment to study the p38 inhibition on herpesvirus reactivation *in vivo*.

C57/BL6 mice were intranasally infected with 5*10^4 PFU MHV-68 for 28 days to establish virus latency and subsequently instilled with either CNP (50 µg) or LPS (positive control, 0.1 mg) or an equal amount of H_2O as control. The p38 inhibitor (SB203580, 20 mg/kg) was intraperitoneally injected 1 h before particle instillation. Mouse lungs were perfused and fixed with 4% PFA overnight followed with embedding in paraffin block. 3 µm lung tissue slides were cut and performed immunohistochemistry (IHC) or immunofluorescence (IF) staining.

Briefly, C57/BL6 mice were intranasally infected with MHV-68 for 28 days to establish latency and subsequently instilled with either CNP (50 µg) or LPS (positive control, 0.1 mg) or equal amount of H_2O as control. The p38 inhibitor (SB203580, 20 mg/kg) was intraperitoneally injected 1 h before particle instillation. For those mice exposed for 72 h, additional two times p38 inhibitor was

administrated at day 29 and day 30. Mouse lungs were harvested to investigate the effect of p38 inhibition on MHV-68 reactivation induced by CNP 24 and 72 h thereafter. Mouse lungs were perfused and fixed with 4% PFA overnight followed with embedding in paraffin block. 3µm lung tissue slides were cut and performed immunohistochemistry (IHC) or immunofluorescence (IF) staining. Schematic representation was shown in **Fig. 3.37**.

3.4.2 p38 application attenuates herpesvirus reactivation triggered by pulmonary CNP exposure

First, mouse lung slides were stained with anti-MHV-68 serum to investigate the lytic virus protein expression by IHC staining.

As shown here, during acute infection (6 days after infection) phase, there is a dramatic increase of lytic virus protein expression and mainly localized to epithelial region of lungs (**Fig. 3.38**).

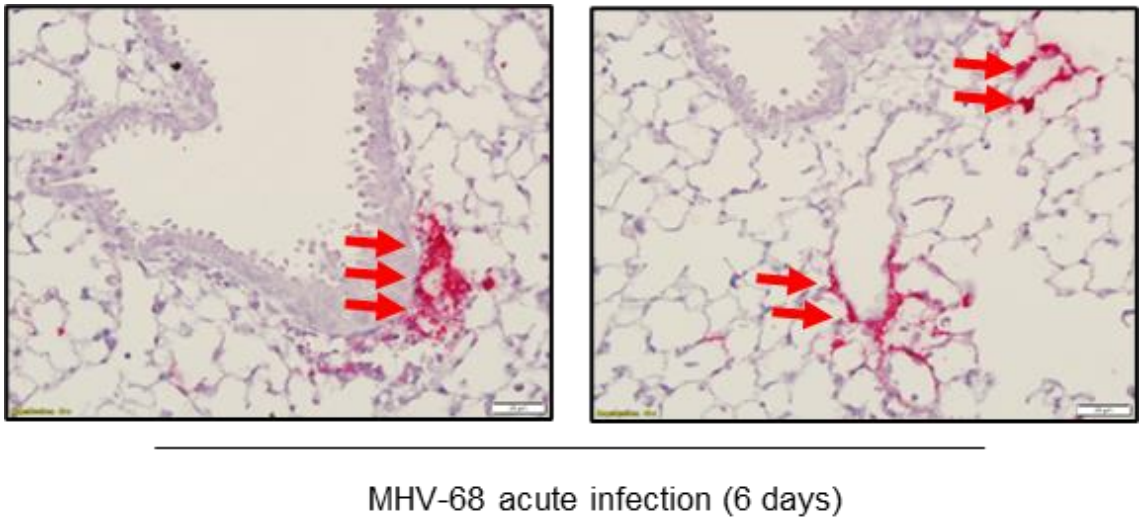

Figure 3.38 anti-MHV-68 serum staining showed an dramatic expression of lytic protein in mouse lungs and mainly localized to epithelial regions.

After 6 days of infection, some mice were harvested and tissue were collected for IHC staining. 3 µm lung tissue slides were stained with anti-MHV-68 serum according to IHC Vulcan fast red method. Slides were imaged with Olympus light microscope. Red arrows indicate the localization of lytic protein expression.

Only few MHV-68 positive cells remain after the establishment of latency (**Fig. 3.39**). CNP instillation triggered an increase of lytic virus protein expression after 24 h. Besides, a stronger effect of by LPS instillation was obtained indicating

more virus reactivating cells. Compared to acute infection, reactivation occurs predominately in infiltrating areas with a single-cell distribution morphology in the lung. This was similar to our former findings.

p38 inhibition pretreatment significantly reduced lytic virus protein expression induced by CNP and LPS. A quantification of reactivation cell number was performed by CAST and as shown in **Fig. 3.39b**, no effect of p38 inhibition was found when administrated to mice alone whereas it significantly attenuated the MHV-68 lytic virus protein stained cells triggered by CNP and LPS, indicating an effect of p38 inhibition on the attenuation of MHV-68 reactivation.

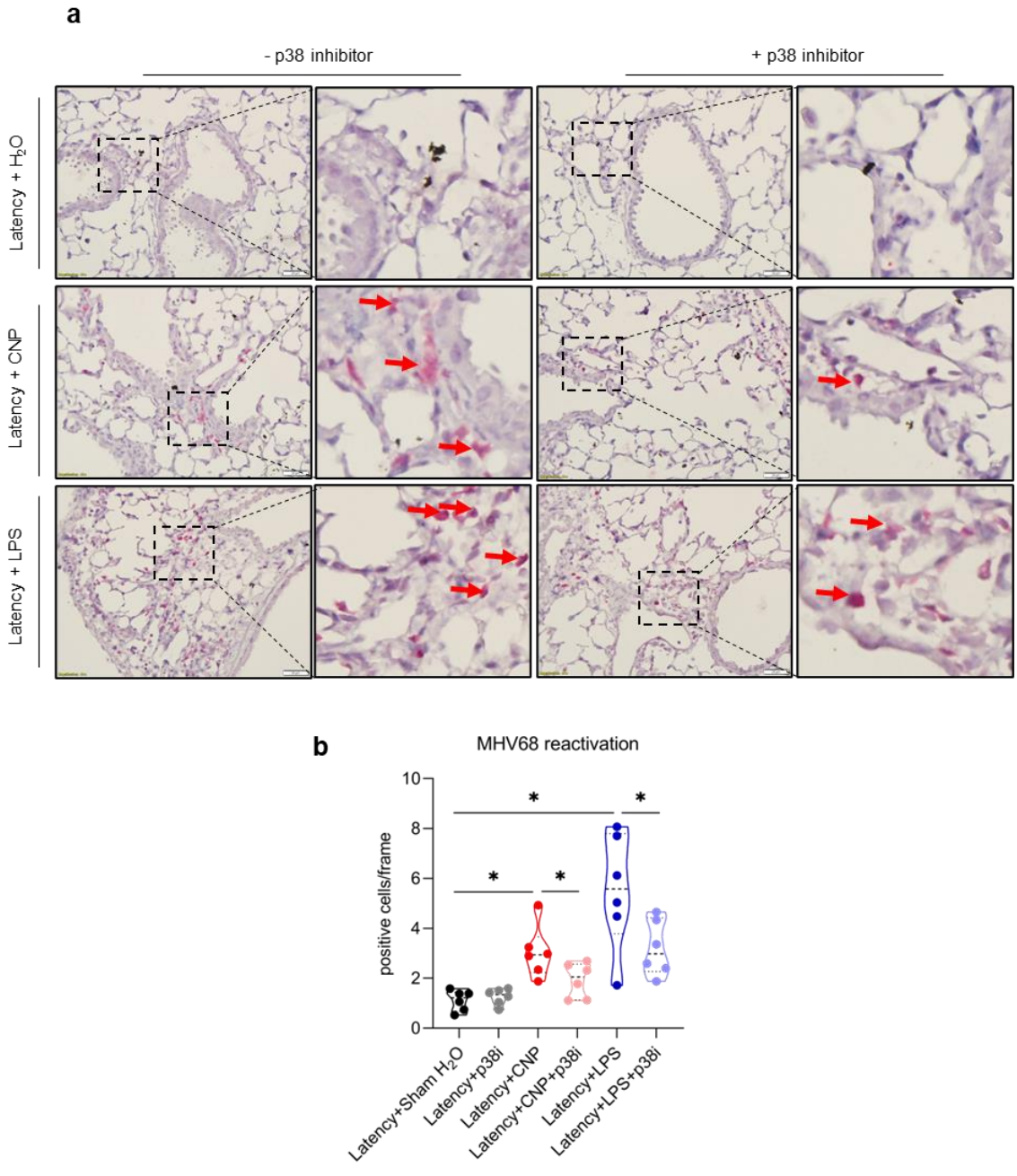

Figure 3.39 p38 inhibition attenuates MHV-68 reactivation induced by CNP exposure.

Mouse lung slides (3 μm) were stained with anti-MHV-68 serum according to IHC Vulcan fast red method. Images with magnification of 40 x were taken with Olympus microscope. Representative images were shown in **a**. Scale bar: 20 μm. MHV-68 reactivation was shown in **b**. Each dots represented left or right lung lobes quantification results of 3 mice. A comparison between "Latency + CNP" and "Latency + CNP + p38 inhibitor", "Latency + LPS" and "Latency + LPS + p38 inhibitor" was made with Student *t* test. * $P < 0.05$. Red arrows indicate the localization of lytic virus protein expression.

Taken together, our findings demonstrated that p38 application also blocked herpesvirus reactivation *in vivo*.

4. Discussion

4.1 Nanoparticle exposure reactivates latent MHV-68 mainly in lung infiltrates

4.1.1 Nanoparticle exposure reactivates latent MHV-68

Herpesvirus is one of the most prevalent virus to human and maintains lifelong latency in the host after primary infection. As reported, EBV infects more than 90% population worldwide (Smatti et al., 2018). During the primary infection stage, herpesvirus infects epithelial cells through respiratory tract and subsequently causes epithelial cell damage. Besides, macrophages, dendritic cells and B lymphocytes in lung tissue are also infected and finally virus reaches spleen via lymph nodes and circulation system. Lytic genes are expressed during lytic infection accompanied with viral DNA replication and eventually produce virus particles. The immune system fights again the acute infection and keeps the infection under control, then virus turns to “silent” and establishes latency in the host, and forms a balance between the virus and host. During latency, virus genomic DNA exists in the nucleus as an episome, and only produces a limited number of latent genes (Murata, 2014).

Studies have revealed that many classical and non-classical stimuli disturb the balance and reactivate latent herpesvirus, termed reactivation. These classical triggers include fever, microbial co-infection, UV light, Stress, tissue injury, cytokines, hyperthermia, toxic stimuli etc. For example, the cytokine TGF-β reactivates latent EBV via activation of Smad signaling in B cells (Iempridee et al., 2011). Some stress factors, like chemotherapy or body irradiation can also reactivate EBV from latency (Hagemeier et al., 2012). Besides, novel triggers of herpesvirus reactivation like components in ambient air pollution, which are also omnipresent in our daily life, need further consideration.

In the previous study, Sattler and colleagues in our group reported that pulmonary exposure of soot-like carbonaceous nanoparticles (CNP) and fiber-shape double walled carbon nanotubes (DWCNT) reactivated latent murine gammaherpesvirus (MHV-68) and restored a signature of acute infection (Sattler et al., 2017). Continuously in the current study, we established the MHV-68 latency model (28

days after MHV-68 infection) as described before, acute infection (6 days after infection), CNP and LPS exposure were included as the consequence of lytic infection and reactivation, respectively. Meanwhile, an equal amount of H_2O was used as a control. Same like before, immunofluorescence staining of serum anti-MHV-68 exhibited an increase of lytic virus protein expression in lung tissue exposed to CNP and LPS after 24 h compared to control, suggesting the occurrence of virus reactivation from latency. A quantification of reactivation cell number revealed that, 2- and 3-fold increase of reactivating cells were triggered by CNP and LPS. Thus, we confirmed that, pulmonary CNP exposure reactivates latent herpesvirus in mouse lung.

However, due to the big size of lung tissue and limited number of tissue sections for analysis, the overview and localization of MHV-68 reactivation in mouse lung remain unclear and need further investigation.

Imaging sample slices in two dimensions (2D) scale based on widefield fluorescence microscopy (WFM) and laser scanning confocal fluorescence microscopy (LSCM) has been widely used to visualize structural changes, cell biology changes and obtain quantitative information of biological samples. In our previous work, we stained paraformaldehyde (PFA)-fixed, paraffin-embedded lung tissue slices with serum anti-MHV-68, to investigate the lytic virus protein expression induced by pulmonary CNP or DWCNT exposure. With further imaging, we observed the increase of lytic protein expression in lung tissue, confirming the virus reactivation caused by nanoparticle exposure. It provided us evidence as a good readout of virus reactivation in a high resolution. However, a deeper understanding of the virus reactivation distribution and localization in three dimensions (3D) of the whole lung needs further establishment and investigations.

In this study, whole lung tissue staining technique and optical tissue clearing in 3D followed by light-sheet fluorescence microscopy (LSFM) were established. This ad hoc technique allowed us to visualize each optical section and entire lung lobes after 3D imaging reconstruction. Followed the protocol, lung lobes from MHV-68 latent infected mice were well cleared and turned transparent for subsequent imaging and 3D reconstruction steps. Importantly, dark CNP particles remains appearing inside tissue uniformly after instillation. In one hand,

it proved a good performance of instillation, allowing a stable and comparable establishment of nanoparticle pulmonary exposure. However, in the other hand, nanoparticles are still remaining during the antibody staining and optical clearing procedures and bring difficulties to the following imaging steps and interfere 3D structure reconstitution due to its absorbance ability. Consequently, low imaging depth and poor resolutions especially in the centra part of lung lobes was formed, and a less clear lung structure was reconstituted in CNP exposed lungs. From our attempt, imaging of each lung lobe separately rather than whole lung tissue was better to get a relative high resolution of imaging. Thus, we always cut whole lung into different lobes and continued imaging within the scale. Besides, adjustment of light width and depth of LSFM also improved imaging. However, these endeavors only ameliorate imaging to a limited degree, and we were not able to reconstitute the lytic protein expression in the 3D structure of whole lungs triggered by dark nanoparticles. Deeper investigation on the cellular localizations of lytic protein remained as an challenge and need to be improved by other methods.

As the fact that lung tissue exhibits high autofluorescence, no further staining but just imaging via Alexa Fluor 488 channel is already enough to visualize lung structure, which has been reported before by some studies (Yang et al., 2019, Mzinza et al., 2018). Besides, serum anti-MHV-68 staining and imaging reconstructed the overview of lytic virus protein expression during MHV-68 acute infection, latency as well as reactivation in a whole lung lobe scale.

We observed a massive MHV-68 lytic protein expression in lungs and predominantly localized in epithelial regions after nanoparticle exposure. This finding fits the pathogenesis of herpesvirus acute infection that, infection causes massive virus genomic load in the lung, increase of lytic virus protein expression as well as a great number of infectious virus particles release. Besides, epithelial cells in the airway are the main targets and widely infected, therefore the initial infection results in epithelial damage (Barton et al., 2011). Then, along with the establishment of latency, infection are limited and only spontaneous MHV-68 lytic protein are expressed exhibiting basal level of signals. From our LSFM images, a relative low and basal fluorescence was observed. CNP as well as LPS reactivate latent MHV-68, CNP triggered an moderate increase of lytic protein

expression whereas LPS caused even stronger lytic protein expression in the whole lung lobe.

There are other publications which also investigated lung biological alterations in inflammation using LSFM approach and quantitative analysis. As reported by Mzinza and colleagues, an in-depth visualization of bronchus-associated lymphoid tissue (BALT) was well established and used to assess entire distribution in the whole lung (Mzinza et al., 2018). Furthermore, with the application of CD3 and B220 antibody staining, the localization and composition of BALT, including T lymphocytes and B lymphocytes can be also visualized. Same to us, autofluorescence exhibited the entire lung anatomy in both 3D and sectional views.

Thus, 3D optical tissue clearing and LSFM techniques bring benefit on investigation of herpesvirus pathogenesis in an entire tissue scale.

To this end, we confirmed MHV-68 reactivation according to the increased lytic virus protein expression induced by nanoparticle exposure. In the meantime, we also investigated lytic viral gene expression as a readout of virus reactivation. Open Reading Frame 50 (ORF50) is expressed in the lytic phase of virus life cycle and Open Reading Frame 73 (ORF73) is continuously expressed in all phases of virus life cycle. In our previous study, we use the ratio of ORF50 and ORF73 to show the lytic viral gene expression. However, we did not observe an increase of ORF50 expression in mouse lung homogenates after 24 h exposure to CNP or LPS. Furthermore, ORF73 is even too low expressed to be detected by qPCR. One reason could be the low percentage of reactivating cells in the whole lung homogenates used for RNA isolation. As shown in **Fig. 3.3**, there are less than 5% reactivating cells in lung tissue (around 1.5% of control, and around 3% or 5% after CNP or LPS exposure, respectively). Thus, a low abundance of the gene may be under the detection limit. The other reason is the time point for gene expression detection, that 24 h is too late to catch the peak of lytic gene expression. In our *in vitro* model, we found the peak of lytic viral gene expression is 24 h for nanoparticle exposure and 12 h for LPS exposure in Ana-1/MHV-68 cells in a submerged cell model. In this condition, cells were cultured and treated with nanoparticles in medium. Thus, the exposure route and interactions between nanoparticles and cells are different compared to real exposure in mouse model.

Further considered the deposition of nanoparticle in lung, we assumed that, there is a fast and early response to nanoparticles and thus caused a rapid upregulation of lytic viral gene expression. We plan to add one early time point, such as 6 h and 12 h, to harvest lungs and investigate the kinetic of lytic viral gene expression.

After exposed to nanoparticle, herpesvirus were reactivated in the lung by increasing virus production, and thus may induce herpesvirus-specific antibody increase via the humoral immune responses. Considering the persistent effect of nanoparticle exposure and time consumption of immune regulations, 3 days after nanoparticle exposure was included to analysis MHV-68 specific antibody alterations. However, no change of that antibody was detected after CNP or LPS treatment compared to control. We guess the detection after 3 days remains too short to show B lymphocytes response and detect the antibody in sera. As reported by Ruiss and colleagues, Glycoprotein 150 (gp150) is a positional homolog of gp350/220 of EBV and reported as a suitable vaccine antigen to protect from EBV-associated diseases (Ruiss et al., 2012). In this context, they studied the specific antibody either after two weeks of MHV-68 infection or 19 days afterward two times vaccines and observed a strong immune responses. Steer *et al*. established the determination of MHV-68 specific antibody detection. In the former work, MHV-68 specific antibody was detected 17 or 42 days after MHV-68 infection (Steer et al., 2016). Thus, we take the detection time points into consideration and have planned to harvest serum from mice a week after CNP exposure during latency and try to determine the MHV-68 specific antibody in the further project, and gain more insight to the herpesvirus reactivation induced by pulmonary nanoparticle exposure.

Besides the herpesvirus reactivation, pulmonary nanoparticle exposure also triggered a pro-inflammatory response *in vivo*. BAL cells characterization showed that CNP exposure after 24 h caused an increase of cell numbers after lavage and cell types differentiation indicated that the majority of those cells are neutrophils, suggesting a neutrophilic inflammation. Previously, we defined the time course of inflammatory responses caused by CNP intratracheal instillation (Chen et al., 2016). There we found that, CNP at dose of 20 μg induced an dynamic accumulation of neutrophils in air space in a time dependent manner, which started after 12 h and was most abundant after 18 and 24 h. In the current study, exposure of CNP at 50 μg also showed a massive accumulation of

neutrophils after 24 h. A transcriptomic study also revealed that, CNP exposure during virus latency induced a cluster of genes upregulation compared to control (Sattler et al., 2017). Some upregulated genes in our mice exposed to CNP, Saa3, Cxcl1, Timp1, Slc26a4, Cd14, Lcn2 and Ch25h were also reported in other studies (Husain et al., 2015). Furthermore, some genes were also expressed during MHV-68 acute infection, such as Saa3, Cxcl1, Lcn2 and Timp1. Further pathway analysis showed that, immune cell response pathways, such as activation of leukocytes, invasion of cells and cell proliferation were both activated by CNP exposure as well as MHV-68 acute infection. Thus, CNP exposure in MHV-68 latently infected mice exhibited signature not only a common pro-inflammation, but also similar immune responses as of the acute infection.

4.1.2 MHV-68 reactivation induced by CNP mainly localizes in CD11b+ macrophage-like infiltrates in mouse lungs

Upon pulmonary nanoparticle exposure, alveolar macrophages in air space act as the first defense against exposure and phagocytose inhaled nanoparticles (Barlow et al., 2005), the interaction between nanoparticles and alveolar macrophages after phagocytosis determines the subsequent cellular responses in the lung. As our group reported formerly, CNP agglomerate was mainly phagocytoses by alveolar macrophages analyzed in lung tissue and BAL cell cytospins (Chen et al., 2016). Nanoparticle uptake by lung epithelial cells is in contrast only rarely observed (Geiser et al., 2013). Thus, alveolar macrophages might be the first candidate to be taken into consideration for the occurrence of virus reactivation.

Since alveolar macrophages mainly localize in alveolar space and show distinct morphology, together with high expression of the integrin marker CD11c, we can well distinguish alveolar macrophages from other macrophages which are usually positive for the integrin CD11b. We observed particles are appeared in alveolar macrophages either from histological examination of lung tissue as well as BAL cell cytosins after CNP exposure during latency. However, we did not detect significant MHV-68 lytic protein expression in these cells in lung tissue. In BAL cells, CNP exposure during MHV-68 latency caused an increase of total BAL cell number and mainly from neutrophils, indicating a neutrophilic inflammation. No significant macrophage number change was found after CNP exposure. Indeed,

almost all BAL macrophages exhibit CD11c expression, identifying them as alveolar macrophages. However, rarely little MHV-68 lytic protein expression occurs in these CD11c positive cells. Thus, we concluded that alveolar macrophages are not the major site of MHV-68 latency and virus reactivation. Similarly, we were not able to establish a stable infected alveolar macrophage cell line, but succeeded using bone marrow derived cell line. This may be due to the defensive role of alveolar macrophages, to limit and reduce virus replication. Farrell and colleagues found that, another type of herpesvirus, murine cytomegaloviruses (MCMVs) directly infect alveolar epithelial type 2 cells and alveolar macrophages after 24 h (Farrell et al., 2015). The depletion of alveolar macrophages however increased virus infection. Thus, alveolar macrophages play an essential role in defending virus replication and no latency is established in these cells. When we quantified BAL macrophage during MHV-68 acute infection (day 6 after infection), we found a significant decrease of alveolar macrophage numbers in BAL fluid, indicating that lytic MHV-68 may also cause the dysfunction or depletion of alveolar macrophages. In this context, Ghoneim and colleagues used the fluorescent probe PKH26 to specifically label alveolar macrophages in the lung and found that, influenza infection results in depletion of PKH26-labeled alveolar macrophages (Ghoneim et al., 2013).Taken together, alveolar macrophages are targets of herpesvirus primary infection and help host to control virus replication but are not the main sites for virus latency and reactivation.

During infection or inflammation, bone marrow- / monocytes-derived macrophages are recruited to infiltrating areas of lung tissue (Evren et al., 2020). In 1999, Weck *et al*. reported that, besides B lymphocytes, peritoneal macrophages exhibiting F4/80 expression, a pan macrophage marker, are also targets of MHV-68 latency (Weck et al., 1999). The relevance of bone marrow- or monocyte-derived macrophages as major reservoirs of MHV-68 latency and reactivation is less described.

In our investigation using CD11b as marker for recruited macrophages, we found most lytic MHV-68 proteins localized to CD11b+ macrophage-like cells in infiltrating distinct regions of the mouse lung. The source of MHV-68 latency and reactivating cells currently remains a crucial question to us. One of the key question is, whether these CD11b+ cells, which show MHV-68 reactivation upon

particle exposure, are i) cells accumulating in response to infection and latency development, as known for T cells, or ii) whether they are recruited during particle induced inflammation, and undergo reactivation upon monocyte to macrophage differentiation (Stoeger and Adler, 2018, Dupont and Reeves, 2016).

Our quantification of CD11b+ cells in lung tissue indicates only a tendency for the increase of CD11b+ cells upon MHV-68 acute infection (**Fig.3.4b**), which however, along with the establishment of MHV-68 latency, declined again to a similar level as observed for non-infected control animals. Our data therefore does not support an increase of recruited CD11b+ macrophages into lungs upon infection which stay in the tissue for e longer time to establish latency. MHV-68 lytic protein staining rather demonstrated that spontaneous MHV-68 reactivation also occurs during latency and our quantification demonstrated that more than 60% CD11b+ cells harbor spontaneous reactivation. During the acute pro-inflammatory responses, both CNP and particularly LPS instillation triggered a significant recruitment of CD11b cells into lung tissue (**Fig. 3.4c**) while in parallel, MHV-68 reactivation was triggered (**Fig. 3.3b**). The release of CCL2 after CNP and LPS exposure measured in BAL fluid by my colleague (data not shown) also indicates the regulation of macrophages recruitment inro lungs. The percentage of CD11b+ cells showing MHV-68 reactivation however still remained steady in the range of 60% to 70%, similar as compared to latency.

Thus, the majority of latently infected and reactivating cells that account for the source of lytic MHV-68 protein expression, are likely not local CD11b+ macrophages in the lung tissue, but CD11b+ infiltrating inflammatory monocytes/macrophages. As reported by Dupont *et al.*, Human cytomegalovirus (HCMV) latency is established in bone marrow precursors, and monocytes derived from these precursors also carry latency. Stimuli that trigger monocytes differentiation into macrophages reactivate HCMV from latency (Dupont and Reeves, 2016). In summary, circulating CD11b+ monocytes seem to account for the main latency cell types. Due to the pro-inflammatory responses induced by CNP or LPS, monocytes get recruited into lung tissue and differentiate to CD11b+ macrophages and exhibit MHV-68 reactivation. However, whether monocytes can be latently infected and get reactivation are not yet well investigated.

CCR2 is a marker for inflammatory monocytes. As reported by Yang *et al*., vaccinia virus causes severe pneumonia and systemic dissemination in mouse lung according to the response of type 2 alveolar epithelial cells (ACEIIs) The response of ACEIIs induces the recruitment and activation of CCR2+ inflammatory monocytes and subsequently differentiated into Lyve1- interstitial macrophages (Yang et al., 2022). From our unpublished single-cell RNA sequencing data, the strongest CD11b expression was detected in Fn1+ macrophages. These cells are showing low CCR2 expression, and can be well-identified from infiltrating monocytes and differentiating macrophages (data not shown). Thus, a double staining of CCR2 and CD11b can help us to distinguish inflammatory monocytes and recruited macrophages in the current project. As shown in **Fig. 3.4e**, CCR2+ cells show different size and morphology to CD11b+ cells, which are smaller compared to CD11b+ cells. Furthermore, little colocalization was observed. Thus, coupled with our former findings, monocytes are latently infected and due to CNP exposure, monocytes are recruited and differentiate to macrophages showing CD11b expression, and finally get MHV-68 reactivation. However, to get a deeper understanding of latency and reactivation states in monocytes and macrophages, a double staining of CCR2 and anti-MHV-68 serum is necessary to be done in the future.

In the other hand, our *in vitro* model established with BMDM-derived macrophages (Ana-1) also exhibited the ability to harbor latency, NP or LPS treatment also triggered MHV-68 reactivation. Thus, whether bone marrow cells harbor MHV-68 latency and can be reactivated need to be investigated in the future.

Taken together, we conclude that nanoparticle triggered MHV-68 reactivation mainly localizes in CD11b+ macrophage-like infiltrates in the lung.

4.2 CNP activates latent MHV-68 via a p38 MAPK dependent signaling pathway

To study the mechanism of MHV-68 reactivation induced by nanoparticle exposure, we established the Ana-1/MHV-68 cell line. Flow cytometry analysis revealed a marked high expression of CD11b but not CD11c, providing us good a cell line to mimic the main MHV-68 reactivating cell types *in vivo*.

In the *in vitro* model, a fiber-shape double walled carbon nanotube (DWCNT) was also included in the study. Some mouse studies reveled that, DWCNT is more toxic and causes a persistent inflammation compared to CNP. Thus, there may be different effects of two distinct NPs on herpesvirus reactivation. Cell viability study revealed that both CNP and DWCNT triggered the decrease of metabolic activity in a dose dependent manner. In the range of high concentrations, NPs killed macrophages before induced upregulation of virus genome. Thus, a non-severe cytotoxicity concentration (50 μg/ml) was considered for the following experiments. NPs reactivated latent MHV-68, accompanied by significantly upregulated lytic viral gene expression after 24 h, increased lytic virus protein expression after 24 h as well as infectious virus production and release after 72 h. Thus, we successfully mimic the events of MHV-68 reactivation in CD11b+ infiltrates in lung.

In our previous study, 72 h was the time point to study both viral gene expression and infectious virus production. But the peak of lytic viral gene expression should be prior to massive virus production to be detected. According to the kinetic investigation, we found that the peak of lytic viral gene expression induced by NPs is 24 h in the culture model. As a positive control, LPS caused no metabolic activity decrease, but induced stronger lytic viral gene expression. Not like NPs, the peak was earlier at 12 h. Due to the producing and assemble time of virus particle, the infectious virus can be only detected until 72 h.

In the current study, we used submerged *in vitro* culture model and the milestone time point for lytic viral gene expression detection was 24 h. Considering the fact that, NPs are faster deposited and interact with cells *in vivo*, the response machinery and the lytic viral gene expression may be earlier upregulated compared to *in vitro* condition. Thus, a more realistic *in vitro* model, such as air-liquid interface (ALI) culture model is need to mimic the *in vivo* biological condition. Lenz *et al.* (PMID: 23484138) compared the oxidative stress and pro-inflammatory responses induced by zinc oxide (ZnO) nanoparticles between submerged and ALI culture conditions. In alveolar epithelial cells, ZnO showed comparable cell viability decline and oxidative stress related genes expression. However, ZnO triggered higher level of pro-inflammatory genes expression, such as IL-6, IL-8 and GM-CSF in ALI culture model compared to submerged model. Similarly, Volckens and colleagues also proved that, coarse ambient particulate

matter also induced higher IL-8 expression in ALI culture model cultured with human primary bronchial epithelial cells (Volckens et al., 2009). Thus, Ana-1/MHV-68 cell cultured under ALI model to study the course of NPs exposure induced lytic viral gene expression is under consideration for further *in vitro* studies.

4.2.1 CNP but not DWCNT triggered MHV-68 reactivation is depending on p38 MAPK signaling

MAPK signaling is a common stress related signaling and has been reported to be associated with certain nanoparticle-cell interaction. Many studies have focused on the toxicity of macrophages induced by carbon based nanomaterials (Yuan et al., 2019). MAPK signaling is activated due to oxidative stress potential of nanomaterials, and contributes to pro-inflammatory responses, mitochondrial damage and apoptosis. To better understand MAPK signaling activation, silica nanoparticles provide us good particle exposure model. As widely reported, silica causes severe and permanent lung inflammation and damage, even cause silicosis and lung cancer. A cluster of pathways are activated by silica exposure, such as oxidative stress, MAPK signaling, TGF-β signaling, inflammasome and pyroptosis (Tomaru and Matsuoka, 2011, Rabolli et al., 2014, Peeters et al., 2013, Peeters et al., 2014). We found that, silica at dose of 50% cell viability decline induced a progressive activation of p38 and JNK MAPK activation up to 6 h in Ana-1 cells. Differently, silica caused a fast ERK MAPK activation. Likewise, silica nanoparticle activated MAPK signaling pathway in a dose and time dependent manner, and was associated with following pro-inflammatory responses in RAW264.7 macrophages (Fritsch-Decker et al., 2018). p38, ERK and JNK MAPK were phosphorylated at dose of 50 µg/ml and 100 µg/ml and peaked after 4 h exposure. Thus, MAPK signaling was fast activated in response to silica nanoparticle exposure in macrophages.

Similar in current study, our data demonstrated that CNP and DWCNT activate p38, JNK and ERK MAPK signaling in Ana-1/MHV-68 cells in an even rapid pattern after exposure compared to the effect of silica in Ana-1 cells. The peak was either 30 min or 1 h after exposure. This may due to the establishment of latency, some viral transcription factors resemble those factors of MAPK signaling to help virus production. For instance, one of the most important

regulator of EBV is a viral transcription factor called Zta or BZLF1, resembling the cellular activator protein 1 (AP1) transcription factor (Sinclair, 2013). AP-1 is one transcription factor of MAPK signaling. Hence, under this condition, cells are more sensitive to phosphorylate p38, ERK and JNK upon stimuli. When NPs were exposed to cells, NPs not only switch on phosphorylation due to the interactions with cells, but also perturb the latent virus, the dual effects fasten the activation of MAPK signaling in Ana-1/MHV-68 cells.

MAPK signaling has been proved to contribute to pro-inflammatory responses. Silica nanoparticles trigger a pro-inflammatory response depending on MAPK signaling, especially Tnf gene expression and cytokine release in macrophages, and JNK and ERK inhibition significantly attenuated Tnf in gene and protein expression level (Fritsch-Decker et al., 2018). Likewise, Frank and colleagues reported that MWCNT triggered TNF and IL1β release at dose of 400 μg/ml in MHS cells is dependent on p38 and JNK MAPK signaling (Frank et al., 2015). We have to point out that, this is a super high dose of MWCNT and caused nearly all cell viability decline. These findings suggested the role of MAPK signaling in the elaboration of macrophages in responses to nanoparticles exposure.

Upon MAPK signaling activation, a number of transcriptional responses occur, including typical transcriptional factors activation. In our microarray analysis, no classical pro-inflammatory signature was observed in Ana-1/MHV-68 cells in response to NPs exposure. Some classical pro-inflammatory genes, such as Tnf, Nos2, Il1b, Cox2, have been widely reported to be induced downstream of MAPK signaling activation. However, they are not upregulated by either CNP or DWCNT after 3 or 9 h, indicating no classical pro-inflammatory response in macrophages. In contrast, LPS significantly triggered these genes upregulation at two different time points. The data fits to a former study (Ban et al., 2011). They found that the same concentration of LPS triggered 1073 genes upregulation in RAW264.7 macrophages, including Tnf, Il1a, Il1b, Cxcl2 and Cxcl10, which were also induced in our experiment. As addressed by many studies, LPS binds to Toll-like receptor 4 (TLR4) in the cell surface and later recruits downstream adaptors, like MyD88. TGF-β activating protein kinase 1 (TAK1) and MAPK signaling is rapidly activated and strengthen pro-inflammatory responses (Yesudhas et al., 2014). How macrophages recognize nanomaterials and the activation of certain receptors may determine the downstream transcriptional responses. Tsugita and

colleagues identified that class B scavenger receptor (SR-B1) specifically recognizes crystalline and amorphous silica, silica further activates NLRP3 inflammasome and promote IL1β release during lung inflammation (Tsugita et al., 2017). However, SR-B1 is not responsive to recognize titanium dioxide nanoparticles, latex nanoparticles or monosodium urate crystals. However, the surface receptors for carbon nanoparticles recognition still remains unclear to us, and special receptors activation for CNP and DWCNT determines the inflammatory responses in macrophages.

Another reason is, the activation or the response of epithelial cells is necessary to facilitate macrophage responses upon nanomaterials exposure. We previously found that, alveolar epithelial cells but not macrophages are involved in the initiation of acute inflammatory response in mice exposed to CNP (Chen et al., 2016). Upon CNP exposure, alveolar macrophages showed no pro-inflammatory signatures, with genes of Nos2, Tnf, Il1b, Cxcl1, Cxcl2 and Cxcl5 unchanged. However, Cxcl5 was highly expressed due to CNP exposure in alveolar epithelial cells, indicating the initiative role of epithelial cells but not macrophages on inflammation. The study support that, responses from epithelial cells to macrophages play important role in inflammatory responses. Hence, in our current *in vitro* model, signaling or stimuli from epithelial cells upon nanoparticle exposure are missing to activate macrophages. Thus, a crosstalk between epithelial cells and macrophages on MAPK signaling activation, MHV-68 reactivation and in turn, whether released virus particles from macrophages affect epithelial cells need further investigations. In the future, a co-culture of alveolar epithelial cells and Ana-1/MHV-68 cells is needed to establish to study the interaction between epithelial cells and macrophages on MHV-68 reactivation triggered by nanoparticle exposure.

MAPK signaling has also been reported to contribute to herpesvirus infection and reactivation. Ye and colleagues showed that oxidative stress reactivates KSHV from latency via p38, ERK and JNK MAPK signaling (Ye et al., 2011). Antioxidant as well as MAPK inhibition application reduced KSHV lytic replication and prolong lifespan in mice. In human. the reactivation of KSHV contribute to Kaposi's sarcoma (KS) development, which remains the most common cancer for AIDS patients. Thus, investigation on the mechanism underlying herpesvirus reactivation provide us opportunity to identify therapeutic target on reducing

herpesvirus reactivation and related diseases. From above studies, anti-MAPK signaling activation, anti-inflammation or antioxidants can be potential targets.

In our study, three specific MAPKs inhibitors were also applied to study their roles on blocking herpesvirus reactivation. Firstly, we spent effort to seek proper concentrations to guarantee no toxic effect of inhibitors themselves and importantly, exhibit effective role on MAPK signaling. We found that, p38 MAPK signaling inhibition dramatically reduced lytic viral gene expression as well as infectious virus production induced by CNP. However, only a mild but not significant effect was found in DWCNT treatment. Meanwhile, p38 inhibition also significantly blocks LPS triggered MHV-68 reactivation, exhibiting a similar effect as observed in CNP. Likewise, ERK, JNK and p38 MAPK signaling mediate KSHV reactivation induced by TPA in BCBL-1 cells. Mechanically, inhibition of three MAPKs reduced the lytic viral gene expression of RTA and infectious virus production (Xie et al., 2008).

Since p38 MAPK also contributes to cell proliferation, it could happen that, inhibition of p38 reduced Ana-1/MHV-68 cells proliferation, and there are less cells compared to CNP treatment after 24 h. Thus, less cells showed reactivation. To answer the question, we checked the effect of p38 inhibitor on cell viability and cytotoxicity. From our results, the p38 inhibition did not reduce metabolic activity and trigger more cytotoxicity to Ana-1/MHV-68 cells, there was no cell proliferation attenuation. Besides, after 24 h, we isolated relative equal concentration of RNAs from different groups, also provided no blocking on cell proliferation. Thus, MHV-68 reactivation reduction by the p38 inhibition is due to the effect on lytic replication machinery but not cell proliferation.

For KSHV reactivation, protein of RTA plays the central role for host cells to switch on lytic virus replication. As reported, TPA induced KSHV reactivation via RTA activation is mediated by AP-1, which is a downstream target of MAPK signaling (Xie et al., 2008). RTA is encoded by ORF50. Thus, in our case, p38 MAPK activation may also activate transcriptional factor AP-1 and further upregulate ORF50 expression, to trigger MHV-68 reactivation from latency in Ana-1/MHV-68 cells.

According the microarray results discussed above, we did not observe any classical pro-inflammatory signatures after p38 MAPK activation, our data

supported that the effect of p38 MAPK signaling on herpesvirus reactivation in latently MHV-68 infected macrophages is beyond the transcriptional responses. CNP activated both p38 as well as downstream MAPKAPK2 phosphorylation. Beyond activating several transcriptional factors, MAPKAPK2 plays other important role in various cellular functions, for instance cytokine release and inflammation, cell cycle and tumorigenesis (Soni et al., 2019). Importantly, MAPKAPK2 mediates mRNA stability. As shown by Winzen and colleagues, p38 MAPK signaling pathway contribute to IL-6 and IL-8 mRNA expression via a MAPKAPK2 dependent mRNA stabilization function (Winzen et al., 1999). Thus, the determination of mRNA stability may also explain the direct role of MAPKAPK2 on lytic viral gene expression to contribute to MHV-68 reactivation induced by CNP. MAPKAPK2 phosphorylation could increase the stability of lytic viral genes (ORF50), and in turn, ORF50 expression is downregulated by pretreatment with p38 inhibitor.

Beyond p38 MAPK, there is additional signaling that involved in DWCNT induced MHV-68 reactivation. As a fiber-shape nanomaterial, CNT causes specific toxic effects differing from soot-like CNP. In recent years, CNT is widely reported to cause lysosomal membrane permeabilization (LMP), and the lysosomal damage contribute to related cell death (Jessop et al., 2017). Meunier and colleagues found, DWCNT triggered IL-1β release via inflammasome activation (Meunier et al., 2012). The inflammasome activation is depending on LMP and subsequent Cathepsin B release from damaged lysosomes. Cathepsin B inhibition by CA074-Me attenuated IL-1β release in response to DWNCT. MWCNT also triggered Cathepsin B release in macrophage-differentiated THP-1 cells and plays as a key molecular event on NLRP3 inflammasome activation and IL-1β release. Cathepsin B inhibition also rescued the release of IL-1β release (Keshavan et al., 2021). Thus, LMP may be a potential mechanism that regulates MHV-68 reactivation in response to DWCNT. The application of the Cathepsin B inhibitor reduced lytic viral gene expression to some degree but not significantly. There are other protease of lysosome, like cathepsin L S, C, V and K. A potential mix combination of several cathepsins contributes to MHV-68 reactivation induced by DWCNT. Thus, a pan-cathepsins inhibitor (e.g. K777) application is under consideration to investigate the involvement of LMP in MHV-68 reactivation, and would provide insight into CNT specific toxic effect in herpesvirus reactivation.

However, ERK and JNK MAPK signaling is not contributing to MHV-68 reactivation, since we observed a further high lytic viral gene expression and infectious virus production after inhibitor treatment, demonstrating elevated reactivation. ERK inhibition was reported to reduce cell viability and induce apoptosis. We found that cleaved caspase3 expression was significantly induced by ERK inhibition, indicating the apoptosis activation. As for apoptosis, Bcl-2 protein family determine the fate of cells whether they commit to apoptosis (Czabotar et al., 2014). MHV-68 M11 is homological to Bcl-2 and study showed that, M11 encoded protein MHV-68Bcl-2 protects epithelial cells from apoptosis (Roy et al., 2000). Meanwhile, M11 is persistently expressed during lytic and latent infection of MHV-68, which helps virus to maintain latency. We assumed that ERK and JNK MAPK signaling activation triggers apoptosis and impairs the protection role of M11, resulting in MHV-68 reactivation from latency. Thus, ERK and JNK MAPK play more important role in MHV-68 latency maintenance rather than reactivation.

Oxidative stress or ROS is known to activate MAPK signaling. Many studies have proved the oxidative stress potential of nanomaterials, and ROS subsequently activates MAPK and is associated with pro-inflammatory response. For instance, Particulate matter (PM) triggered ROS and MAPK signaling activation in human bronchial epithelial cells, pretreatment of NAC scavenger abolished ROS level, MAPK activation, as well as downstream inflammatory gene expression, including COX-2, IL-1β, IL-6, IL-8 (Wang et al., 2017). NAC pretreatment also attenuate acute lung inflammation induced by PM exposure in mice. Similarly, we found both NPs exposure caused intracellular ROS production in a rapid response manner. However, treatment with antioxidant NACA failed to attenuate MHV-68 reactivation induced by NPs exposure. H_2O_2 was used as a positive control and induced massive ROS production, compared to our NPs exposure. Indeed, Ye and colleagues reported H_2O_2 triggered KSHV reactivation and was abolished by NAC treatment (Ye et al., 2011).

Meanwhile, we also tried different antioxidants to investigate their effect on MHV-68 reactivation induced by NPs. Resveratrol (3,5,4’-trihydroxy-trans-stilbene) is a natural phenol found in many fruits. As one type of antioxidant, resveratrol possesses anti-oxidant and anti-inflammation potentials, studies has also addressed its role in disease protection (Leonard et al., 2003). However,

pretreatment of resveratrol showed no effect on MHV-68 lytic viral gene expression in response to NPs (data not shown). Another attempt is Vitamin E, which also possesses antioxidant potential. Similarly, no attenuation of lytic viral gene expression of different concentrations of Vitamin E (data not shown).

Given the fact that different types of antioxidants exhibit no effect on MHV-68 reactivation in our case, we assumed that both CNP and DWCNT exposure only induced a low level of oxidative stress, to a degree which is still under control by self-antioxidant effect and is not sufficient to trigger herpesvirus reactivation.

The other reason may be that the type of radicals triggered by NPs and detected by DCFH-DA are different to H_2O_2, and NACA, resveratrol or Vitamin E targeted in other radicals cannot be sufficient to block MHV-68 reactivation induced by NPs exposure (Ates et al., 2008, Baschieri and Amorati, 2021).

4.3 Pharmacological p38 inhibition attenuates MHV-68 reactivation caused by pulmonary CNP exposure

In vitro, we proved that CNP reactivates MHV-68 from latency, p38 inhibition attenuates MHV-68 reactivation via significantly reducing lytic viral gene expression and infectious virus production in Ana-1/MHV-68 cells.

p38 MAPK is widely reported as a target for acute lung injury (ALI). Li and colleagues proved the role of p38 MAPK signaling on suppressing ALI and lung inflammation in mice exposed to lipopolysaccharide (LPS) and its potential effect on macrophage pyroptosis. As a table established model, intratracheally LPS exposure at 5 mg/kg triggered acute lung injury and inflammation, with thickened alveolar septal and hemorrhage appearing from histological analysis, LPS caused increase of protein concentration as total cell numbers in BAL fluid. By p38 inhibitor pretreatment (SB203580; 20 mg/kg), mouse lungs were protected to produce less protein content and BAL cell number, and exhibit less inflammation compared to LPS. Moreover, p38 inhibition also prevent mice from weight loss. Interestingly, p38 MAPK blockage reduced IL-1β release. As macrophages are main target of the cytokine release, the massive release often points to the occurrence of pyroptosis. Thus, the effect of p38 MAPK on NLRP3 inflammasome formation and pyroptosis in macrophages was then proved. Similarly, Li *et al.* also found that, p38 inhibitor pretreatment (40 mg/kg) reduced

MPO, IL-6 and TNF release and neutrophil numbers from BAL fluid induced by LPS (Li et al., 2020). Another p38 inhibitor, SB239063 showed similar effect on intestinal ischemia reperfusion (II/R) injury induced ALI in mouse model (Xiong et al., 2016). Thus, targeting p38 MAPK signaling is a protective or preventive strategy on acute lung injury. Here in our study, translating our *in vitro* findings to *in vivo* helps us to understand the effect of p38 MAPK signaling as a protective target for MHV-68 reactivation as well as related chronic lung diseases induced by nanoparticle exposure.

In vivo, we again confirmed that the administration of p38 inhibitor significantly attenuates MHV-68 reactivation induced by pulmonary CNP exposure. Thus, p38 is a potential protective target in ambient particle exposure induced herpesvirus reactivation and related exacerbations of chronic lung diseases. Other studies also proved the role of p38 MAPK on KSHV reactivation and the contribution on Kaposi's sarcoma development.

As a common signaling pathway, targeting on p38 MAPK may also bring benefit to other virus infection, like influenza virus, accompanied with severe human respiratory symptoms and high morbidity and mortality. Growcott and colleagues tested p38 MAPK inhibitor (BCT194) or related drugs to study their roles on reducing influenza viral replication (Growcott et al., 2018). However, the BCT194 inhibitor showed no effect, but BCT197, which is a closely related p38 MAPK inhibitor, even did not reduce virus replication, was still useful to reduce mice weight loss and improve survival. The concentration of BCT197 in the study was relevant to clinical trials of COPD exacerbations (ClinicalTrials.gov Identifier: NCT01332097).

SARS-CoV-2 infection and COVID-19 pandemic remains a highly concerned global health issue, COVID-19 has a high morbidity and mortality because of the massive inflammatory effects by infection. Some studies also addressed that, p38 MAPK could serve as a potential therapeutic target due to its general effect on pro-inflammatory responses and acute lung injury protection (Grimes and Grimes, 2020). Besides, studies also focused on the coinfection of herpesvirus during COVID-19. A single-center retrospective study revealed that, more than 55% COVID-19 patients was EBV sera antibody detectable, these EBV and SARS-CoV-2 coinfection patients showed significant high risk to develop fever

symptoms (3.9 folds) and high C-reaction protein (CRP) and aspartate aminotransferase (AST) compared to patients only with COVID-19 (Chen et al., 2021). Thus, SARS-CoV-2 infection may be a trigger of EBV reactivation, and EBV reactivation subsequently promote the severity of COVID-19, targeting p38 MAPK both on EBV reactivation as well as inflammatory effect during SARS-CoV-2 infection reduces symptoms and attenuates the development of diseases. This is even worthy to consider for those who are suffering fundamental from chronic lung diseases, like COPD and IPF.

With efforts of epidemiological studies, herpesvirus reactivation is suggested to be associated with IPF development. Herpesvirus DNA is consistently detectable in IPF patients lungs (Tang et al., 2003). Pulkkinen and colleagues also found more than 80% IPF patients lungs are HHV6 DNA positive whereas only 30% for controls, and the detection of HHV6 in IPF patients suggested virus reactivation (Pulkkinen et al., 2012). Another study demonstrated that HHV6 is associated with higher mortality in allogeneic hematopoietic cell transplantation recipients with lower respiratory tract disease (Hill et al., 2019). A meta-analysis showed that the presence of EBV, Cytomegalovirus (CMV), HHV7 and HHV8 significantly increase the risk of developing IPF but not HHV6 (Sheng et al., 2020). All these studies proved that herpesvirus reactivation may act as a driver to promote IPF development, targeting shared therapeutic or treatment strategy would in one hand reduce virus replication, and in the other hand, decrease the effects of IPF.

In 2011, pirfenidone, a p38 target drug, has been approved for a treatment of IPF in Europe (Moran, 2011). Clinical trials leaded by CAPACITY study group tested the effect of pirfenidone oral administration for IPF patients in 110 centers in North America, Australia and Europe (Noble et al., 2011). The phase 2 study revealed that treatment with pirfenidone reduced the decline of lung function of IPF patients, and to a degree, less overall deaths happened. Some side effects are shown in pirfenidone patients, such as nausea, dyspepsia, vomiting and anorexia. Another multi-center clinical trial also assessed the safety and efficacy of pirfenidone for IPF patients (Maher et al., 2020). Despite the side effects, pirfenidone are safe and protective to reduce lung function decline.

Experimental study showed that pirfenidone inhibited the p38 phosphorylation in alveolar epithelial cells (Neri et al., 2016). Thus, pirfenidone treatment on blocking

p38 MAPK signaling exhibited potential effect to attenuate herpesvirus reactivation and is potentially benefit to related CLDs.

Another p38 target drug is Ambroxol, a common cough reliver for CLD patients to help remove bronchial mucus. Ricciardolo and colleagues reported that Ambroxol inhibited p38 phosphorylation as well as pro-inflammatory response induced by LPS in human bronchial epithelial (BEAS-2B) cells (Ricciardolo et al., 2015). Importantly, lung epithelial injury followed by herpesvirus reactivation could contribute to profibrotic response. Thus, experimental as well as epidemiological evidence of these p38 MAPK targeting therapeutic drugs on blocking or controlling herpesvirus reactivation and as a bridge, herpesvirus reactivation related disease exacerbations need to be studied in the future.

4.4 Schematic representation of the study

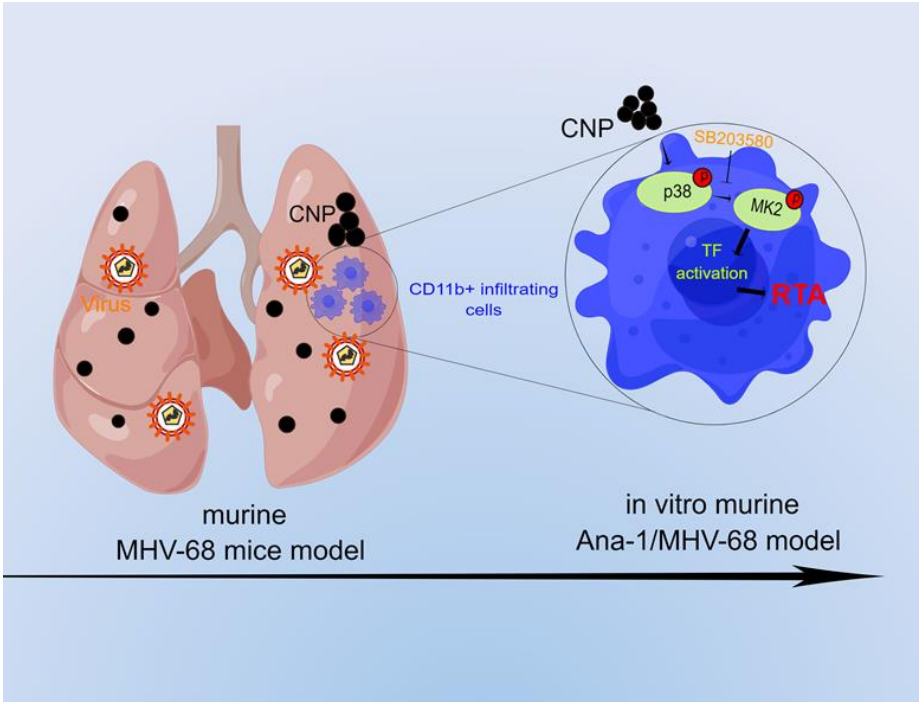

(generated by Figdraw)

The key findings of the current study are:

1. In the murine MHV-68 model, pulmonary CNP exposure induced MHV-68 reactivation mainly localized to CD11b+ infiltrating macrophage-like cells in lung.

2. CNP triggered MHV-68 reactivation via a p38 MAPK dependent signaling and p38 inhibition significantly attenuated MHV-68 reactivation induced by CNP.

5. Conclusion and Outlook

5.1 Conclusion

Our study demonstrated that carbon nanoparticles exposure reactivates latent gammaherpesvirus via a p38 MAPK dependent signaling pathway and inhibition of p38 strongly attenuates lytic virus production after CNP but only weakly after DWCNT exposure *in vitro*. Mechanism underlying nanoparticle induced herpesvirus reactivation is material-shape dependent.

Pulmonary CNP exposure triggers reactivation of latent herpesvirus in mouse lung via a p38 MAPK dependent signaling pathway. pharmacological p38 inhibition might thus alleviates ambient particle exposure related adverse effects and disease exacerbations.

5.2 Outlook

1. Our preliminary result showed that, besides p38 MAPK signaling, there are additional mechanisms for DWCNT induced MHV-68 reactivation. Lysosomal damage is potentially involved. A further study is needed to investigate the underlying mechanism additionally contribute to DWCNT induced MHV-68 reactivation.

2. *In vitro*, we currently use submerge culture model to treat cells whereas an air-liquid interface *in vitro* culture model as well as 3D co-culture is approaching to mimic a more reliable exposure way and investigate the crosstalk between epithelial cells and macrophages during herpesvirus reactivation induced by nanoparticle exposure.

3. A translational study is need to investigate environmental nanoparticle exposure and human herpesvirus reactivation as well as related chronic lung diseases.

4. We concluded that p38 inhibition attenuates herpesvirus reactivation, which demonstrating a potential therapeutic target. However, we are trying to link the attenuation of herpesvirus reactivation by p38 MAPK signaling with diseases exacerbations. Thus, p38 associated medication administration on herpesvirus

reactivation as well as chronic lung disease development in human need further investigation and the further cooperation need build with epidemiology studies.

5. With our current experimental setting *in vivo*, mice were instilled with NPs one time. However, the way of exposure is not mimicking human relevant exposure. Inhalation of nanoparticles to mice would be considered in the further plans. Furthermore, a more frequent exposure times will be performed in the further to mimic a more realistic research model.

6. In the current study, we mainly focus on carbon nanoparticles exposure, other omnipresent or emerging components of ambient pollution as well as environmental factors, e.g, metal particles, microplastics, pollens would be also necessary to be investigated in the further.

7. More experimental methods to identify herpesvirus reactivation, e.g. specific antibody against MHV-68 and lytic viral gene expression in early time points need to be considered in the future projects.

References

AGUILAR, P. M., CARRERA, L. G., SEGURA, C. C., SáNCHEZ, M. I. T., PEñA, M. F., HERNáN, G. B., RODRíGUEZ, I. E., ZAPATA, R. M. R., LUCAS, E. Z., ÁLVAREZ, P. D., BUENO, E. V., SáNCHEZ, C. P. & WALTHER, R. 2021. Relationship between air pollution levels in Madrid and the natural history of idiopathic pulmonary fibrosis: severity and mortality. *J Int Med Res,* 49**,** 3000605211029058.

ALESSANDRINI, F., SCHULZ, H., TAKENAKA, S., LENTNER, B., KARG, E., BEHRENDT, H. & JAKOB, T. 2006. Effects of ultrafine carbon particle inhalation on allergic inflammation of the lung. *J Allergy Clin Immunol,* 117**,** 824-30.

ANDRé, E., STOEGER, T., TAKENAKA, S., BAHNWEG, M., RITTER, B., KARG, E., LENTNER, B., REINHARD, C., SCHULZ, H. & WJST, M. 2006. Inhalation of ultrafine carbon particles triggers biphasic pro-inflammatory response in the mouse lung. *Eur Respir J,* 28**,** 275-85.

ANEJA, K. K. & YUAN, Y. 2017. Reactivation and Lytic Replication of Kaposi's Sarcoma-Associated Herpesvirus: An Update. *Front Microbiol,* 8**,** 613.

ATES, B., ABRAHAM, L. & ERCAL, N. 2008. Antioxidant and free radical scavenging properties of N-acetylcysteine amide (NACA) and comparison with N-acetylcysteine (NAC). *Free Radic Res,* 42**,** 372-7.

AWASTHI, K., SRIVASTAVA, A. & SRIVASTAVA, O. N. 2005. Synthesis of carbon nanotubes. *J Nanosci Nanotechnol,* 5**,** 1616-36.

BAN, J. Y., KIM, B. S., KIM, S. C., KIM, D. H. & CHUNG, J. H. 2011. Microarray Analysis of Gene Expression Profiles in Response to Treatment with Melatonin in Lipopolysaccharide Activated RAW 264.7 Cells. *Korean J Physiol Pharmacol,* 15**,** 23-9.

BARBARINO, M. & GIORDANO, A. 2021. Assessment of the Carcinogenicity of Carbon Nanotubes in the Respiratory System. *Cancers (Basel),* 13.

BARLOW, P. G., CLOUTER-BAKER, A., DONALDSON, K., MACCALLUM, J. & STONE, V. 2005. Carbon black nanoparticles induce type II epithelial cells to release chemotaxins for alveolar macrophages. *Part Fibre Toxicol,* 2**,** 11.

BARTON, E., MANDAL, P. & SPECK, S. H. 2011. Pathogenesis and host control of gammaherpesviruses: lessons from the mouse. *Annu Rev Immunol,* 29**,** 351-97.

BASCHIERI, A. & AMORATI, R. 2021. Methods to Determine Chain-Breaking Antioxidant Activity of Nanomaterials beyond DPPH(•). A Review. *Antioxidants (Basel),* 10.

BEYELER, S., STEINER, S., WOTZKOW, C., TSCHANZ, S. A., ADHANOM SENGAL, A., WICK, P., HAENNI, B., ALVES, M. P., VON GARNIER, C. & BLANK, F. 2020. Multi-walled carbon nanotubes activate and shift polarization of pulmonary macrophages and dendritic cells in an in vivo model of chronic obstructive lung disease. *Nanotoxicology,* 14**,** 77-96.

BLASI, E., MATHIESON, B. J., VARESIO, L., CLEVELAND, J. L., BORCHERT, P. A. & RAPP, U. R. 1985. Selective immortalization of murine macrophages from fresh bone marrow by a raf/myc recombinant murine retrovirus. *Nature,* 318**,** 667-70.

BOSHOFF, C. & WEISS, R. A. 2001. Epidemiology and pathogenesis of Kaposi's sarcoma-associated herpesvirus. *Philos Trans R Soc Lond B Biol Sci,* 356**,** 517-34.

BOURDON, J. A., SABER, A. T., JACOBSEN, N. R., JENSEN, K. A., MADSEN, A. M., LAMSON, J. S., WALLIN, H., MøLLER, P., LOFT, S., YAUK, C. L. & VOGEL, U. B. 2012. Carbon black nanoparticle instillation induces sustained inflammation and genotoxicity in mouse lung and liver. *Part Fibre Toxicol,* 9**,** 5.

BROWN, H. J., SONG, M. J., DENG, H., WU, T. T., CHENG, G. & SUN, R. 2003. NF-kappaB inhibits gammaherpesvirus lytic replication. *J Virol,* 77**,** 8532-40.

CASS, S. P., MEKHAEL, O., THAYAPARAN, D., MCGRATH, J. J. C., REVILL, S. D., FANTAUZZI, M. F., WANG, P., REIHANI, A., HAYAT, A. I., STEVENSON, C. S., DVORKIN-GHEVA, A., BOTELHO, F. M., STäMPFLI, M. R. & ASK, K. 2021. Increased Monocyte-Derived CD11b(+) Macrophage Subpopulations Following Cigarette Smoke Exposure Are Associated With Impaired Bleomycin-Induced Tissue Remodelling. *Front Immunol,* 12**,** 740330.

CHAUDHARY, P. M., JASMIN, A., EBY, M. T. & HOOD, L. 1999. Modulation of the NF-kappa B pathway by virally encoded death effector domains-containing proteins. *Oncogene,* 18**,** 5738-46.

CHEN, C. L., HUANG, Y., MARTINEZ-GARCIA, M. A., YUAN, J. J., LI, H. M., DE LA ROSA-CARRILLO, D., HAN, X. R., CHEN, R. C., GUAN, W. J. & ZHONG, N. S. 2020. The Role of Epstein-Barr Virus in Adults With Bronchiectasis: A Prospective Cohort Study. *Open Forum Infect Dis,* 7**,** ofaa235.

CHEN, S., YIN, R., MUTZE, K., YU, Y., TAKENAKA, S., KöNIGSHOFF, M. & STOEGER, T. 2016. No involvement of alveolar macrophages in the initiation of carbon nanoparticle induced acute lung inflammation in mice. *Part Fibre Toxicol,* 13**,** 33.

CHEN, T., SONG, J., LIU, H., ZHENG, H. & CHEN, C. 2021. Positive Epstein-Barr virus detection in coronavirus disease 2019 (COVID-19) patients. *Sci Rep,* 11**,** 10902.

CHRISTIANI, D. C. 2021. Ambient Air Pollution and Lung Cancer: Nature and Nurture. *Am J Respir Crit Care Med,* 204**,** 752-753.

CIENIEWICZ, B., SANTANA, A. L., MINKAH, N. & KRUG, L. T. 2016. Interplay of Murine Gammaherpesvirus 68 with NF-kappaB Signaling of the Host. *Front Microbiol,* 7**,** 1202.

COLLABORATORS, G. R. F. 2018. Global, regional, and national comparative risk assessment of 84 behavioural, environmental and occupational, and metabolic risks or clusters of risks for 195 countries and territories, 1990-2017: a systematic analysis for the Global Burden of Disease Study 2017. *Lancet,* 392**,** 1923-1994.

COX, G. W., MATHIESON, B. J., GANDINO, L., BLASI, E., RADZIOCH, D. & VARESIO, L. 1989. Heterogeneity of hematopoietic cells immortalized by v-myc/v-raf recombinant retrovirus infection of bone marrow or fetal liver. *J Natl Cancer Inst,* 81**,** 1492-6.

CZABOTAR, P. E., LESSENE, G., STRASSER, A. & ADAMS, J. M. 2014. Control of apoptosis by the BCL-2 protein family: implications for physiology and therapy. *Nat Rev Mol Cell Biol,* 15**,** 49-63.

DE SANJOSE, S., MBISA, G., PEREZ-ALVAREZ, S., BENAVENTE, Y., SUKVIRACH, S., HIEU, N. T., SHIN, H. R., ANH, P. T., THOMAS, J., LAZCANO, E., MATOS, E., HERRERO, R., MUñOZ, N., MOLANO, M., FRANCESCHI, S. & WHITBY, D. 2009. Geographic variation in the prevalence of Kaposi sarcoma-associated herpesvirus and risk factors for transmission. *J Infect Dis,* 199**,** 1449-56.

DEUTSCH, E., COHEN, A., KAZIMIRSKY, G., DOVRAT, S., RUBINFELD, H., BRODIE, C. & SARID, R. 2004. Role of protein kinase C delta in reactivation of Kaposi's sarcoma-associated herpesvirus. *J Virol,* 78**,** 10187-92.

DUKE, K. S. & BONNER, J. C. 2018. Mechanisms of carbon nanotube-induced pulmonary fibrosis: a physicochemical characteristic perspective. *Wiley Interdiscip Rev Nanomed Nanobiotechnol,* 10**,** e1498.

DUPONT, L. & REEVES, M. B. 2016. Cytomegalovirus latency and reactivation: recent insights into an age old problem. *Rev Med Virol,* 26**,** 75-89.

EPA 2022. Particulate Matter (PM) Basics.

EVREN, E., RINGQVIST, E. & WILLINGER, T. 2020. Origin and ontogeny of lung macrophages: from mice to humans. *Immunology,* 160**,** 126-138.

FARRELL, H. E., LAWLER, C., OLIVEIRA, M. T., DAVIS-POYNTER, N. & STEVENSON, P. G. 2015. Alveolar Macrophages Are a Prominent but Nonessential Target for Murine Cytomegalovirus Infecting the Lungs. *J Virol,* 90**,** 2756-66.

FRANK, E. A., BIRCH, M. E. & YADAV, J. S. 2015. MyD88 mediates in vivo effector functions of alveolar macrophages in acute lung inflammatory responses to carbon nanotube exposure. *Toxicol Appl Pharmacol,* 288**,** 322-9.

FRITSCH-DECKER, S., MARQUARDT, C., STOEGER, T., DIABATé, S. & WEISS, C. 2018. Revisiting the stress paradigm for silica nanoparticles: decoupling of the anti-oxidative defense, pro-inflammatory response and cytotoxicity. *Arch Toxicol,* 92**,** 2163-2174.

GANGULY, K., ETTEHADIEH, D., UPADHYAY, S., TAKENAKA, S., ADLER, T., KARG, E., KROMBACH, F., KREYLING, W. G., SCHULZ, H., SCHMID, O. & STOEGER, T. 2017. Early pulmonary response is critical for extra-pulmonary carbon nanoparticle mediated effects: comparison of inhalation versus intra-arterial infusion exposures in mice. *Part Fibre Toxicol,* 14**,** 19.

GEISER, M., QUAILE, O., WENK, A., WIGGE, C., EIGELDINGER-BERTHOU, S., HIRN, S., SCHäFFLER, M., SCHLEH, C., MöLLER, W., MALL, M. A. & KREYLING, W. G. 2013. Cellular uptake and localization of inhaled gold nanoparticles in lungs of mice with chronic obstructive pulmonary disease. *Part Fibre Toxicol,* 10**,** 19.

GHONEIM, H. E., THOMAS, P. G. & MCCULLERS, J. A. 2013. Depletion of alveolar macrophages during influenza infection facilitates bacterial superinfections. *J Immunol,* 191**,** 1250-9.

GRIMES, J. M. & GRIMES, K. V. 2020. p38 MAPK inhibition: A promising therapeutic approach for COVID-19. *J Mol Cell Cardiol,* 144**,** 63-65.

GROWCOTT, E. J., BAMBA, D., GALARNEAU, J. R., LEONARD, V. H. J., SCHUL, W., STEIN, D. & OSBORNE, C. S. 2018. The effect of P38 MAP kinase inhibition in a mouse model of influenza. *J Med Microbiol,* 67**,** 452-462.

HAGEMEIER, S. R., BARLOW, E. A., MENG, Q. & KENNEY, S. C. 2012. The cellular ataxia telangiectasia-mutated kinase promotes epstein-barr virus lytic reactivation in response to multiple different types of lytic reactivation-inducing stimuli. *J Virol,* 86**,** 13360-70.

HAMRA, G. B., GUHA, N., COHEN, A., LADEN, F., RAASCHOU-NIELSEN, O., SAMET, J. M., VINEIS, P., FORASTIERE, F., SALDIVA, P., YORIFUJI, T. & LOOMIS, D. 2014. Outdoor particulate matter exposure and lung cancer: a systematic review and meta-analysis. *Environ Health Perspect,* 122**,** 906-11.

HILL, J. A., VANDE VUSSE, L. K., XIE, H., CHUNG, E. L., YEUNG, C. C. S., SEO, S., STEVENS-AYERS, T., FISHER, C. E., HUANG, M. L., STEWART, F. M., JEROME, K. R., ZERR, D. M., COREY, L., LEISENRING, W. M. & BOECKH, M. 2019. Human Herpesvirus 6B and Lower Respiratory Tract Disease After Hematopoietic Cell Transplantation. *J Clin Oncol,* 37**,** 2670-2681.

HSU, M. J., WU, C. Y., CHIANG, H. H., LAI, Y. L. & HUNG, S. L. 2010. PI3K/Akt signaling mediated apoptosis blockage and viral gene expression in oral epithelial cells during herpes simplex virus infection. *Virus Res,* 153**,** 36-43.

HUANG, Y., ZHU, M., JI, M., FAN, J., XIE, J., WEI, X., JIANG, X., XU, J., CHEN, L., YIN, R., WANG, Y., DAI, J., JIN, G., XU, L., HU, Z., MA, H. & SHEN, H. 2021. Air Pollution, Genetic Factors, and the Risk of Lung Cancer: A Prospective Study in the UK Biobank. *Am J Respir Crit Care Med,* 204**,** 817-825.

HUSAIN, M., KYJOVSKA, Z. O., BOURDON-LACOMBE, J., SABER, A. T., JENSEN, K. A., JACOBSEN, N. R., WILLIAMS, A., WALLIN, H., HALAPPANAVAR, S., VOGEL, U. & YAUK, C. L. 2015. Carbon black nanoparticles induce biphasic gene expression changes associated with inflammatory responses in the lungs of C57BL/6 mice following a single intratracheal instillation. *Toxicol Appl Pharmacol,* 289**,** 573-88.

IEMPRIDEE, T., DAS, S., XU, I. & MERTZ, J. E. 2011. Transforming growth factor beta-induced reactivation of Epstein-Barr virus involves multiple Smad-binding elements cooperatively activating expression of the latent-lytic switch BZLF1 gene. *J Virol,* 85**,** 7836-48.

INOUE, K., TAKANO, H., YANAGISAWA, R., HIRANO, S., SAKURAI, M., SHIMADA, A. & YOSHIKAWA, T. 2006. Effects of airway exposure to nanoparticles on lung inflammation induced by bacterial endotoxin in mice. *Environ Health Perspect,* 114**,** 1325-30.

INOUE, K., TAKANO, H., YANAGISAWA, R., SAKURAI, M., ICHINOSE, T., SADAKANE, K. & YOSHIKAWA, T. 2005. Effects of nano particles on antigen-related airway inflammation in mice. *Respir Res,* 6**,** 106.

JANSSEN, W. J., BARTHEL, L., MULDROW, A., OBERLEY-DEEGAN, R. E., KEARNS, M. T., JAKUBZICK, C. & HENSON, P. M. 2011. Fas determines differential fates of resident and recruited macrophages during resolution of acute lung injury. *Am J Respir Crit Care Med,* 184**,** 547-60.

JESSOP, F., HAMILTON, R. F., JR., RHODERICK, J. F., FLETCHER, P. & HOLIAN, A. 2017. Phagolysosome acidification is required for silica and engineered nanoparticle-induced lysosome membrane permeabilization and resultant NLRP3 inflammasome activity. *Toxicol Appl Pharmacol,* 318**,** 58-68.

JOHANNSON, K. A., VITTINGHOFF, E., MORISSET, J., WOLTERS, P. J., NOTH, E. M., BALMES, J. R. & COLLARD, H. R. 2018. Air Pollution Exposure Is Associated With Lower Lung Function, but Not Changes in Lung Function, in Patients With Idiopathic Pulmonary Fibrosis. *Chest,* 154**,** 119-125.

KEET, C. A., KELLER, J. P. & PENG, R. D. 2018. Long-Term Coarse Particulate Matter Exposure Is Associated with Asthma among Children in Medicaid. *Am J Respir Crit Care Med,* 197**,** 737-746.

KESHAVAN, S., GUPTA, G., MARTIN, S. & FADEEL, B. 2021. Multi-walled carbon nanotubes trigger lysosome-dependent cell death (pyroptosis) in macrophages but not in neutrophils. *Nanotoxicology,* 15**,** 1125-1150.

KOLOSNJAJ-TABI, J., JUST, J., HARTMAN, K. B., LAOUDI, Y., BOUDJEMAA, S., ALLOYEAU, D., SZWARC, H., WILSON, L. J. & MOUSSA, F. 2015. Anthropogenic Carbon Nanotubes Found in the Airways of Parisian Children. *EBioMedicine,* 2**,** 1697-704.

KOTAKI, K., IKEDA, H., FUKUDA, T., YUHEI, K., YUKI, F., KAWASAKI, M., WAKAMATSU, K. & SUGAHARA, K. 2019. Trends in the prevalence of COPD in elderly individuals in an air-polluted city in Japan: a cross-sectional study. *Int J Chron Obstruct Pulmon Dis,* 14**,** 791-798.

KROKER, M., SYDLIK, U., AUTENGRUBER, A., CAVELIUS, C., WEIGHARDT, H., KRAEGELOH, A. & UNFRIED, K. 2015. Preventing carbon nanoparticle-induced lung inflammation reduces antigen-specific sensitization and subsequent allergic reactions in a mouse model. *Part Fibre Toxicol,* 12**,** 20.

KURMI, O. P., SEMPLE, S., SIMKHADA, P., SMITH, W. C. & AYRES, J. G. 2010. COPD and chronic bronchitis risk of indoor air pollution from solid fuel: a systematic review and meta-analysis. *Thorax,* 65**,** 221-8.

LABO, N., MILEY, W., BENSON, C. A., CAMPBELL, T. B. & WHITBY, D. 2015. Epidemiology of Kaposi's sarcoma-associated herpesvirus in HIV-1-infected US persons in the era of combination antiretroviral therapy. *Aids,* 29**,** 1217-25.

LANDRIGAN, P. J., FULLER, R., ACOSTA, N. J. R., ADEYI, O., ARNOLD, R., BASU, N. N., BALDé, A. B., BERTOLLINI, R., BOSE-O'REILLY, S., BOUFFORD, J. I., BREYSSE, P. N., CHILES, T., MAHIDOL, C., COLL-SECK, A. M., CROPPER, M. L., FOBIL, J., FUSTER, V., GREENSTONE, M., HAINES, A., HANRAHAN, D., HUNTER, D., KHARE, M., KRUPNICK, A., LANPHEAR, B., LOHANI, B., MARTIN, K., MATHIASEN, K. V., MCTEER, M. A., MURRAY, C. J. L., NDAHIMANANJARA, J. D., PERERA, F., POTOČNIK, J., PREKER, A. S., RAMESH, J., ROCKSTRöM, J., SALINAS, C., SAMSON, L. D., SANDILYA, K., SLY, P. D., SMITH, K. R., STEINER, A., STEWART, R. B., SUK, W. A., VAN SCHAYCK, O. C. P., YADAMA, G. N., YUMKELLA, K. & ZHONG, M. 2018. The Lancet Commission on pollution and health. *Lancet,* 391**,** 462-512.

LEONARD, S. S., XIA, C., JIANG, B. H., STINEFELT, B., KLANDORF, H., HARRIS, G. K. & SHI, X. 2003. Resveratrol scavenges reactive oxygen species and effects radical-induced cellular responses. *Biochem Biophys Res Commun,* 309**,** 1017-26.

LI, N., HAO, M., PHALEN, R. F., HINDS, W. C. & NEL, A. E. 2003. Particulate air pollutants and asthma. A paradigm for the role of oxidative stress in PM-induced adverse health effects. *Clin Immunol,* 109**,** 250-65.

LI, T., WU, Y. N., WANG, H., MA, J. Y., ZHAI, S. S. & DUAN, J. 2020. Dapk1 improves inflammation, oxidative stress and autophagy in LPS-induced acute lung injury via p38MAPK/NF-κB signaling pathway. *Mol Immunol,* 120**,** 13-22.

LI, X., FENG, J. & SUN, R. 2011. Oxidative stress induces reactivation of Kaposi's sarcoma-associated herpesvirus and death of primary effusion lymphoma cells. *J Virol,* 85**,** 715-24.

LI, Z., XU, X., LENG, X., HE, M., WANG, J., CHENG, S. & WU, H. 2017. Roles of reactive oxygen species in cell signaling pathways and immune responses to viral infections. *Arch Virol,* 162**,** 603-610.

LIANG, L., CAI, Y., LYU, B., ZHANG, D., CHU, S., JING, H., RAHIMI, K. & TONG, Z. 2022. Air pollution and hospitalization of patients with idiopathic pulmonary fibrosis in Beijing: a time-series study. *Respir Res,* 23**,** 81.

LIU, S., ZHOU, Y., WANG, X., WANG, D., LU, J., ZHENG, J., ZHONG, N. & RAN, P. 2007. Biomass fuels are the probable risk factor for chronic obstructive pulmonary disease in rural South China. *Thorax,* 62**,** 889-97.

LIU, X. & COHEN, J. I. 2015. The role of PI3K/Akt in human herpesvirus infection: From the bench to the bedside. *Virology,* 479-480**,** 568-77.

LOK, S. S., HAIDER, Y., HOWELL, D., STEWART, J. P., HASLETON, P. S. & EGAN, J. J. 2002. Murine gammaherpes virus as a cofactor in the development of pulmonary fibrosis in bleomycin resistant mice. *Eur Respir J,* 20**,** 1228-32.

MAHER, T. M., CORTE, T. J., FISCHER, A., KREUTER, M., LEDERER, D. J., MOLINA-MOLINA, M., AXMANN, J., KIRCHGAESSLER, K. U., SAMARA, K., GILBERG, F. & COTTIN, V. 2020. Pirfenidone in patients with unclassifiable progressive fibrosing interstitial lung disease: a double-blind, randomised, placebo-controlled, phase 2 trial. *Lancet Respir Med,* 8**,** 147-157.

MARZOUK, K., CORATE, L., SALEH, S. & SHARMA, O. P. 2005. Epstein-Barr-virus-induced interstitial lung disease. *Curr Opin Pulm Med,* 11**,** 456-60.

MCMANUS, T. E., MARLEY, A. M., BAXTER, N., CHRISTIE, S. N., ELBORN, J. S., O'NEILL, H. J., COYLE, P. V. & KIDNEY, J. C. 2008. High levels of Epstein-Barr virus in COPD. *Eur Respir J,* 31**,** 1221-6.

MCMILLAN, T. R., MOORE, B. B., WEINBERG, J. B., VANNELLA, K. M., FIELDS, W. B., CHRISTENSEN, P. J., VAN DYK, L. F. & TOEWS, G. B. 2008. Exacerbation of established pulmonary fibrosis in a murine model by gammaherpesvirus. *Am J Respir Crit Care Med,* 177**,** 771-80.

MEUNIER, E., COSTE, A., OLAGNIER, D., AUTHIER, H., LEFèVRE, L., DARDENNE, C., BERNAD, J., BéRAUD, M., FLAHAUT, E. & PIPY, B. 2012. Double-walled carbon nanotubes trigger IL-1β release in human monocytes through Nlrp3 inflammasome activation. *Nanomedicine,* 8**,** 987-95.

MISHARIN, A. V., MORALES-NEBREDA, L., MUTLU, G. M., BUDINGER, G. R. & PERLMAN, H. 2013. Flow cytometric analysis of macrophages and dendritic cell subsets in the mouse lung. *Am J Respir Cell Mol Biol,* 49**,** 503-10.

MOLDOBAEVA, A., ZHONG, Q., ELDRIDGE, L. & WAGNER, E. M. 2018. CD11b(+) interstitial macrophages are required for ischemia-induced lung angiogenesis. *Physiol Rep,* 6**,** e13721.

MOORE, P. S., BOSHOFF, C., WEISS, R. A. & CHANG, Y. 1996a. Molecular mimicry of human cytokine and cytokine response pathway genes by KSHV. *Science,* 274**,** 1739-44.

MOORE, P. S., GAO, S. J., DOMINGUEZ, G., CESARMAN, E., LUNGU, O., KNOWLES, D. M., GARBER, R., PELLETT, P. E., MCGEOCH, D. J. & CHANG, Y. 1996b. Primary characterization of a herpesvirus agent associated with Kaposi's sarcomae. *J Virol,* 70**,** 549-58.

MORAN, N. 2011. p38 kinase inhibitor approved for idiopathic pulmonary fibrosis. *Nat Biotechnol,* 29**,** 301.

MURATA, T. 2014. Regulation of Epstein-Barr virus reactivation from latency. *Microbiol Immunol,* 58**,** 307-17.

MZINZA, D. T., FLEIGE, H., LAARMANN, K., WILLENZON, S., RISTENPART, J., SPANIER, J., SUTTER, G., KALINKE, U., VALENTIN-WEIGAND, P. & FöRSTER, R. 2018. Application of light sheet microscopy for qualitative and quantitative analysis of bronchus-associated lymphoid tissue in mice. *Cell Mol Immunol,* 15**,** 875-887.

NEL, A., XIA, T., MäDLER, L. & LI, N. 2006. Toxic potential of materials at the nanolevel. *Science,* 311**,** 622-7.

NERI, T., LOMBARDI, S., FAìTA, F., PETRINI, S., BALìA, C., SCALISE, V., PEDRINELLI, R., PAGGIARO, P. & CELI, A. 2016. Pirfenidone inhibits p38-mediated generation of procoagulant microparticles by human alveolar epithelial cells. *Pulm Pharmacol Ther,* 39**,** 1-6.

NOBLE, P. W., ALBERA, C., BRADFORD, W. Z., COSTABEL, U., GLASSBERG, M. K., KARDATZKE, D., KING, T. E., JR., LANCASTER, L., SAHN, S. A., SZWARCBERG, J., VALEYRE, D. & DU BOIS, R. M. 2011. Pirfenidone in patients with idiopathic pulmonary fibrosis (CAPACITY): two randomised trials. *Lancet,* 377**,** 1760-9.

PAN, H., XIE, J., YE, F. & GAO, S. J. 2006. Modulation of Kaposi's sarcoma-associated herpesvirus infection and replication by MEK/ERK, JNK, and p38 multiple mitogen-activated protein kinase pathways during primary infection. *J Virol,* 80**,** 5371-82.

PATHAK, U., GUPTA, N. C. & SURI, J. C. 2020. Risk of COPD due to indoor air pollution from biomass cooking fuel: a systematic review and meta-analysis. *Int J Environ Health Res,* 30**,** 75-88.

PEETERS, P. M., EURLINGS, I. M., PERKINS, T. N., WOUTERS, E. F., SCHINS, R. P., BORM, P. J., DROMMER, W., REYNAERT, N. L. & ALBRECHT, C. 2014. Silica-induced NLRP3 inflammasome activation in vitro and in rat lungs. *Part Fibre Toxicol,* 11**,** 58.

PEETERS, P. M., PERKINS, T. N., WOUTERS, E. F., MOSSMAN, B. T. & REYNAERT, N. L. 2013. Silica induces NLRP3 inflammasome activation in human lung epithelial cells. *Part Fibre Toxicol,* 10**,** 3.

PETERS, A., DOCKERY, D. W., HEINRICH, J. & WICHMANN, H. E. 1997. Short-term effects of particulate air pollution on respiratory morbidity in asthmatic children. *Eur Respir J,* 10**,** 872-9.

PULKKINEN, V., SALMENKIVI, K., KINNULA, V. L., SUTINEN, E., HALME, M., HODGSON, U., LEHTO, J., JääSKELäINEN, A., PIIPARINEN, H., KERE, J., LAUTENSCHLAGER, I., LAPPALAINEN, M. & MYLLäRNIEMI, M. 2012. A novel screening method detects herpesviral DNA in the idiopathic pulmonary fibrosis lung. *Ann Med,* 44**,** 178-86.

QIN, D., FENG, N., FAN, W., MA, X., YAN, Q., LV, Z., ZENG, Y., ZHU, J. & LU, C. 2011. Activation of PI3K/AKT and ERK MAPK signal pathways is required for the induction of lytic cycle replication of Kaposi's sarcoma-associated herpesvirus by herpes simplex virus type 1. *BMC Microbiol,* 11**,** 240.

RABOLLI, V., BADISSI, A. A., DEVOSSE, R., UWAMBAYINEMA, F., YAKOUB, Y., PALMAI-PALLAG, M., LEBRUN, A., DE GUSSEM, V., COUILLIN, I., RYFFEL, B., MARBAIX, E., LISON, D. & HUAUX, F. 2014. The alarmin IL-1α is a master cytokine in acute lung inflammation induced by silica micro- and nanoparticles. *Part Fibre Toxicol,* 11**,** 69.

REESE, T. A., WAKEMAN, B. S., CHOI, H. S., HUFFORD, M. M., HUANG, S. C., ZHANG, X., BUCK, M. D., JEZEWSKI, A., KAMBAL, A., LIU, C. Y., GOEL, G., MURRAY, P. J., XAVIER, R. J., KAPLAN, M. H., RENNE, R., SPECK, S. H., ARTYOMOV, M. N., PEARCE, E. J. & VIRGIN, H. W. 2014. Helminth infection reactivates latent γ-herpesvirus via cytokine competition at a viral promoter. *Science,* 345**,** 573-7.

RENNE, R., ZHONG, W., HERNDIER, B., MCGRATH, M., ABBEY, N., KEDES, D. & GANEM, D. 1996. Lytic growth of Kaposi's sarcoma-associated herpesvirus (human herpesvirus 8) in culture. *Nat Med,* 2**,** 342-6.

RENWICK, L. C., BROWN, D., CLOUTER, A. & DONALDSON, K. 2004. Increased inflammation and altered macrophage chemotactic responses caused by two ultrafine particle types. *Occup Environ Med,* 61**,** 442-7.

RICCIARDOLO, F. L., SORBELLO, V., BENEDETTO, S. & PALEARI, D. 2015. Effect of Ambroxol and Beclomethasone on Lipopolysaccharide-Induced Nitrosative Stress in Bronchial Epithelial Cells. *Respiration,* 89**,** 572-82.

RON, D. & KAZANIETZ, M. G. 1999. New insights into the regulation of protein kinase C and novel phorbol ester receptors. *Faseb j,* 13**,** 1658-76.

ROY, D. J., EBRAHIMI, B. C., DUTIA, B. M., NASH, A. A. & STEWART, J. P. 2000. Murine gammaherpesvirus M11 gene product inhibits apoptosis and is expressed during virus persistence. *Arch Virol,* 145**,** 2411-20.

RUISS, R., OHNO, S., STEER, B., ZEIDLER, R. & ADLER, H. 2012. Murine gammaherpesvirus 68 glycoprotein 150 does not contribute to latency amplification in vivo. *Virol J,* 9**,** 107.

SARID, R., FLORE, O., BOHENZKY, R. A., CHANG, Y. & MOORE, P. S. 1998. Transcription mapping of the Kaposi's sarcoma-associated herpesvirus (human herpesvirus 8) genome in a body cavity-based lymphoma cell line (BC-1). *J Virol,* 72**,** 1005-12.

SATTLER, C., MORITZ, F., CHEN, S., STEER, B., KUTSCHKE, D., IRMLER, M., BECKERS, J., EICKELBERG, O., SCHMITT-KOPPLIN, P., ADLER, H. & STOEGER, T. 2017. Nanoparticle exposure reactivates latent herpesvirus and restores a signature of acute infection. *Part Fibre Toxicol,* 14**,** 2.

SCHRAUFNAGEL, D. E. 2020. The health effects of ultrafine particles. *Exp Mol Med,* 52**,** 311-317.

SEHRAWAT, S., KUMAR, D. & ROUSE, B. T. 2018. Herpesviruses: Harmonious Pathogens but Relevant Cofactors in Other Diseases? *Front Cell Infect Microbiol,* 8**,** 177.

SHENG, G., CHEN, P., WEI, Y., YUE, H., CHU, J., ZHAO, J., WANG, Y., ZHANG, W. & ZHANG, H. L. 2020. Viral Infection Increases the Risk of Idiopathic Pulmonary Fibrosis: A Meta-Analysis. *Chest,* 157**,** 1175-1187.

SHVEDOVA, A. A., FABISIAK, J. P., KISIN, E. R., MURRAY, A. R., ROBERTS, J. R., TYURINA, Y. Y., ANTONINI, J. M., FENG, W. H., KOMMINENI, C., REYNOLDS, J., BARCHOWSKY, A., CASTRANOVA, V. & KAGAN, V. E. 2008a. Sequential exposure to carbon nanotubes and bacteria enhances pulmonary inflammation and infectivity. *Am J Respir Cell Mol Biol,* 38**,** 579-90.

SHVEDOVA, A. A., KISIN, E., MURRAY, A. R., JOHNSON, V. J., GORELIK, O., AREPALLI, S., HUBBS, A. F., MERCER, R. R., KEOHAVONG, P., SUSSMAN, N., JIN, J., YIN, J., STONE, S., CHEN, B. T., DEYE, G., MAYNARD, A., CASTRANOVA, V., BARON, P. A. & KAGAN, V. E. 2008b. Inhalation vs. aspiration of single-walled carbon nanotubes in C57BL/6 mice: inflammation, fibrosis, oxidative stress, and mutagenesis. *Am J Physiol Lung Cell Mol Physiol,* 295**,** L552-65.

SHVEDOVA, A. A., KISIN, E. R., MERCER, R., MURRAY, A. R., JOHNSON, V. J., POTAPOVICH, A. I., TYURINA, Y. Y., GORELIK, O., AREPALLI, S., SCHWEGLER-BERRY, D., HUBBS, A. F., ANTONINI, J., EVANS, D. E., KU, B. K., RAMSEY, D., MAYNARD, A., KAGAN, V. E., CASTRANOVA, V. & BARON, P. 2005. Unusual inflammatory and fibrogenic pulmonary responses to single-walled carbon nanotubes in mice. *Am J Physiol Lung Cell Mol Physiol,* 289**,** L698-708.

SINCLAIR, A. J. 2013. Epigenetic control of Epstein-Barr virus transcription - relevance to viral life cycle? *Front Genet,* 4**,** 161.

SMATTI, M. K., AL-SADEQ, D. W., ALI, N. H., PINTUS, G., ABOU-SALEH, H. & NASRALLAH, G. K. 2018. Epstein-Barr Virus Epidemiology, Serology, and Genetic Variability of LMP-1 Oncogene Among Healthy Population: An Update. *Front Oncol,* 8**,** 211.

SONI, S., ANAND, P. & PADWAD, Y. S. 2019. MAPKAPK2: the master regulator of RNA-binding proteins modulates transcript stability and tumor progression. *J Exp Clin Cancer Res,* 38**,** 121.

STEER, B., ADLER, B., JONJIC, S., STEWART, J. P. & ADLER, H. 2010. A gammaherpesvirus complement regulatory protein promotes initiation of infection by activation of protein kinase Akt/PKB. *PLoS One,* 5**,** e11672.

STEER, B., STREHLE, M., SATTLER, C., BUND, D., FLACH, B., STOEGER, T., HAAS, J. G. & ADLER, H. 2016. The small noncoding RNAs (sncRNAs) of murine gammaherpesvirus 68 (MHV-68) are involved in regulating the latent-to-lytic switch in vivo. *Sci Rep,* 6**,** 32128.

STöCKMANN, D., SPANNBRUCKER, T., ALE-AGHA, N., JAKOBS, P., GOY, C., DYBALLA-RUKES, N., HORNSTEIN, T., KüMPER, A., KRAEGELOH, A., HAENDELER, J. & UNFRIED, K. 2018. Non-Canonical Activation of the Epidermal Growth Factor Receptor by Carbon Nanoparticles. *Nanomaterials (Basel),* 8.

STOEGER, T. & ADLER, H. 2018. "Novel" Triggers of Herpesvirus Reactivation and Their Potential Health Relevance. *Front Microbiol,* 9**,** 3207.

STOEGER, T., TAKENAKA, S., FRANKENBERGER, B., RITTER, B., KARG, E., MAIER, K., SCHULZ, H. & SCHMID, O. 2009. Deducing in vivo toxicity of combustion-derived nanoparticles from a cell-free oxidative potency assay and metabolic activation of organic compounds. *Environ Health Perspect,* 117**,** 54-60.

SUZUI, M., FUTAKUCHI, M., FUKAMACHI, K., NUMANO, T., ABDELGIED, M., TAKAHASHI, S., OHNISHI, M., OMORI, T., TSURUOKA, S., HIROSE, A., KANNO, J., SAKAMOTO, Y., ALEXANDER, D. B., ALEXANDER, W. T., JIEGOU, X. & TSUDA, H. 2016. Multiwalled carbon nanotubes intratracheally instilled into the rat lung induce development of pleural malignant mesothelioma and lung tumors. *Cancer Sci,* 107**,** 924-35.

TAKANO, H., YANAGISAWA, R., ICHINOSE, T., SADAKANE, K., YOSHINO, S., YOSHIKAWA, T. & MORITA, M. 2002. Diesel exhaust particles enhance lung injury related to bacterial endotoxin through expression of proinflammatory cytokines, chemokines, and intercellular adhesion molecule-1. *Am J Respir Crit Care Med,* 165**,** 1329-35.

TANG, Y. W., JOHNSON, J. E., BROWNING, P. J., CRUZ-GERVIS, R. A., DAVIS, A., GRAHAM, B. S., BRIGHAM, K. L., OATES, J. A., JR., LOYD, J. E. & STECENKO, A. A. 2003. Herpesvirus DNA is consistently detected in lungs of patients with idiopathic pulmonary fibrosis. *J Clin Microbiol,* 41**,** 2633-40.

TASIS, D., TAGMATARCHIS, N., BIANCO, A. & PRATO, M. 2006. Chemistry of carbon nanotubes. *Chem Rev,* 106**,** 1105-36.

TIAN, F., HABEL, N. C., YIN, R., HIRN, S., BANERJEE, A., ERCAL, N., TAKENAKA, S., ESTRADA, G., KOSTARELOS, K., KREYLING, W. & STOEGER, T. 2013. Pulmonary DWCNT exposure causes sustained local and low-level systemic inflammatory changes in mice. *Eur J Pharm Biopharm,* 84**,** 412-20.

TOMARU, M. & MATSUOKA, M. 2011. The role of mitogen-activated protein kinases in crystalline silica-induced cyclooxygenase-2 expression in A549 human lung epithelial cells. *Toxicol Mech Methods,* 21**,** 513-9.

TOTLANDSDAL, A. I., REFSNES, M. & LåG, M. 2010. Mechanisms involved in ultrafine carbon black-induced release of IL-6 from primary rat epithelial lung cells. *Toxicol In Vitro,* 24**,** 10-20.

TSUGITA, M., MORIMOTO, N., TASHIRO, M., KINOSHITA, K. & NAKAYAMA, M. 2017. SR-B1 Is a Silica Receptor that Mediates Canonical Inflammasome Activation. *Cell Rep,* 18**,** 1298-1311.

TZELLOS, S. & FARRELL, P. J. 2012. Epstein-barr virus sequence variation-biology and disease. *Pathogens,* 1**,** 156-74.

VIRGIN, H. W., WHERRY, E. J. & AHMED, R. 2009. Redefining chronic viral infection. *Cell,* 138**,** 30-50.

VOLCKENS, J., DAILEY, L., WALTERS, G. & DEVLIN, R. B. 2009. Direct particle-to-cell deposition of coarse ambient particulate matter increases the production of inflammatory mediators from cultured human airway epithelial cells. *Environ Sci Technol,* 43**,** 4595-9.

VON KLOT, S., WöLKE, G., TUCH, T., HEINRICH, J., DOCKERY, D. W., SCHWARTZ, J., KREYLING, W. G., WICHMANN, H. E. & PETERS, A. 2002. Increased asthma medication use in association with ambient fine and ultrafine particles. *Eur Respir J,* 20**,** 691-702.

WANG, C., XU, J., YANG, L., XU, Y., ZHANG, X., BAI, C., KANG, J., RAN, P., SHEN, H., WEN, F., HUANG, K., YAO, W., SUN, T., SHAN, G., YANG, T., LIN, Y., WU, S., ZHU, J., WANG, R., SHI, Z., ZHAO, J., YE, X., SONG, Y., WANG, Q., ZHOU, Y., DING, L., YANG, T., CHEN, Y., GUO, Y., XIAO, F., LU, Y., PENG, X., ZHANG, B., XIAO, D., CHEN, C. S., WANG, Z., ZHANG, H., BU, X., ZHANG, X., AN, L., ZHANG, S., CAO, Z., ZHAN, Q., YANG, Y., CAO, B., DAI, H., LIANG, L. & HE, J. 2018. Prevalence and risk factors of chronic obstructive pulmonary disease in China (the China Pulmonary Health [CPH] study): a national cross-sectional study. *Lancet,* 391**,** 1706-1717.

WANG, J., HUANG, J., WANG, L., CHEN, C., YANG, D., JIN, M., BAI, C. & SONG, Y. 2017. Urban particulate matter triggers lung inflammation via the ROS-MAPK-NF-κB signaling pathway. *J Thorac Dis,* 9**,** 4398-4412.

WANG, J. & XIA, Y. 2012. Assessing developmental roles of MKK4 and MKK7 in vitro. *Commun Integr Biol,* 5**,** 319-24.

WANG, M., LI, J., DONG, S., CAI, X., SIMAITI, A., YANG, X., ZHU, X., LUO, J., JIANG, L. H., DU, B., YU, P. & YANG, W. 2020. Silica nanoparticles induce lung inflammation in mice via ROS/PARP/TRPM2 signaling-mediated lysosome impairment and autophagy dysfunction. *Part Fibre Toxicol,* 17**,** 23.

WANG, P., NIE, X., WANG, Y., LI, Y., GE, C., ZHANG, L., WANG, L., BAI, R., CHEN, Z., ZHAO, Y. & CHEN, C. 2013. Multiwall carbon nanotubes mediate macrophage activation and promote pulmonary fibrosis through TGF-β/Smad signaling pathway. *Small,* 9**,** 3799-811.

WANG, P., WANG, Y., NIE, X., BRAïNI, C., BAI, R. & CHEN, C. 2015. Multiwall carbon nanotubes directly promote fibroblast-myofibroblast and epithelial-mesenchymal transitions through the activation of the TGF-β/Smad signaling pathway. *Small,* 11**,** 446-55.

WECK, K. E., KIM, S. S., VIRGIN, H. I. & SPECK, S. H. 1999. Macrophages are the major reservoir of latent murine gammaherpesvirus 68 in peritoneal cells. *J Virol,* 73**,** 3273-83.

WEISSENBERG, A., SYDLIK, U., PEUSCHEL, H., SCHROEDER, P., SCHNEIDER, M., SCHINS, R. P., ABEL, J. & UNFRIED, K. 2010. Reactive oxygen species as mediators of membrane-dependent signaling induced by ultrafine particles. *Free Radic Biol Med,* 49**,** 597-605.

WHO 2022. Chronic obstructive pulmonary disease (COPD).

WINTERBOTTOM, C. J., SHAH, R. J., PATTERSON, K. C., KREIDER, M. E., PANETTIERI, R. A., JR., RIVERA-LEBRON, B., MILLER, W. T., LITZKY, L. A., PENNING, T. M., HEINLEN, K., JACKSON, T., LOCALIO, A. R. & CHRISTIE, J. D. 2018. Exposure to Ambient Particulate Matter Is Associated With Accelerated Functional Decline in Idiopathic Pulmonary Fibrosis. *Chest,* 153**,** 1221-1228.

WINZEN, R., KRACHT, M., RITTER, B., WILHELM, A., CHEN, C. Y., SHYU, A. B., MüLLER, M., GAESTEL, M., RESCH, K. & HOLTMANN, H. 1999. The p38 MAP kinase pathway signals for cytokine-induced mRNA stabilization via MAP kinase-activated protein kinase 2 and an AU-rich region-targeted mechanism. *Embo j,* 18**,** 4969-80.

XIE, J., AJIBADE, A. O., YE, F., KUHNE, K. & GAO, S. J. 2008. Reactivation of Kaposi's sarcoma-associated herpesvirus from latency requires MEK/ERK, JNK and p38 multiple mitogen-activated protein kinase pathways. *Virology,* 371**,** 139-54.

XIE, J., PAN, H., YOO, S. & GAO, S. J. 2005. Kaposi's sarcoma-associated herpesvirus induction of AP-1 and interleukin 6 during primary infection mediated by multiple mitogen-activated protein kinase pathways. *J Virol,* 79**,** 15027-37.

XIONG, L. L., TAN, Y., MA, H. Y., DAI, P., QIN, Y. X., YANG, R. A., XU, Y. Y., DENG, Z., ZHAO, W., XIA, Q. J., WANG, T. H. & ZHANG, Y. H. 2016. Administration of SB239063, a potent p38 MAPK inhibitor, alleviates acute lung injury induced by intestinal ischemia reperfusion in rats associated with AQP4 downregulation. *Int Immunopharmacol,* 38**,** 54-60.

YANG, L., FEUCHTINGER, A., MöLLER, W., DING, Y., KUTSCHKE, D., MöLLER, G., SCHITTNY, J. C., BURGSTALLER, G., HOFMANN, W., STOEGER, T., DANIEL, R., WALCH, A. & SCHMID, O. 2019. Three-Dimensional Quantitative Co-Mapping of Pulmonary Morphology and Nanoparticle Distribution with Cellular Resolution in Nondissected Murine Lungs. *ACS Nano,* 13**,** 1029-1041.

YANG, N., LUNA, J. M., DAI, P., WANG, Y., RICE, C. M. & DENG, L. 2022. Lung type II alveolar epithelial cells collaborate with CCR2(+) inflammatory monocytes in host defense against poxvirus infection. *Nat Commun,* 13**,** 1671.

YE, F., ZHOU, F., BEDOLLA, R. G., JONES, T., LEI, X., KANG, T., GUADALUPE, M. & GAO, S. J. 2011. Reactive oxygen species hydrogen peroxide mediates Kaposi's sarcoma-associated herpesvirus reactivation from latency. *PLoS Pathog,* 7**,** e1002054.

YESUDHAS, D., GOSU, V., ANWAR, M. A. & CHOI, S. 2014. Multiple roles of toll-like receptor 4 in colorectal cancer. *Front Immunol,* 5**,** 334.

YONG, H. Y., KOH, M. S. & MOON, A. 2009. The p38 MAPK inhibitors for the treatment of inflammatory diseases and cancer. *Expert Opin Investig Drugs,* 18**,** 1893-905.

YOON, H. Y., KIM, S. Y., KIM, O. J. & SONG, J. W. 2021. Nitrogen dioxide increases the risk of mortality in idiopathic pulmonary fibrosis. *Eur Respir J,* 57.

YOU, R., LU, W., SHAN, M., BERLIN, J. M., SAMUEL, E. L., MARCANO, D. C., SUN, Z., SIKKEMA, W. K., YUAN, X., SONG, L., HENDRIX, A. Y., TOUR, J. M., CORRY, D. B. & KHERADMAND, F. 2015. Nanoparticulate carbon black in cigarette smoke induces DNA cleavage and Th17-mediated emphysema. *Elife,* 4**,** e09623.

YUAN, X., ZHANG, X., SUN, L., WEI, Y. & WEI, X. 2019. Cellular Toxicity and Immunological Effects of Carbon-based Nanomaterials. *Part Fibre Toxicol,* 16**,** 18.

ZHONG, W. & GANEM, D. 1997. Characterization of ribonucleoprotein complexes containing an abundant polyadenylated nuclear RNA encoded by Kaposi's sarcoma-associated herpesvirus (human herpesvirus 8). *J Virol,* 71**,** 1207-12.

ZHU, F. X., CUSANO, T. & YUAN, Y. 1999. Identification of the immediate-early transcripts of Kaposi's sarcoma-associated herpesvirus. *J Virol,* 73**,** 5556-67.

Apendix A:

Apendix B:

Acknowledgements

From October 2017, I started my PhD program under the supervision of Prof. Dr. Annette Peters in Ludwig-Maximilians Universität München. I have been working for my PhD project for more than four years in Dr. Tobias Stoeger lab in Institute of Lung Health and Immunity, Comprehensive Pneumology Center (LHI/CPC) in Helmholtz Zentrum München in Munich, Germany. In the same time, Prof. Dr. Heiko Adler is my additional supervisor on my PhD project.

First, I want to thank to my supervisors, Prof. Annette Peters, Dr. Tobias Stoeger and Prof. Dr. Heiko Adler for their professional supervisions in the past years. It was my great pleasure to work together with them. Every meet and discussion makes the project always ongoing and achieve a lot. As my university supervisor, Prof. Dr. Annette Peters gave great support on university issues, thesis committee (TC) meeting discussion as well as project maintenance. Besides, I feel so lucky to work together with Dr. Tobias Stoeger. He is a talent scientist and a nice person, I learned a lot, improved a lot in research. What I achieved in the last years with Dr. Tobias Stoeger brings me confidence and enthusiasm and keep me stay in scientific work in the future. I also would like to thank to Prof. Dr. Heiko Adler, who is a professional virologist in my project, and provides me great support.

I want to thank to all the supports from our group Dynamics of Pulmonary Inflammation of the Institute of Lung Health and Immunity (LHI) for their support and help: Verena Haefner, David Kutschke, Anna Fuchs, Beatrix Steer, Dr. Carola Voss, Dr. Markus Rehberg, Hongyu Ren, Chenxi Li, Qiongliang Liu, Yasmin Shaalan, Eva Guenther, Miriam Kastlmeier, Qiaoxia Zhou, Xiaoying Wang,

I also want to thank to all the supports from our Institute of Lung Health and Immunity (LHI) for their support and help: Dr. Ali Önder Yildirim, Dr. Aicha Jeridi, Dr. Thomas Mark Conlon, Xiaomei Tan, Dr. Hengshuo Liu, Dr. Gizem Günes, Dr. Carmela Morrone, Dr. Claudia Staab-Weijnitz, Dr. Doreen Franke, Christine Hollauer. I am grateful to our secretary Silke Lauer and Kaori Sumikawa. They are always nice and helpful in the past years.

Thanks to all our collaborators: Dr. Martin Irmler, Prof. Dr. Johannes Beckers, Dr. Annette Feuchtinger. We cannot conduct well without nice techniques, analysis and so on.

Thanks to my friends, Bing Han, Mengwen He, Xinyuan Wang. I had a super nice time with them in the past years. Scientific discussion with them also provide me great support.

Last but not least, thanks to my family, especially my parents and my elder sister for their warm, continuous support to me in the past years. I cannot finish my PhD without them.

Affidavit

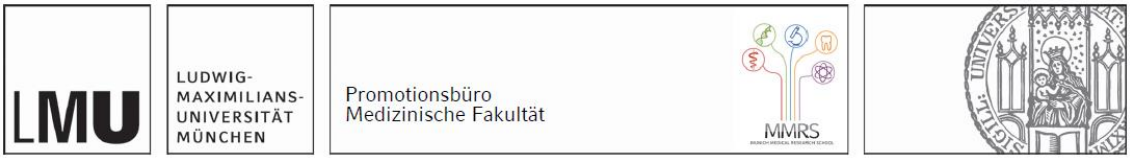

Affidavit

Han, Lianyong
_____
Surname, first name

Forstenrieder Allee, 78-5.OG
_____
Street

81476, Munich, Germany
_____
Zip code, town, country

I hereby declare, that the submitted thesis entitled:

Mechanism underlying environmental nanoparticle exposure triggered gammaherpesvirus reactivation

is my own work. I have only used the sources indicated and have not made unauthorized use of services of a third party. Where the work of others has been quoted or reproduced, the source is always given.

I further declare that the submitted thesis or parts thereof have not been presented as part of an examination degree to any other university.

Munich, Germany 08.08.2023 — place,date

Lianyong Han — Signature doctoral candidate

List of publications

Han L, Haefner V, Yu Y, Han B, Ren H, Irmler M, Beckers J, Feuchtinger A, Flexeder C, Schulz H, Peters A, Adler H, Stoeger T. Preventive p38 inhibition mitigates particle triggered herpesvirus reactivation (***ACS Nano; under revision***)

Han B, Lü Y, Moser D, Zhou X, Woehrle T, **Han L**, Osterman A, Rudelius M, Choukér A, Lei P. Cell surface GRP78 functions as an alternative virus entry receptor on monocytes during SARS-CoV-2 infection. (***eBioMedicine; under revision***)

Zhang Q, Tu W, Tian K, **Han L**, Wang Q, Chen P, Zhou X. Sirtuin 6 inhibits myofibroblast differentiation via inactivating transforming growth factor-β1/Smad2 and nuclear factor-κB signaling pathways in human fetal lung fibroblasts. J Cell Biochem. 2019 Jan;120(1):93-104.

Chen P, Tian K, Tu W, Zhang Q, **Han L**, Zhou X. Sirtuin 6 inhibits MWCNTs-induced epithelial-mesenchymal transition in human bronchial epithelial cells via inactivating TGF-β1/Smad2 signaling pathway. Toxicol Appl Pharmacol. 2019 Jul 1;374:1-10.

Tu W, Zhang Q, Liu Y, **Han L**, Wang Q, Chen P, Zhang S, Wang A, Zhou X. Fluoride induces apoptosis via inhibiting SIRT1 activity to activate mitochondrial p53 pathway in human neuroblastoma SH-SY5Y cells. Toxicol Appl Pharmacol. 2018 May 15;347:60-69.

Tian K, Chen P, Liu Z, Si S, Zhang Q, Mou Y, **Han L**, Wang Q, Zhou X. Sirtuin 6 inhibits epithelial to mesenchymal transition during idiopathic pulmonary fibrosis via inactivating TGF-β1/Smad3 signaling. Oncotarget. 2017 May 9;8(37):61011-61024.